1-21-2016

Continuous Processing of Liposomes to Control and Predict Physical Properties

Antonio P. Costa
University of Connecticut, apc0331@gmail.com

Continuous Processing of Liposomes to Control and Predict Physical Properties

Antonio P. Costa, PhD

University of Connecticut, 2016

Liposomes are specialized drug delivery systems that deliver drugs efficiently and may be used in targeted and/or extended-release applications. Currently, the processing and manufacturing of these drug products is by batch processing in the pharmaceutical industry. Batch processing has disadvantages such as scalability, irreproducibility, down-time between batches and other issues leading to reduced product availability, product waste and increased monetary costs. As a way to circumvent traditional problems associated with batch processing, the U.S. FDA has published guidance focusing on the continuous manufacturing of drug products, quality by design and the incorporation of process analytical technology.

In the current work, a continuous process for the formation of liposomes was developed. This process was based on the ethanol-injection process, which includes injecting ethanol with dissolved lipid into an aqueous phase. The process included additional downstream processes such as in-line dilution, in-line concentrating, and at-line particle size analysis. National Instruments (NI) LabVIEW was used to develop the entire process into an automatic, continuous process. All control and measurement devices were controlled by a single computer program. The computer program contained algorithms that enabled prediction measurement of liposomal characteristics (*e.g.* particle size, particle size distribution and lipid concentration). Moreover, a quality-by-design (QbD) approach was followed from the onset of the project. Following QbD minimized the overall risk in developing the system and established an extensive understanding of liposomes. With the use of multiple design of experiment studies, algorithms and prediction equations were included in the custom-built computer program and established accurate control over the liposome formation process.

Continuous Processing of Liposomes to Control and Predict Physical Properties

Antonio Paul Costa

B.A., University of Connecticut, **2010**

B.S., University of Connecticut, **2010**

M.S., University of Connecticut, **2011**

A Dissertation

Submitted in Partial Fulfillment of the

Requirements for the Degree of

Doctor of Philosophy

at the

University of Connecticut

2016

APPROVAL PAGE

Doctor of Philosophy Dissertation

Continuous Processing of Liposomes to Control and Predict Physical Properties

Presented by

Antonio P. Costa, B.S., B.A., M.S.

Major Advisor _____
Diane J. Burgess

Associate Advisor _____
Mansoor A. Khan

Associate Advisor _____
Fotios Papadimitrakopoulos

Associate Advisor _____
Xiuling Lu

Associate Advisor _____
Xiaoming Xu

University of Connecticut
2016

Dedication

To Gosia and my parents

Acknowledgments

I would like to first thank my wife and parents. I thank my wife for her love and for staying by my side over these past years. I greatly appreciate her understanding with my constant studying and to the tremendous amount of time that I spent in the lab. In addition, being a student for nearly eleven years would not have been possible without the love and support from my parents.

I thank Dr. Burgess, my advisor, for her endless support over the years, which started during my undergraduate studies. She has prepared me for future endeavors in many ways, such as bettering my scientific writing skills, forming a fundamental basis to critically review scientific papers, improving my time management skills and, most importantly, becoming a well-rounded, astute scientist.

I would like to thank all of my other committee members, Dr. Mansoor Khan, Dr. Fotios Papadimitrakopoulos, Dr. Xiuling Lu and Dr. Xiaoming Xu for their support and guidance. I would like to especially thank Dr. Xiaoming Xu as he has been an excellent mentor and was the person that introduced me and taught me much about liposomes, which became the basis of my doctoral research.

Additionally, I would like to acknowledge previous and current lab members in Dr. Burgess' lab. Being surrounded by pleasant individuals provides for an atmosphere where great achievements can be met. I would especially like to thank Dr. Jie Shen for discussion and guidance over the years.

I would also like to thank the remaining Pharmaceutics faculty, Dr. Michael Pikal, Dr. Devendra Kalonia, Dr. Robin Bogner and Dr. Bodhi Chaudhuri for their instruction during course offerings and scientific support outside of the classroom.

The University of Connecticut offers many outstanding resources such as machine shops and electron microscopy labs. I thank Peter Glaude for allowing me to use the engineering machine shop. With his support, I was able to rapidly prototype/ machine parts for the system that I developed. Also, I thank Dr. M. Cantino, Stephen Daniels and Dr. X. Sun from the Biosciences Electron Microscope Laboratory of the Physiology and Neurobiology Department at the University of Connecticut for their work on cryo-SEM and negative stain TEM micrographs.

I would like to acknowledge the U.S. FDA (Grant#: HHSF223201310117C) for their support for much of this work. In addition, I would like to acknowledge the FDA White Oak Nanotechnology Core Facility for instrument use, scientific and technical assistance.

Lastly, I would like to also acknowledge the American Foundation for Pharmaceutical Education (AFPE) for selecting me as an AFPE fellow. I personally feel becoming an AFPE fellow was a significant achievement and highlighted the importance of my doctoral endeavors.

Table of Contents

List of Figures xiii
List of Tables xviii

Chapter 1

Liposomes as Drug Delivery Systems

1.1 Abstract 1
1.2 Liposomal Basic Principles 1
1.2.1 Properties of Lipid Molecules 1
1.2.2 Thermodynamics of Liposome Formation 4
1.2.3 Liposomal Physicochemical Properties 5
1.2.4 Liposome Formulation Techniques 6
1.2.5 Intercalation of Molecules in the Liposomal Membrane 7
1.2.6 Passive Encapsulation: Freeze-Thaw Cycling 8
1.2.7 Active or “Remote” Loading of Molecules 9
1.2.8 Liposomal Drug Products Overview 9
1.3 Continuous Processing of Liposomal Drug Products 10
1.3.1 Batch vs. Continuous Manufacturing 10
1.3.2 Process Analytical Technology 11

Chapter 2

Specific Aims and Tasks

2.1. Specific Aim 1 14
2.1.1 Task 1 15
2.1.2 Task 2 15
2.1.3 Task 3 16
2.2 Specific Aim 2 17
2.2.1 Task 1 18
2.2.3 Task 2 19
2.3. Figures 20

Chapter 3

Quality by Design: Risk Assessment of Continuous Processing Stages

3.1 Introduction 22
3.2 Risk Assessments 23
3.2.1 Liposomal Process Selection 23
3.2.2 Ethanol injection Process Stages: A Risk Analysis 24
3.2.2.1 System Requirements 25
3.2.2.2 Lipid Mixing 26
3.2.2.3 Liposome Formation with Dilution 27
3.2.2.4 Concentrating Liposomes 27
3.2.3 Risk Analysis of Process Analytical Technology 28
3.2.3.1 Particle Size Analysis 29
3.2.3.2 NIR Turbidity Sensor 30
3.2.4 Material and Process Parameters on Particle Size Formation 31
3.3 Conclusion 32
3.4 Figures 33

Chapter 4

Liposome Formation using a Coaxial Turbulent Jet in Co-Flow

4.1 Abstract 39
4.2 Abbreviations 40
4.3 Introduction 41
4.4 Materials and Methods: 43
4.4.1. Overview of Process with Turbulent Mixer 43
4.4.2. Liposome Preparation 44
4.4.3 Dynamic Light Scattering for Particle Size and Zeta-Potential 44
4.4.4 Flow Visualizations 45
4.4.5 Nanoparticle Tracking Analysis 45
4.4.6 Negative Stain Transmission Electron Microscopy (NS-TEM) 45
4.4.7 Cryo-Transmission Electron Microscopy (cryo-TEM) 46
4.4.8 Design of Experiment Study 46

4.4.9 Reynolds Number and Flow Velocity Ratio Calculations 47
4.5. Results 48
4.5.1 Mixing of Ethanol and Aqueous Phase 48
4.5.2 Relationship between Fluid Flow Properties and Liposomal Polydispersity Index 48
4.5.3 Design of Experiment: Lipid Concentration vs. Particle Size 50
4.5.4 Types of Lipid on Liposome Particle Size 51
4.5.5 Aqueous Phase Additives on Liposome Particle Size 51
4.5.6 Comparison of Particle Size and Size Distribution using Multiple Measurement Techniques 52
4.5.7 Negative Stain TEM Micrographs of Liposomes 53
4.5.8 Cryo-TEM Micrographs of Liposomes 53
4.6 Discussion 54
4.6.1 Liposome Monodispersity via a Coaxial Turbulent Jet 54
4.6.2 Liposome Formation Model using a Coaxial Turbulent Jet 55
4.6.3 Particle Size Analysis using Multiple Measurement Techniques 59
4.7 Conclusion 61
4.8 Tables 62
4.9 Figures 63

Chapter 5

Continuous Processing of Liposomes with in-line Dilution and at-line Particle Size Analysis

5.1. Abstract 74
5.2 Introduction 74
5.3 Materials and Methods 78
5.3.1 Materials 78
5.3.2 Experimental Methods 78
5.3.2.1. Liposome Formation and Dilution 78
5.2.2.2. Data Acquisition System and Computer Software 79
5.2.2.3. Experimental Outline for Liposomal Dilution 80
5.2.2.4. Temperature Effects on Liposome Formation and Dilution 81
5.2.2.5. Particle Size Measurements 81
5.2.2.6. Automatic Particle Size Control 82
5.3 Results 83

5.3.1. Effect of Contactor prior to Ethanol Dilution 83
5.3.2. Temperature Effects on Liposome Formation and Dilution 83
5.3.3. DLS Measurement Analysis 84
5.3.4. At-line Particle Size Analysis - Approach 1: Continuous Flow Mode 85
5.3.5. Approach 2: Load/Stop Mode 86
5.3.5. Ionic Strength on Liposomal Physical Properties 88
5.3.6. Automatic Particle Size Control 88
5.4. Discussion 89
5.4.1. In-line Liposomal Dilution 89
5.4.2. Variables that Influence Particle Size Measurements 91
5.4.3. At-line Particle Size Measurements Comparisons 94
5.4.4. Ionic Strength on Liposome Formation 94
5.4.5. Automatic Particle Size Control 96
5.5. Conclusions 96
5.6. Tables 98
5.7. Figures 99

Chapter 6

Continuous Processing of Liposomes with In-line Concentrating

6.1 Abstract 113
6.2. Introduction 113
6.2. Materials and Methods 115
6.2.1. Materials 115
6.2.2. Experimental Methods 116
6.2.2.1. Liposome Formation and Dilution 116
6.2.2.2. Data Acquisition System and Computer Software 117
6.2.2.3. Particle Size Measurements 117
6.2.2.4. NIR (Turbidity) Measurements 118
6.2.2.5. Tangential Flow Filtration System 119
6.2.2.6. Lipid Concentration Analysis via the Stewart Assay 119
6.2.2.6. Lipid Concentration Analysis via high pressure liquid chromatograph – Mass spectrometry 119
6.2.2.6. Lipid Concentration Prediction Equation 120

6.3. Results 121
6.3.1. Prediction Models 121
6.3.2. Polydispersity on the NIR Signal 122
6.4. Discussion 123
6.4.1 Lipid Concentration Models 123
6.4.2 Polydispersity on NIR Detection 125
6.5. Conclusions 125
6.5. Tables 126
6.6. Figures 128

Chapter 7

Freeze-Anneal-Thaw Cycling of Unilamellar Liposomes: Effect on Encapsulation Efficiency

7.1 Abstract 133
7.2 Abbreviations 134
7.3 Introduction 135
7.4 Materials and Methods 136
7.4.1 Preformed Empty Liposomes Preparation 136
7.4.2 Drug Encapsulation Process 137
7.4.3 Encapsulation Efficiency (EE%) 138
7.4.4 Particle Size and Zeta-Potential 138
7.4.5 Cryo-SEM Imaging 138
7.4.6 Differential Scanning Calorimetry 139
7.5 Results 139
7.5.1 Particle Size 139
7.5.2 Zeta-Potential 140
7.5.3 Encapsulation Efficiency (Post-Extrusion) 140
7.5.4 Two Freeze-Anneal-Thaw Cycles (Pre-Extrusion) 141
7.5.5 Cryo-SEM Imaging 141
7.5.6 Differential Scanning Calorimetry Thermogram 142
7.6 Discussion 142
7.7 Conclusion 145
7.8 Disclaimer 146
7.9 Acknowledgement 146

7.10 Tables 146
7.11 Figures 148

Chapter 8

Conclusions and Suggested Studies

8.1 Conclusions 153
8.2 Suggested Studies 156
8.2.1 Continuous Processing of Liposomes 156
8.2.2 Freeze-Anneal-Thaw Cycling 157

9. References 158

List of Figures

Figure 2.1: Block diagram of the entire system. Arrows indicate the flow direction of the process.

Figure 2.2: Front panel of the custom computer program. The computer program is divided into five parts: lipid mixing, aqueous phase/buffer, aqueous phase dilution, tangential flow filtration (TFF) system and particle size.

Fig. 3.1 A risk assessment comparing two processing techniques to make liposomes with the intention to develop the current process into a continuous process.

Fig 3.2: A cause and effect diagram highlighting the main stages of the continuous process with subdivisions for each main stage.

Fig 3.3: The control design for the concentrating system. This design uses feedback control (pump flow rate) and feedforward control (particle size analyzer and an NIR sensor) to determine the lipid concentration. The particle size data and data from the NIR sensor are incorporated into a mathematical model used to predict the lipid concentration.

Fig 3.4: A cause and effect diagram outlining variables that result in obtaining accurate particle size data for a continuous process.

Fig 3.5: A cause and effect diagram outlining variables that affect the lipid concentration detection via a NIR sensor.

Fig 3.6: A cause and effect diagram outlining variables that affect the liposome formation process with respect to material and process variables.

Fig. 4.1 Overall schematic of the lipid mixing process and the injection port (not shown to scale). Ethanol or lipid dissolved in ethanol is added to the pressurized tanks. NI LabVIEW is used to control the entire process and sensors such as flow meters are installed to control/monitor the flow conditions.

Fig. 4.2 The design space of the DOE study on the impact of lipid concentration and aqueous phase flow rate on particle size. The initial design consisted of 2 factors at 4-levels (black circles) and center points (red star). The design was augmented with additional runs to extend the model design space (blue triangles).

Fig. 4.3 Schematics and photographic image of the injection port that allows formation of a coaxial turbulent jet. Both the aqueous and ethanol streams are flowing in the same direction (co-flow). Arrows indicate the direction of liquid flow. The photograph is of lipid dissolved in ethanol (visualized through the use of Nile Red) that is being injected in the center of the aqueous stream. Additionally, the jet location is shown as a schematic where there is a limited mixing zone followed by a concentration gradient of the ethanol+lipid phase.

Fig. 4.4 Relationship between liposome polydispersity index and flow properties. 4a) Flow velocity ratio (FVR) *vs*. the mixture Reynolds Number ($Re_{mixture}$). The region above the solid line produced monodispersed liposomes (PDI <0.10) and the region below the solid line formed polydispersed liposomes (PDI >0.10). 4b) Flow images corresponding to locations (1, 2, 3, and 4) from Fig. 4a demonstrating flow profiles leading to monodispersed or polydispersed systems. To cover a range of FVR and $Re_{mixture}$, the ethanol containing inner tube diameter (d_E) and the aqueous containing outer tube diameter (d_A) were changed accordingly. 4c) Z-average particle size vs. $Re_{mixture}$ for only monodispersed liposomes. d_{A1} = 3.175 mm, d_{A2} = 4.572 mm, d_{E1} = 0.508 mm, d_{E2}=1.016 mm.

Fig. 4.5 A Surface profile plot of the Z-average particle size vs. the aqueous phase flow rate (AFR) and lipid concentration. The liposome particle size increases with an increase in the injected lipid concentration and/or a decrease in aqueous phase flow rate

Fig. 4.6 The effect of lipid type (*i.e.* DMPC, DPPC, DSPC, DOPC) on mean particle size and PDI. The formed liposomes were mostly monodispersed with the majority of PDI values ≤ 0.05. Some polydispersity was evident for DOPC liposomes and for liposomes formed at low aqueous phase flow rates. The dotted line in the bottom plot represents the limit on monodispersity (PDI<0.10). The standard deviation from the Z-Average particle size plot was less than the symbols representing the data.

Fig. 4.7 The effect of aqueous phase additives on mean particle size. The aqueous phase consisted of 10 mM phosphate buffer plus the addition of certain additives (*i.e.* NaCl, glycerol and ethanol). All additives were pre-mixed with the aqueous phase prior to liposome formation. The 10 mM Phosphate buffer sample was used as a control. The Z-average particle size measured by DLS and PDI are plotted above.

Fig. 4.8 Comparison of different particle sizing techniques (dynamic light scattering, nanoparticle tracking and particle counting *via* NS-TEM to assess liposome mean particle size and particle size distribution. DLS and nanoparticle tracking are in good agreement with both mean size and size distribution. NS-TEM produces a larger particle size and size distribution. For all three techniques, the mean particle size trend is the same, *i.e.* an increase in mean particle size for a decrease in the aqueous phase flow rate. Ethanol flow rate = e (mL/min); Aqueous flow rate = a (mL/min).

Fig. 4.9 Liposome mean particle size and standard deviations for DLS, nanoparticle tracking, NS-TEM and Cryo-TEM. The z-average standard deviation was calculated from the PDI (*i.e.* $\sigma = [\text{mean}*\text{PDI}]^{1/2}$). The intensity standard deviation was reported directly from the intensity width. The nanoparticle tracking standard deviation was reported by the Nanosight® software. The NS-TEM standard deviation was from the Gaussian distribution fit ($R^2 \geq 0.913$ for all cases). Error bars represent the standard deviation for the multiple data sets. No error bars were reported for Cryo-TEM since the particle count was limited. Ethanol flow rate = e (mL/min); Aqueous flow rate = a (mL/min).

Fig. 4.10 Negative stain TEM micrographs of liposomes for three liposome samples produced using different flow conditions. a) 40e:100a sample, b) 40e:150a, c) 40e:375a and d) 40e:375a zoomed. Ethanol flow rate = e (mL/min); Aqueous flow rate = a (mL/min).

Fig. 4.11 Cryo-TEM micrographs of liposomes for three liposome samples produced using different flow conditions. a) 40e:100a sample, b) 40e:150a and c) 40e:375a. Ethanol flow rate = e (mL/min); Aqueous flow rate = a (mL/min).

Fig. 4.12 Proposed model for liposome formation from a coaxial turbulent jet mixer in co-flow. A schematic of a turbulent jet is shown with a radial ethanol concentration gradient (top left). In the liposome formation model, lipid and ethanol molecules aggregate (forming pro-liposomes) as the ethanol concentration decreases. The pro-liposomes grow in size by "recruiting" lipid molecules. The growth continues until the ethanol concentration reduces below a critical level. Image not shown to scale.

Fig. 5.1 Schematic representation of the liposome formation stage followed by the ethanol dilution stage. Two temperature readings via thermocouples are taken at each stage and a contactor (degassing unit) is positioned in some cases at the end of the liposome formation stage.

Fig 5.2 Liposome mean particle size and polydispersity index for both *lipid*:Chol:DPPG (4.5:3:0.4 molar ratio) liposomes, where *lipid* refers to either DMPC or DPPC. Both z-average particle size (top) and polydispersity index (PDI, bottom) are plotted vs. aqueous phase I flow rate (mL/min).

Fig 5.3 Liposome mean particle size and polydispersity index for DPPC:Chol:DPPG (4.5:3:0.4 molar ratio) liposomes. The mean particle size and PDI is plotted against the temperature (°C) at the liposome formation site (see Fig 5.1). The aqueous phase I flow rate was kept constant at 80 mL/min.

Fig 5.4 Liposome mean particle size and polydispersity index for DMPC:Chol:DPPG (4.5:3:0.4 molar ratio) liposomes. The mean particle size and PDI is plotted against the temperature (°C) at the liposome formation site (see Fig 5.1). The aqueous phase I flow rate was kept constant at 70 mL/min.

Fig 5.5 A comparison of manual DLS measurement settings on the liposome particle size (z-average), the PDI and the DLS count rate (kcps). All results were from a single run at either 3, 9 or 15 seconds. The liposome formulation was the same for all measurements and had a z-average of 56.50 ± 0.03 nm, a PDI of 0.05 ± 0.02 and a count rate of 401.4 ± 2.77 kcps.

Fig 5.6 Liposome mean particle size and polydispersity index for DPPC:Chol:DPPG (4.5:3:0.4 molar ratio) liposomes. The mean particle size and PDI is plotted against aqueous phase I flow rate. The flow rates in the bottom plot in red are the DLS flow rates or the flow rate of the sample during the DLS measurement.

Fig 5.7 Liposome mean particle size and polydispersity index (PDI) for DMPC:Chol:DPPG (4.5:3:0.4 molar ratio) liposomes in 10 mM Phosphate Buffer. The mean particle size, PDI and

aqueous phase I flow rate is plotted over a period of time. The DLS flow rate was fixed at 1 mL/min. The aqueous phase was initially at 15°C prior to liposome formation.

Fig 5.8 Liposome mean particle size and polydispersity index (PDI) for DPPC:Chol:DPPG (4.5:3:0.4 molar ratio) liposomes in 10 mM Hepes buffer. The mean particle size, PDI and aqueous phase I flow rate is plotted over a period of time. The DLS flow rate was fixed at 1 mL/min.

Fig 5.9 Liposome mean particle size and polydispersity index (PDI) for DPPC:Chol:DPPG (4.5:3:0.4 molar ratio) liposomes in 10 mM NaCl. The mean particle size, PDI and aqueous phase I (AFR I) flow rate is plotted over a period of time.

Fig 5.10 Liposome mean particle size and polydispersity index (PDI) for DPPC:Chol:DPPG (4.5:3:0.4 molar ratio) liposomes in 75 mM NaCl. The mean particle size, PDI and aqueous phase I (AFR I) flow rate is plotted over a period of time.

Fig 5.11 Liposome mean particle size and polydispersity index (PDI) for DPPC:Chol:DPPG (4.5:3:0.4 molar ratio) liposomes in 140 mM NaCl. The mean particle size, PDI and aqueous phase I (AFR I) flow rate is plotted over a period of time.

Fig 5.12 Liposome mean particle size (z-average, d.nm) for DPPC:Chol:DPPG (4.5:3:0.4 molar ratio) liposomes in 10-140 mM NaCl (green, red, blue) and 10 mM PB (orange). The mean particle size is plotted against the aqueous phase I flow rate and the ionic strength.

Fig 5.13 Liposome zeta potential for DPPC:Chol:DPPG (4.5:3:0.4 molar ratio) liposomes in 10-140 mM NaCl and 10 mM phosphate buffer. The zeta potential is plotted against the aqueous phase I flow rate.

Fig 5.14 An example of automatic particle size control for HSPC:Chol:DPPG (4.5:3:0.4 molar ratio) liposomes prepared in 10 mM NaCl is shown. The mean particle size, polydispersity index (PDI), count rate (kcps) and aqueous phase I flow rate (mL/min) is plotted against time (s). The arrows indicate when the user changed the particle size set point in the software.

Fig 6.1: Schematic of the lipid concentration stage consisting of multiple components such as pumps, a tangential flow filtration unit, a flow meter and an NIR turbidity sensor.

Fig 6.2: Experimental design of the lipid concentration prediction model based on scattered light from an NIR turbidity sensor.

Fig 6.3: Model 2 experimental design for the lipid concentration with factors including particle size (d.nm), polydispersity index (PDI), ppm and CU. The PDI was from 0.03 – 0.21, with “low PDI” as PDI $\leq$ 0.1 and “high PDI” as PDI > 0.1.

Fig 6.4: Surface Profile plot for the lipid concentration [Lipid] prediction model. The scattered light from the NIR turbidity detector was measured in units of ppm. ppm vs. particle size (d.nm) vs. the total lipid concentration (mM) was plotted.

Fig 6.5: The Lipid Concentration prediction model equation based on the study outlined in Fig. 6.2 and Fig. 6.4.

Fig 6.6: The Lipid Concentration prediction model equation for Model 2. The response for the model is the total lipid concentration denoted as [Lipid] and has four factors: particle size (d.nm), polydispersity (PDI), ppm and CU. Both ppm and CU are detected by an NIR turbidity meter.

Fig 6.7: An example of how the NIR signal output in PPM is affected by the polydispersity of a liposomal formation. The polydispersity index (PDI) was approximately 0.16 for the high PDI sample and was <0.1 for the low PDI sample. In the case of larger liposomes, the NIR scattered light signal should be greater.

Fig. 7.1. Particle size of liposomes under various conditions. Samples either underwent a freeze-thaw (FT) cycle or a freeze-anneal-thaw ($FA_{NN}T$) cycle. All liposomes were frozen in liquid nitrogen (-196°C). All $FA_{NN}T$ samples were thawed at 65°C. Both pre-extrusion and post-extrusion particle size properties are detailed above. The error bar represents the PDI distribution width. The inset above each group of data represents the PDI of the samples for pre- and post-extrusion.

Fig. 7.2. Zeta-potential of the liposome formulation. The zeta-potential is provided for both pre- and post-extrusion for the samples listed in Fig. 7.1.

Fig. 7.3. Encapsulation efficiency for samples thawed under various conditions. All samples were frozen in liquid nitrogen at -196°C. The samples thawed directly at 65°C represent normal freeze-thaw cycling. All other samples underwent a single freeze-thaw or freeze-anneal-thaw cycle. The effects on EE% of thawing at temperatures above 0°C and annealing at subzero temperatures is demonstrated (n=3).

Fig. 7.4. Cryo-SEM images of PFE-liposomes with tenofovir. In all the images, the smooth/darker areas represent the ice phase while the non-smooth/lighter regions are liposomes. (A) Sample frozen to -196°C, magnification (mag.) 5,000x. (B) 30,000x mag. of sample from A with liposomes clearly visible. (C) Sample frozen to -196°C, annealed at -20°C overnight, and then refrozen to -196°C prior to imaging, mag. 5,000x. (D) 30,000x mag. of sample from C. In D, the top right hand corner is ice while the rest of the image is of liposomes in an apparent fused state. (D Inset) 30,000x mag. of a thin channel of liposomes between the ice-phases.

Fig. 7.5. DSC profile of annealed liposomes. Samples were first frozen in liquid nitrogen (-196°C) and heated to the annealing temperature (-22°C or -1.4°C) and held at that temperature for 10 min (not shown). The sample was then re-cooled to -60°C (shown above). HEPES buffer without liposomes was shown as a control. All samples were run in triplicate and the average standard deviation was <0.4 in all cases.

List of Tables

Table 4.1 DOE on Lipid Concentration vs. Particle Size - Model Parameter Estimates Sorted by Statistical Significance. The aqueous phase flow rate (AFR) and the lipid concentration terms both have statistical significance. In addition, higher order AFR terms are required due to the non-linearity of the response (*i.e.* particle size).

Table 5.1. Variables that Influence Continuous Particle Size Measurements

Table 6.1: TSQ HPLC-MS ESI Operating Conditions used in the Analysis of Lipid Concentration Quantitation.

Table 6.2: Sorted parameter estimates and model terms for Model 1.

Table 6.3: Sorted parameter estimates and model terms for Model 2.

Table 6.4: Validation data points for both lipid concentration ([Lipid]) models. Model 1 is based on particle size and ppm, whereas Model 2 includes particle size, polydispersity index (PDI), ppm and CU.

Table 7.1: Experimental outline for 60 mM DSPC:Chol:DSPG (6:3:1 molar ratio) liposomes. A single freeze-thaw cycle was performed in all cases, with differences in the thawing temperature. The difference in thawing time was needed to accommodate complete thawing. Liposomes were held at 65°C for 10 minutes before extrusion to prevent membrane fouling

Table 7.2. Pre-Extrusion Results for Two FANNT(-196/-1.436min/65) Cycles (n=3)

Chapter 1

Liposomes as Drug Delivery Systems

1.1 Abstract

There has been extensive research over the years focusing on liposomes as drug delivery systems. Liposomes are vesicles composed of a single lipid-bilayer or multiple/concentric lipid-bilayers that surround an aqueous core. Liposomal drug delivery systems are designed to encapsulate drug substances in the aqueous core and/or incorporate drug substances into the lipid-bilayer. The route of administration is often parental but may also be via other routes such as intra-muscular or oral. This chapter explains the basic principles of liposomes and is divided into two major sections. The first section outlines the liposome formation mechanism and liposomal physicochemical properties. The second section outlines liposomal processing techniques.

1.2 Liposomal Basic Principles

1.2.1 Properties of Lipid Molecules

Lipid is one of the four classes of biological compounds and the compounds in this class share the chemical property of being insoluble in water. Unlike the other classes such as proteins, nucleic acids and carbohydrates, lipid compounds have a high degree of structural diversity[1]. For example, lipid compounds may be further subdivided into fatty acids, surfactants, triglycerides, phospholipids, terpenes, steroids, and lipid soluble vitamins. Lipids that are typically used in the

formulation of liposomes are amphiphilic in that these compounds have both a hydrophilic and a hydrophobic region. The chemical structure of these lipid compounds consist of a backbone region (*e.g.* glycerol or sphingosine), a hydrophilic head group (*e.g.* phosphatidylcholine), and two hydrophobic hydrocarbon tails. The head group and hydrocarbon tails are esterified to the backbone and form specific classes of lipids (*e.g.* glycerophospholipids). Many different esterified groups exist, forming an abundance of lipids. With respect to head groups, these groups may be neutral/zwitterionic (*e.g.* phosphatidyl choline) or have either a positive or negative charge. Moreover, hydrocarbon chains may be saturated or unsaturated and may be derived naturally or synthetically. Saturated lipids do not have double bonds in the hydrocarbon chains while unsaturated do. Typically, unsaturated lipids used in liposomes consist of either only one or two sites of double bonds, as highly unsaturated lipids would not form liposomes as a result of their packing parameters as detailed below.

Individual lipid molecules have an important property known as the lipid phase transition temperature. This property outlines a transition where the lipid molecule goes from a gel, solid-ordered phase (below the T_c) to a fluid, disordered phase (above the T_c)[2]. This transition can be determined by differential scanning calorimetry[3-4]. With respect to liposomes, this transition may cause in increase in membrane permeability[5]. Saturated lipids generally have a higher lipid phase-transition compared to unsaturated lipids. A high lipid phase-transition keeps the lipids in the gel form at physiological temperature or above; which can increase liposomal *in vitro* and *in vivo* stability. For lipids with a low phase transition temperature, the lipid may be disordered in the lipid bilayer at storage and processing conditions, leading to increased molecular permeability[6] (*e.g.* drug leakage) and reduced liposomal stability. The incorporation of

cholesterol in a lipid bilayer is known to be an important addition to liposomes as it broadens or diminishes the lipid phase-transition and increases liposomal stability[7-8]. Cholesterol does this by forming a new phase, the liquid, ordered phase[9]. This phase exists below and above the lipid phase transition temperature of the pure lipid component and reduce the intensity of the phase transition[10]. Therefore, it may be important to incorporate cholesterol into liposomal formulations for drug delivery applications.

Depending on the application, different types of lipid may be incorporated into liposomes to modify liposomal properties. For example, fusogenic lipids such as DOPE are used in cellular delivery of nucleic acids to improve endosomal escape. The fusogenic property is one that causes the liposomes to fuse with the cellular membrane[11-12] or with the endosomal membrane[13], resulting in the release of contents into the cytoplasm. The liposomes fuse with the endosomal membrane post cellular uptake[14] causing the liposome and the nucleic acid to reach the cytoplasm. Another type of lipid is DSPE-mPEG and its derivatives. The chemical structure of these lipids consists of a phosphoglycerol lipid (*e.g.* DSPE) linked to a long chained polyethylene-glycol (*e.g.* mPEG-2000). This class of lipids adds a polymer layer to the outside of the liposome and enhances liposomal stability. These liposomes were originally termed “stealth” liposomes[15] as the hydrated polymer layer considerably delays liposomal cellular uptake once administered *in vivo*. In addition, these polymer lipids may be modified to introduce targeting moieties to the outer-leaflet of the lipid-bilayer. These targeting moieties are important for a variety of applications when *in vivo* passive targeting is insufficient.

Another property of lipid molecules is the critical packing parameter. The critical packing parameter, ***P***, is defined as:

$$\boldsymbol{P} = \frac{V}{a * l}$$

Where V is the volume of the hydrophobic region of the lipid, *a* is the cross-sectional polar head group area where the head group connects with the hydrophobic region, and *l* is the length of the hydrocarbon chains. The importance of the critical packing parameter is that it indicates the lipid structure/phase that may form for that individual lipid. Different lipid structures include: lamellar phase (p~1), hexagonal I phase (P<1) and hexagonal II phase (P>1)[10]. Lipid molecules that have P~1 will form liposomes under certain conditions (see section 1.2.2), whereas lipid molecules with P<1 and P>1 will form micelles or inverted micelles, respectively. In addition, this packing parameter can be used to determine whether lipid mixtures will form liposomes, *i.e.* certain weight ratios of lipids of different phases may result in an average packing parameter of approximately 1, thus forming liposomes. Moreover, critical packing parameters are known for the vast majority of lipids used in liposomal applications.

1.2.2 Thermodynamics of Liposome Formation

Since lipid molecules used in liposome preparations are amphiphiles and have a large hydrophobic region, these molecules are insoluble in aqueous medium. Depending on the aqueous phase weight percentage with respect to lipid weight percentage and temperature, different structures may form. For lipids with a P~1 and at high lipid weight percentages, a stacked lamellar network will form. For lipids with P>1 or P<1, stacked hexagonal I phase

cylinders or stacked hexagonal II phase cylinders will form, respectively. In order to form liposomes, the lipid weight percentage must be low and sufficient energy must be applied to the system. Due to these constraints, liposomes are best defined as being in a thermodynamically metastable state. Along the same line of thinking, liposomal bilayers may be considered as kinetic energy traps. With this in mind, liposomes will tend to aggregate over time and approach a thermodynamically stable state, *i.e.* a stacked lamellar phase. Therefore, the addition of charged lipids or polymeric lipids must be added to the lipid mixtures to establish long term physical stability of liposomes.

1.2.3 Liposomal Physicochemical Properties

Physicochemical properties of liposomes include hydrodynamic radius (size), polydispersity, lamellarity, mechanical properties, gel-liquid phase-transition temperature, surface properties (*e.g.* zeta-potential and polymers), oxidation and hydrolysis. All of these properties are important for both formulation stability and pharmaceutical application.

The particle size of liposomes ranges from 30 nm to >1000 nm. Liposomes can be formed as uni-lamellar or multi-lamellar vesicles. Moreover, unilamellar liposomes are normally classified as small-unilamellar vesicles (SUVs, < 100 nm in diameter) or large uni-lamellar vesicles (LUVs, ≥100 nm in diameter). The zeta-potential is an important characteristic that may signify liposome stability. The zeta-potential is the electric potential at the shear plane of the particle, where the shear plane is an imaginary layer of ions bound to the surface of the particle. Particles are considered to exhibit full electrostatic stabilization when the zeta-potential is > |30| mV, or >|60|

mV for optimum stability.[16] In addition, polymers such as polyethylene-glycol (PEG) increase the liposomal steric stability and increase *in vivo* circulation times (biological stability)[17-18].

1.2.4 Liposome Formulation Techniques

There are a vast number of techniques to formulate liposomes. Each technique has its advantages and drawbacks. Some of the more common methods include thin-film hydration, reverse-phase evaporation, adaptive-focused acoustic (AFA) technology and ethanol (or organic solvent) injection.

Briefly, the thin-film hydration method includes dissolving the lipid (in powder form) to chloroform and subsequently removing the chloroform/methanol followed by hydration (with an aqueous phase). This method is simple but uses large amounts of United States Pharmacopeia (USP) Class 2 residual solvents[19]. Under this class, the permitted daily exposure (PDE) of chloroform is 60 ppm and the PDE of methanol is 3000 ppm[19]. Reverse-phase evaporation is a demulsifaction method where an immiscible organic solvent (*e.g.* diethyl ether) is depleted. AFA, on the other hand, does not require any organic solvents. AFA uses focused ultrasound to induce cavitation and break apart the lipid powder/formed liposomes in an aqueous medium. The downside to this technique is that it requires a relatively long amount of time to dissolve the lipid/form liposomes and some drug substances may not be stable during sonication. The last method is the ethanol injection method. This method was chosen for the current work since it is naturally a continuous process. Briefly, lipid is dissolved in ethanol and the ethanol is injected into an aqueous medium. During this process, liposomes are formed. This process can be controlled by a variety of factors, but the exact mechanism is remains unclear. In addition,

ethanol is considered a USP class 3 residual solvent and is acceptable under 5000 ppm or 50 mg/day[19], which is more attractive than class 2 residuals solvents.

Once the liposomes are formed, additional steps must be included to produce a final drug product. These steps include the addition of drug molecules, downsizing techniques, concentration and purification. For the ethanol injection technique, drug molecules may be added to the ethanol phase or to the aqueous phase (depending on solubility). Drug substances may even be added after the liposomes are formed, and an additional step such as freeze-thaw cycling would need to be incorporated to encapsulate the drug substance.

1.2.5 Intercalation of Molecules in the Liposomal Membrane

For the ethanol injection method, drug substances can be added to the aqueous and/or organic phase prior to liposome formation or to the aqueous phase after liposome formation. Drug substances that are soluble in an organic phase, *e.g.* ethanol, may interact with the nonpolar, hydrocarbon chain of the lipid. In this way, these molecules will be either fully or partially embedded in the lipid-bilayer. Molecules that are water-soluble may be added to the aqueous phase and these molecules will be entrapped by the liposomes upon formation. One downside to the ethanol injection method for water-soluble drugs is that this method is highly dilutive; meaning the amount of lipid injected into the aqueous phase is very low. For this reason, the amount of drug entrapped during the liposome formation process will be extremely low (*e.g.* ~1%). Therefore, the drug must be lipophilic or additional techniques will need to be implemented to encapsulate the drug. One way to encapsulate larger quantities of water-soluble drugs is to concentrate the liposomes and then undergo freeze-thaw cycling (*see section 1.2.6*).

This approach is suitable for small molecules and proteins. For weak acids and weak bases that are able to permeate the lipid membrane, another approach termed active loading has been widely used (see section 1.2.7).

1.2.6 Passive Encapsulation: Freeze-Thaw Cycling

Freeze-thaw cycling is a processing technique that impacts the liposomes in multiple ways. This technique has been shown to: reduce the lamellarity of multi-lamellar liposomes[20]; form a more monodispersed system from a polydispersed system by disrupting the lipid-bilayer[21]; and increase drug diffusion into the liposomes – resulting in higher drug encapsulation efficiency[22-24]. Briefly, this technique consists of mixing pre-formed liposomes with drug followed by immersion in a << 0°C bath (typically liquid nitrogen). The sample is allowed to completely freeze and is then thawed in a second bath above 0°C (typically 25-50°C). This cycle may be repeated multiple times. During each cycle, drug diffuses into the aqueous core of the liposome and become passively encapsulated. The encapsulated quantity is highly dependent on the lipid concentration and liposomal particle size[25]. Achieving large trapping volumes >40-50% is generally not feasible with this approach. A modified freeze-thaw cycling technique termed freeze-anneal-thaw cycling has been developed to reduce the number of freeze-thaw cycles and increase liposome permeability, thus allowing more drug molecules to enter the liposomes[26]. Moreover, this technique takes advantage of cryo-concentration of drug substances to increase the amount of drug molecules encapsulated. However, this approach also suffers from relatively low trapping volumes.

1.2.7 Active or "Remote" Loading of Molecules

Active loading is a suitable technique to load weak acids or weak bases into the aqueous core and achieve high load efficiencies (>90%)[27-28]. This technique has been used for the FDA-approved Doxil® drug product. There are different strategies to active loading, and each strategy is typically drug dependent. However, the basic idea behind each strategy is to establish an ion gradient or pH gradient[29-31]. Briefly, the liposomes are first formed with a large amount of salt in the liposomal interior (*e.g.* 300 mM ammonium sulfate, pH=6). The external phase salt is exchanged *via* dialysis or other means with an isotonic medium with a pH near the pKa of the drug. The difference in pH of the internal phase and external phase, along with an ion gradient, establishes an electrochemical gradient across the lipid bilayer[32]. The drug is then added to the external phase and is partially unionized since the pH is close to the pKa. The unionized form of the drug permeates the lipid bilayer and ionizes inside the liposomes since the pH << pKa (*i.e.* for a weak base). Since ionized drugs do not permeate through the lipid bilayer the drug then becomes trapped inside the liposomes.

1.2.8 Liposomal Drug Products Overview

Liposomes as drug delivery carriers have been successfully developed and marketed in the pharmaceutical industry. To date, liposomes have been used to treat or mitigate cancer, macular degeneration, fungal infections and vaccines with approved products such as Doxil®, Ambisome®, and Exparel®, respectively[33]. Currently, there are eight FDA-approved drug product lines classified as "injectable, liposomal" according to the drugs@FDA database. In addition, there are over 100 open clinical trials that are investigating new liposomal drugs, drug combinations or new indications for existing liposomal drug products[34].

1.3 Continuous Processing of Liposomal Drug Products

1.3.1 Batch vs. Continuous Manufacturing

A batch-type manufacturing process is one in which bulk material is charged and processed as a unit and that entire unit is processed from stage to stage. Upon completion, the entire product is discharged. For multiple stage processing operations, all material must be finished processing in the first stage before being charged into the next stage. A continuous manufacturing process is one in which raw material is constantly charged while the product is discharged[35]. For processing at multiple stages, material is constantly being charged and discharged through each stage until the material reaches the final stage. In this case, there is a final product at one end with raw material at the other. For a continuous process, the term “batch” or “lot” is still applicable and refers to a drug product that has uniform character and quality produced over a unit time.

There are advantages and disadvantages of both systems and in some cases; continuous manufacturing may not be entirely possible. The conventional approach of batch processing has been successful in the pharmaceutical industry. However, recent advances in technology such as those related to process analytical technology (PAT) have opened the door for improvements in the manufacturing and regulation of pharmaceutical processing. In general, batch manufacturing has disadvantages related to open system transfers, batch-to-batch variations, scale-up issues, and supervised production. As the production of liposomes is a multi-stage process, the transfer of material from each stage may lead to material loss and contamination. Both of which will further result in batch-to-batch variations and possibly a low quality product. In some cases, quality assurance of a batch process may be high by rejecting batches; however, this results in wasting material and increasing processing and production timelines. Lastly, scaling up a batch process

typically leads to further problems. Since smaller batches are made for clinical trials, larger batches may result in formulation differences in the final product. Due to the possibility of formulation differences, additional testing needs to be performed to validate and confirm that the increase in batch size did not alter the formulation – this increases production time and regulatory burden.

On the other hand, a continuous manufacturing process avoids many of the issues associated with batch processing. There are no open system transfers (except possibly for the final product), low variations in the formulation as long as the system is running under set conditions, minimal supervision is required and no scale-up issues. To increase the amount of final product, the only variable that needs to be adjusted for is time. Ideally the same equipment can be used for a small pilot study and for large production batches. To this end, continuous manufacturing may reduce production time, costs and regulatory burden compared to a batch process.

1.3.2 Process Analytical Technology

Process analytical technology is a framework outlined by the U.S. FDA that combines components such as multivariate tools, process analyzer and process control tools as a means to measure and control critical quality attributes of drug products.[36] For continuous measurements, measurements are either taken in-line, at-line or on-line. In-line refers to measurements taken where the sample was not removed from the process stream. At-line measurements refer to samples being removed from the process stream, analyzed and discarded. On-line measurements refer to samples being removed from the process stream, analyzed and may be diverted back to the process. One such process analyzer is for particle size and zeta potential measurements. Two

techniques considered for the current work were: (1) dynamic light scattering (DLS), or (2) acoustic (particle size) and electro-acoustic (zeta-potential) spectroscopy. Both dynamic light scattering and acoustic spectroscopy will be explained in more detail in Chapter 5.

In order for these techniques to be implemented in the continuous process, a flow cell is required that connects the process stream to the process analyzer. In addition, the process analyzer must have a means of communication to a computer and/or data acquisition device. For example, the Malvern Zetasizer® can be used in conjunction with Malvern Link-2 software to communicate with National Instruments (NI) LabVIEW™. A custom computer program can be written in NI LabVIEW™ that controls the entire continuous process[37]. The Malvern Link-2 software uses an OPC server/client architecture and provides a way to extract data such as the particle size and zeta potential and to send measurement information from and to the Malvern Zetasizer, respectively. In the current work, the goal was to add *real time* particle size analysis (necessary) and zeta-potential (if possible) measurements to the system.

Raman spectroscopy may also be utilized as a PAT analyzer. This technique has the ability to be used for both quantitative and qualitative purposes.[38] The fundamentals of Raman spectroscopy are based on the inelastic scattering of electromagnetic radiation by exciting the sample at a specific wavelength. The excitation wavelength will depend on the laser source and may range from the visible light to the near infrared wavelengths. The outputs of this technique are Raman bands or vibrational modes of a molecule. Moreover, the intensity of the Raman bands is proportional to the inverse fourth power of the excitation wavelength. This means that a laser source with a shorter wavelength would provide a more intense signal. However, molecules may

also fluoresce in the visible light range, which would create background noise. To avoid this noise, a higher wavelength may be chosen. There are numerous applications of Raman spectroscopy and it can be used to quantify and understand a process. For example, metoprolol tartrate was quantified in the range from 10-40% (g/100mL).[39] Moreover, a qualitative study on doxorubicin interacting with malignant hepatocytes and the overall impact on the lipid content in the hepatocytes was reported.[40] Lastly, Raman spectroscopy may be used to determine drug crystallinity or amorphous content.[41]

Chapter 2

Specific Aims and Tasks

2.1. Specific Aim 1

Design and Fabrication of a Continuous Process to form Liposomes based on the Ethanol Injection Technique

The ethanol injection method was chosen since this method does not require the use of potentially carcinogenic organic solvents. Moreover, this method is inherently a continuous method since lipid dissolved in ethanol is injected into an aqueous phase and the liposomes form during this process. The control of processing conditions was achieved by creating a custom-built computer program (National Instruments (NI) LabVIEW) to communicate with the entire process/system. A block diagram of the process is outlined in Fig. 2.1. A computer program connected to a data acquisition device controlled the entire process (Fig. 2.2). The first stage was the lipid mixing stage, where multiple sources of lipid dissolved in ethanol were mixed at the specified ratio. The next stage was the liposome formation stage, where an aqueous stream was mixed with the lipid+ethanol stream. This stage also included a second aqueous stream that was used to dilute the ethanol down to approximately 5% vol. ethanol. The last major stage was the concentrating stage, where the liposomes were concentrated in-line to a desired concentration. **It was hypothesized** that by controlling processing conditions in the continuous process based on the ethanol injection method, critical quality attributes of liposomes (*e.g.* particle size, size distribution and zeta-potential) would be precisely controlled.

2.1.1 Task 1

Implement a QbD Approach to Design/Fabricate the Ethanol-Injection System

As an initial step, a QbD approach was implemented to reduce the overall risk associated with different aspects of this work. A risk assessment outlining each processing step to increase chances of success was conducted. This approach aids in developing a full understanding of each stage before fabrication to avoid unnecessary costs and to support time management.

2.1.2 Task 2

QbD Approach to Determine Factors involved with Liposome Formation

As a continuation of the QbD approach, design of experiment studies were completed to understand how liposomes were formed and to ultimately determine a mechanism of liposome formation. The first step was to understand the current system and its limitations. For example, it was necessary to determine the minimum and maximum controllable flow rates for both the ethanol and aqueous phases. Also, the system initially needed to be adaptable such that tubing and other parts could be exchanged to test the impact of different dimensioned parts. Once the limitations of the system were known, a list of factors was generated that were thought to impact the liposome formation. This list of factors was generated from a literature review and known system constraints. Below is a list of factors that may impact liposome formation: (1) lipid concentration; (2) ethanol flow-rate; (3) water flow rate; (4) ethanol-phase temperature; (5) water-phase temperature; (6) tubing diameters (both water and ethanol).

The outcomes or responses of the DOE study for the liposome formation process were critical quality attributes of liposomes such as particle size, polydispersity index (PDI) and zeta-potential. Factors that demonstrated statistical significance for critical quality attributes are considered key factors and were studied in more detail.

2.1.3 Task 3

Introduce Process Analytical Technology to the System

The overall goal of PAT is consistent with the FDA's drug quality system: "…quality cannot be tested into products; it should be built-in or should be by design."[42] When quality is built into a system, the product quality is ensured, the products are processed to achieve certain characteristics based on a mechanistic understanding, *real time* quality assurance is provided, the manufacturing is more likely to accommodate current regulatory policies and procedures, and lastly, the risk-based approach reduces the chances of poor product quality.

A PAT tool is any tool that fits under the following categories: (1) acquire/analyze data (multivariate capable); (2) processing analyzer; (3) process control tool; and (4) management tool that allow for continuous improvement and knowledge of a process. Multivariate tools may be statistical designs of experiments described previously. Combining these DOE studies with some type of computer software (as a process control tool) to control and alter processing conditions would fit under this category. In this case, a predictive equation or results from a DOE study is then used to adjust the final formulation when process variations are encountered. Process analyzing tools can be implemented in three ways: (1) at-line, or where a sample is removed and isolated from a system; (2) on-line, or where a sample is diverted, measured and

returned to the process; or (3) in-line, or where a sample is measured directly in the process. Process analyzers generate large amounts of data that can be collected and stored for quality control purposes and reporting. Lastly, analysis of data to build on the understanding of the overall process will aid in a continuous learning and improvement of the processing stream, which will facilitate regulatory acceptance and provide evidence to support alterations to an existing process.

An example of a possible at-line or on-line measurement is using the Malvern Zetasizer with a flow-cell attachment. A solenoid valve opens and directs the flow of the sample to the Zetasizer flow cell and closes once enough sample is loaded in the cell. The Zetasizer then performs a measurement and this information is sent to the custom-built LabVIEW program. In the LabVIEW program, this value is analyzed and process conditions (*e.g.* flow rates) are altered based on the aforementioned DOE studies to re-adjust the particle size to be within quality control limits.

2.2 Specific Aim 2

Impact of Freeze-Anneal-Thaw Cycling on Liposomal Drug Encapsulation Efficiency and Particle Size

Freeze-Thaw cycling is a technique used for multiple purposes, one of which is to encapsulate drug substances inside liposomes. By understanding the mechanism in which drug substances enter a liposome, it may be possible to incorporate this technique in the continuous processing of liposomes detailed in Specific Aim 1.

Once liposomes are formed, the only way for water soluble drugs to enter liposomes is *via* active or "remote" loading. However, active loading is only suitable for weak acids/bases. Other water-soluble molecules such as proteins, nucleic acids, and small molecules cannot diffuse into the liposomes. The only way to get these molecules into liposomes is to break the liposomes or cause the lipid-bilayer to become permeable enough to allow diffusion of these molecules into the core of the liposome. **It was hypothesized** that a more detailed understanding of a possible mechanism on how drug substances enter liposomes during the freeze-thaw cycling technique will aid in the development of a modified method for entrapping drug substances. It is further hypothesized that due to permeability changes in the lipid-bilayer during freezing, in conjunction with cryo-concentration of liposomes and drugs, increased amounts of drugs will enter the liposomes and become encapsulated. Additionally, it is necessary to maintain physical properties of the liposomes such as particle size and zeta-potential during this process.

2.2.1 Task 1

Design a Formulation that is Stable against Freezing (i.e. minimal changes in physical properties).

To determine the impact that freezing has on the liposomal encapsulation efficiency, it is important to perform these studies with a formulation that will not change liposomal critical quality attributes throughout this process. Moreover, comparing the encapsulation efficiency from a monodispersed population of liposomes to a polydispersed population of liposomes is incorrect. Therefore, a stable liposome formulation was investigated and the addition of cryo-protectants (*e.g.* sugars) to the formulation was assessed.

2.2.3 Task 2

Determine Factors that may Influence Drug Substance Encapsulation Efficiency.

During the freeze-thaw cycling step, the following factors were thought to impact how drug substances enter liposomes: (1) freezing rate; (2) final freeze temperature; (3) thawing rate; (4) final thawing temperature; (5) annealing (or holding) time at subzero temperatures; (6) annealing temperature. The first four factors have been previously reported on in the literature, but only in the release of drug substances or chemical markers, not in the encapsulation. **It was further hypothesized** that water crystallization and ice growth and subsequently cryo-concentration will influence the amount of drug substance that enters the liposomes. In this case, annealing the sample at a specified subzero temperature for a period of time promotes ice growth followed by increased drug encapsulation.

2.3. Figures

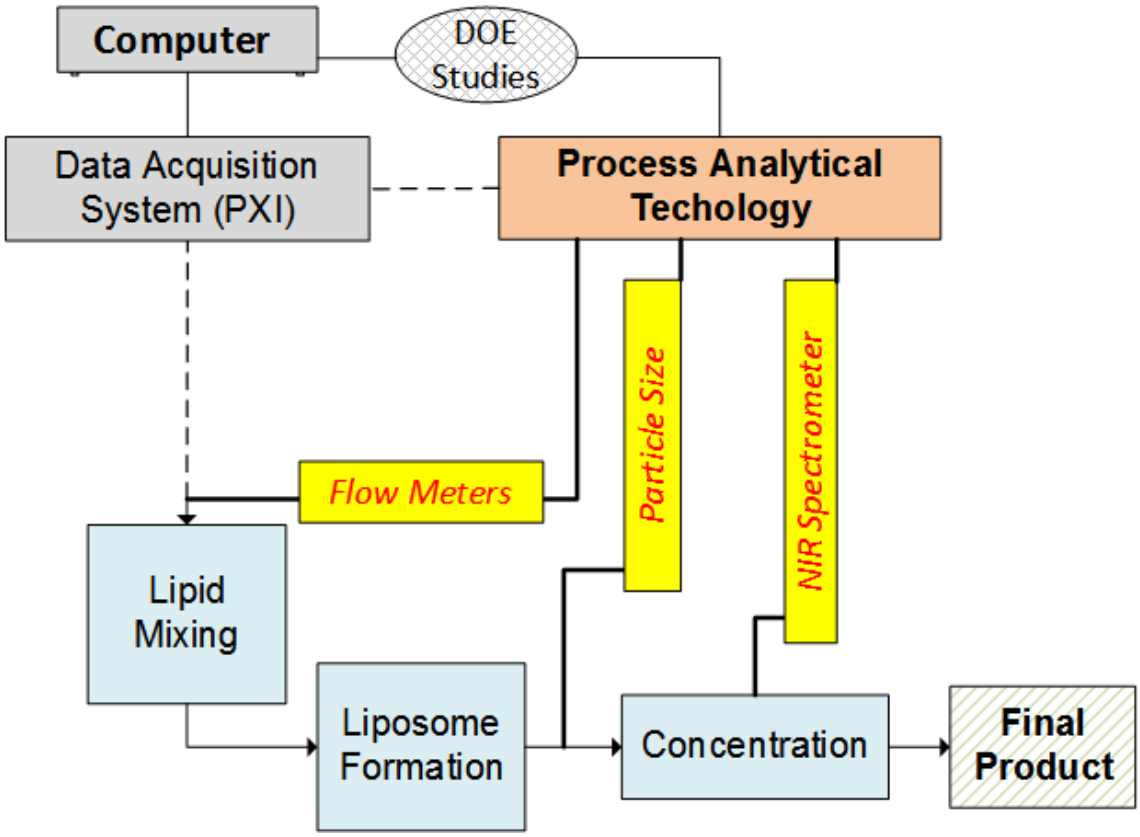

Figure 2.1: Block diagram of the entire system. Arrows indicate the flow direction of the process.

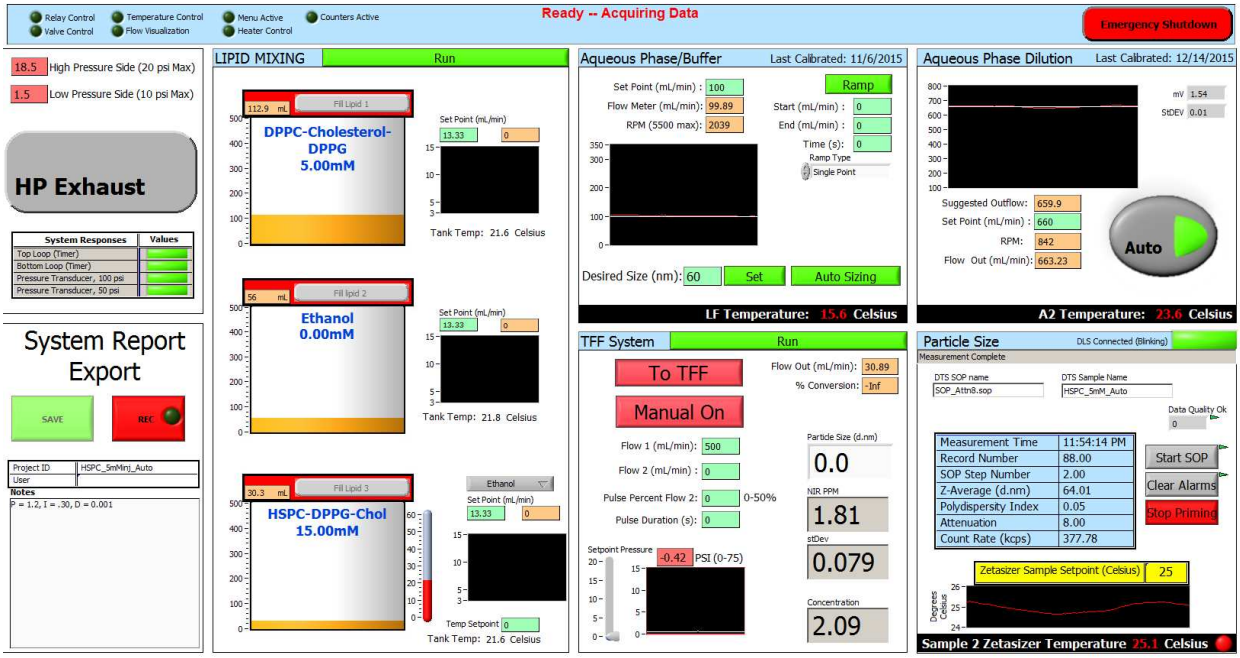

Figure 2.2: Front panel of the custom computer program. The computer program is divided into five parts: lipid mixing, aqueous phase/buffer, aqueous phase dilution, tangential flow filtration (TFF) system and particle size.

Chapter 3

Quality by Design: Risk Assessment of Continuous Processing Stages

3.1 Introduction

The quality by design (QbD) framework is a set of principles that aids in maintaining quality and managing risks associated with product development. Some of these principles applicable to the current work include: (1) identifying/determining critical quality attributes (CQAs), (2) selecting an appropriate process, (3) identifying material and processing parameters that impact the CQAs and (4) form a relationship between material and process parameters.[43] To identify material and process parameters, risk assessment tools such as cause and effect diagrams and a severity/frequency analysis chart were generated. In addition, to form relationships between materials and process parameters, design of experiment studies were used. A more detailed explanation for drug product development is outlined in the Q8(R2) Pharmaceutical Development[43].

In the case of liposomes, CQAs may include particle size, particle size distribution, zeta-potential, drug loading (lipophilic drug), encapsulation efficiency (hydrophilic drug), final drug/lipid weight ratio and drug release rates. In the current work, the focus was primarily on the first three CQAs listed above. Since a part of this work was to develop a continuous process to form liposomes, different liposome preparation techniques were compared and analyzed at the onset of the work to determine whether an existing approach could be modified into a continuous

process. After a literature review and preliminary experiments, material and process parameters were identified that would impact CQAs. Lastly, design of experiment studies were performed for multiple stages of the continuous process that related material properties to process properties.

3.2 Risk Assessments

3.2.1 Liposomal Process Selection

Prior to any work being completed, an initial task was to compare different liposome processing techniques and attempt to de-risk implementing the process as a fully continuous process. As described chapter 1, there are many approaches to process liposomes. Two approaches that were initially considered were the thin-film hydration method[44] and the ethanol injection method[45-46]. At the onset, it was known that the thin film hydration method would end up being a semi-continuous process, as opposed to continuous. One way to form a risk assessment is by using a severity-frequency analysis. This type of analysis identifies risks associated with each process. In this case, the severity is an indication of how likely the risk may negatively impact the ability of each technique to be used in a continuous process. The frequency indicated how often the risk would occur. Even though a risk analysis may be subjective in some cases, it does provide significant insight into what may develop into future problems. From Fig. 3.1, it is clear that for the listed risks, the ethanol injection process has an overall lower risk when compared to the thin-film hydration method. Three key risks are the lipid loss, lipid solubility and whether the system is inherently continuous. When considering the thin-film hydration process, this approach requires dissolving the lipid in an organic solvent followed by solvent removal and then adding an aqueous phase to promote lipid hydration. This process would resemble more of a batch

process and only additional downstream processing may be continuous, resulting in a semi-batch process followed by a continuous process. In addition, this approach would most likely lead to lipid loss since the hydrated lipid may cause the aqueous phase to be highly viscous. As it is more difficult to transfer a high viscosity mixture, the risk associated with sample loss would be higher.

To the contrary, the ethanol injection approach is inherently continuous, *i.e.* the ethanol with dissolved lipid is injected directly into the aqueous phase forming liposomes. In addition, lipid loss would be negligible since the entire amount of dissolved lipid should form liposomes. However, one drawback is that not all of the phospholipids (especially charged lipid) may be soluble in ethanol at high concentrations. This low solubility may introduce limitations on preparing some liposomal formulations using this technique. The overall risk is lower for the ethanol injection approach compared to the thin-film hydration method; therefore, the ethanol injection approach was selected as the process for this work.

3.2.2 Ethanol injection Process Stages: A Risk Analysis

A risk analysis was performed on the processing stages to adequately outline any possible issues that may arise during the fabrication and development of the system. From Fig. 2.1, the main stages include: (1) data acquisition, (2) lipid mixing, (3) liposome formation and (4) liposome concentrating. In addition to these main stages, process analytical technology (PAT) was incorporated into the process and was used to control the entire process. Each PAT was further analyzed in an attempt to de-risk the implementation process. Fig. 3.2 is a risk analysis for the entire process with the single effect of forming a “quality liposome formulation”. For a quality

liposome formulation, the process would need to achieve sufficient control (*e.g.* control of particle size and particle size distribution), be reproducible and accurate, and have the ability to be adaptable to cover formulation changes. For example, if liposomes with a mean diameter of 80 nm are initially sought, but after in-vitro and/or in-vivo studies it is determined liposomes with a mean diameter of 150 nm are more efficacious, then the system should be adaptable for such modifications. Limitations for every system exist and these limitations are clearly outlined throughout this work.

3.2.2.1 System Requirements

At the onset of design process, outlining the system requirements to achieve a continuous process was important. One property was the materials that were selected. Since ethanol and lipid interact with certain polymers and metals, the chemical compatibility of different materials were assessed as a basis for selecting processing components such as solenoid valves and tubing. When it was possible, 316 stainless steel was chosen for its high chemical resistance and ruggedness. In addition, many processing components are made up of multiple materials that are in contact with the liquids and each of these materials (*e.g.* o-rings) needs to be confirmed for chemical compatibility.

Other properties were: (1) type of data acquisition system, (2) types of sensors that would be required to monitor/control the entire process and (3) power requirements to run the entire system. Different types of data acquisition systems exist, *e.g.* real-time, embedded systems and PC-based systems. Since it was determined early on that PAT would be incorporated in this process, a PC-based system was chosen as some PAT devices can only be controlled *via*

software packages designed for PC-based systems and not embedded systems. For this reason, a PCI eXtensions for Instrumentation (PXI) data acquisition system was chosen as this system is PC-based, is accurate, an industry standard and is adaptable for many measurement types.

Measurement type refers to the signal that is either being generated or acquired. Examples of measurement types include analog signals and digital signals. Analog signals may be subdivided further, *e.g.* voltage and current signals. Digital signals may also be subdivided, *e.g.* frequency measurements and counters. As noted above, the PXI data acquisition system is capable of generating and acquiring many signals, but such a system requires specific modules designed for each measurement type to be selected. As an example, one module may be only for generating analog/digital signals (typically 0-5 volts) while another module may be only to acquire analog/digital signals (0-10 volt range). Additional modules may be to directly measure the temperature from thermocouples or to measure the frequency of incoming signals (*e.g.* devices referred to as “counters”).

The third property is the power requirement for the various sensors. Only 12 or 24 volt direct current (VDC) sensors were used so that the number of power supplies was reduced. Sensors and devices are available with many different configurations and to successfully implement all of the sensors into a single system; it is desirable for the sensors to share similar characteristics.

3.2.2.2 Lipid Mixing

The system consists of multiple tanks, each of which may hold either pure ethanol or ethanol with dissolved lipid. For the event that multiple types of lipid are required, individual lipid

molecules or drug molecules may be added to each tank. In order to form a homogenous mixture of lipid or lipid and drug prior to forming liposomes, a lipid mixing process was implemented into the design. The lipid mixing process is when the lipid or drug, dissolved in ethanol, is mixed prior to entering the aqueous phase. The mixing was achieved by the use of solenoid valves, flow meters and precise flow control. In addition, a static mixer was incorporated to create turbulence and further induce mixing.

3.2.2.3 Liposome Formation with Dilution

The liposome formation (Chapter 4) with dilution (Chapter 5) stage can be divided into two parts, *i.e.* liposome formation and ethanol dilution. The liposome formation refers to when the ethanol with dissolved lipid or drug is mixed with the aqueous phase, forming liposomes. The dilution stage is in-line with the formation stage and adds an additional amount of aqueous medium to the liposomes, causing a dilution with respect to the ethanol content and the lipid. For both parts of this stage, controlling the flow rate was important as it was previously determined that flow rates impacted the liposome formation process. In addition, tubing diameters and the liposome formation injection port design were also considered. For example, changing the inner diameter of the tubing will cause changes in the velocity of the liquid traveling through the tubing. The flow velocity ratio of the aqueous phase to the ethanol phase was initially considered as a potential critical factor that would influence the formation of liposomes.

3.2.2.4 Concentrating Liposomes

A concentrating stage was implemented after the liposome formation and dilution stages. This stage was added to provide additional control over the final formulation. When forming

liposomes, the initial lipid concentration is low to prevent non-liposomal structures from forming[47]. In addition, a dilution stage was added at the end of the liposome formation stage (Chapter 5). This dilution stage was incorporated to reduce the overall ethanol percentage down to approximately 5% volume ethanol. By reducing the ethanol stage, the total amount of lipid/drug would also be reduced. In order to reach lipid concentrations suitable for pharmaceutical applications, the liposomes were concentrated. For the concentrating stage, the type of filtration unit and the properties of the filtration unit were assessed. For in-line processing, a tangential flow filtration unit was chosen. In order to incorporate this system for the in-line process, it was necessary to investigate possible filtration rates and the hhgenerated filtration pressures.

3.2.3 Risk Analysis of Process Analytical Technology

In addition to the process stages, PAT was incorporated in the overall design. The purpose of adding PAT was to implement enhanced control and monitoring capabilities. The PAT that was implemented into the system included a particle size analyzer (Chapter 5) and a near-infrared (NIR) sensor (Chapter 6). The particle size analyzer took at-line measurements and provided information such as mean particle size and particle size distribution. The NIR sensor was placed within the concentrating stage process loop and was used to determine the total lipid concentration.

To control the lipid concentration, a control loop (Fig. 3.3) was designed that used both feedback and feedforward control. The feedback control consisted of a pump that adjusts to maintain a set flow rate and was used to increase or maintain the lipid concentration. The particle size analyzer

and NIR sensor were both used as feedforward controls in that these measurements were inputs to a predictive model that is used to determine the lipid concentration.

3.2.3.1 Particle Size Analysis

There are many approaches to determine the particle size distribution of liposomes. Since the liposomes in this work are less than 1000 nm, techniques based on macroscopic fitting methods were only considered. These techniques include dynamic light scattering[48-49], acoustic spectroscopy[50], electron microscopy[51-52], x-ray scattering[53-54], etc. Since the process needs to be implemented into a continuous process, the list of techniques was narrowed down to dynamic light scattering and acoustic spectroscopy. Both techniques are suitable to measure the full range of the liposomes being analyzed (*i.e.* 25 nm up to ~500nm) and both techniques have the ability to measure concentrated samples (refer to chapter 6 for a comparison between each measurement technique). For on-line or at-line measurements, one difference between the two techniques is that dynamic light scattering requires either very low flow rates (~1 mL/min) or static conditions (no flow) for accurate measurements whereas acoustic spectroscopy can provide measurements at higher flow rates. A second difference was related to the companies that manufactured these instruments. For the implementation and use as PAT, the particle sizing data would need to be accessible with the custom computer program written in NI LabVIEW. The company of the acoustic spectroscopy device did not provide a direct means to communicate with NI LabVIEW. However, the company that supplied the dynamic light scattering instrument provided an option with direct communication *via* an open platform communications (OPC) client/server. For this reason, dynamic light scattering was chosen as the instrument of choice.

A risk analysis was outlined for the particle size analysis (Fig. 3.4). The effect/outcome of this diagram was the accurate measurement of particle sizing data for a continuous process. The causes were subdivided into flow conditions, flow cell and DLS measurement. The flow conditions outlined how to control the flow of the sample to the instrument (*e.g.* pump selection) and flow requirements (*e.g.* continuous and laminar flow *vs*. stopped flow). The flow cell has limitations such as the total volume of the flow cell and the pressure rating, which would limit the flow rate of the sample through the flow cell. Lastly, DLS measurement parameters will further impact the accuracy of particle sizing data. These parameters include temperature, measurement duration (*e.g.* 10 seconds), number of runs per measurement and the attenuation setting. As DLS uses a macroscopic fitting algorithm to determine the particle size, the sample temperature and photon count rate will impact the particle size analysis. For example, if the temperature is set at 25°C, but the sample temperature is actually 22°C, then the measured particle size may be higher than actual since particles move more slowly at lower temperatures than higher temperatures. In this case, the set temperature and the actual sample temperature must be similar to achieve accurate results. As a second example, the photon count rate is the rate at which photons are detected. For low count rates, there is not enough information for the macroscopic fitting algorithm to determine the particle size. In addition, at higher count rates, the DLS detector may no longer be operating in a linear range. Therefore, a range of count rates should be determined that provide accurate data.

3.2.3.2 NIR Turbidity Sensor

A NIR sensor was implemented into the process as a means to determine the concentration of the liposome sample. A NIR sensor has the ability to detect turbidity changes and these changes can

be related to the lipid concentration *via* an algorithm. Rayleigh scattering is proportional to the sixth power of the particle diameter; therefore, larger particles scatter more light. It was then hypothesized that for a known particle size, the concentration of the liposomes could be determined (Chapter 6). A risk analysis diagram outlines possible factors that will influence concentration detection via a NIR sensor (Fig. 3.5). For instance, there are a two common NIR sensor styles, *i.e.* a probe design or a flow cell design. The probe design may be more prone to air bubble accumulations at the detection window. In addition, the probe design may have a limited optical path length (*e.g.* up to only 10 mm), whereas the flow cell design may have longer optical paths (*e.g.* up to 160 mm). The longer optical path would accommodate samples that scatter a small amount of light (*i.e.* smaller diameter particles at low concentrations). In addition, NIR probes may be designed at a single wavelength or a band of wavelengths and at various angles of detection. For angles of detection that are 0° from the light source, the measurement is referred to as absorbance and measured in units such as CU. Scattered light may be detected at angles such as 11° or 90°. For the scattered light, the unscattered light is used as a reference to account for changes in the aqueous medium.

3.2.4 Material and Process Parameters on Particle Size Formation

There are many material properties in conjunction with process parameters that are thought to influence the formation of liposomes. These material and process parameters are outlined in the cause and effect diagram from Fig. 3.6. The causes are divided into process variables, material variables and lipid molar ratio. The process variables includes types of flow (e.g. laminar vs. turbulent), type of pump (e.g. pulsatile vs. non-pulsatile) and Reynolds number. The Reynolds number is a means to determine the extent of mixing – with a higher Reynolds number indicating

a greater extent of mixing. The Reynolds number is dependent on viscosity, temperature and flow velocities. The material variables are subdivided into type of lipid and aqueous phase. The type of lipid will significantly impact the liposome particle size. For example, each lipid has a transition temperature, which indicates the fluidity of the lipid at a certain temperature. Lipids that may be in the fluid state could possibly form larger liposomes; however, this is not clearly understood at this time. The lipid molar ratio is another cause that my affect the liposome particle size. As many liposomal formulations consist of multiple lipids, the combination of the lipids must result in a packing parameter that supports the lamellar structure; otherwise, liposomes will not form. Therefore, the lipid ratio of, for example, cholesterol and other lipids must equate to approximately 1 in order to support a lamellar phase – which is the phase that will form liposomes.

3.3 Conclusion

The quality by design approach was implemented at the onset of this work and a risk analysis was the initial tool used in this approach. A risk analysis is an important tool for determining critical material and processing parameters than can affect a specific outcome. A risk analysis was outlined for each processing stage, the implementation of PAT and for the formation of liposomes.

3.4 Figures

Key	
Severity	Frequency
1-3	1-3

Risk Assessment for Technique Conversion to a Continuous Process						
Risks	Ethanol Injection			Thin-Film Hydration		
	Severity	Frequency	Total Risk	Severity	Frequency	Total Risk
Organic Solvent Removal	3	2	6	3	3	9
Organic Solvent (Environmental Impact)	2	3	6	3	3	9
Lipid Loss	3	1	3	3	3	9
Lipid Solubility	2	2	4	2	1	2
Inherent Continuous Process	3	1	3	3	2	6
	OVERALL RISK:		4	OVERALL RISK:		7

Fig. 3.1 A risk assessment comparing two processing techniques to make liposomes with the intention to develop the current process into a continuous process.

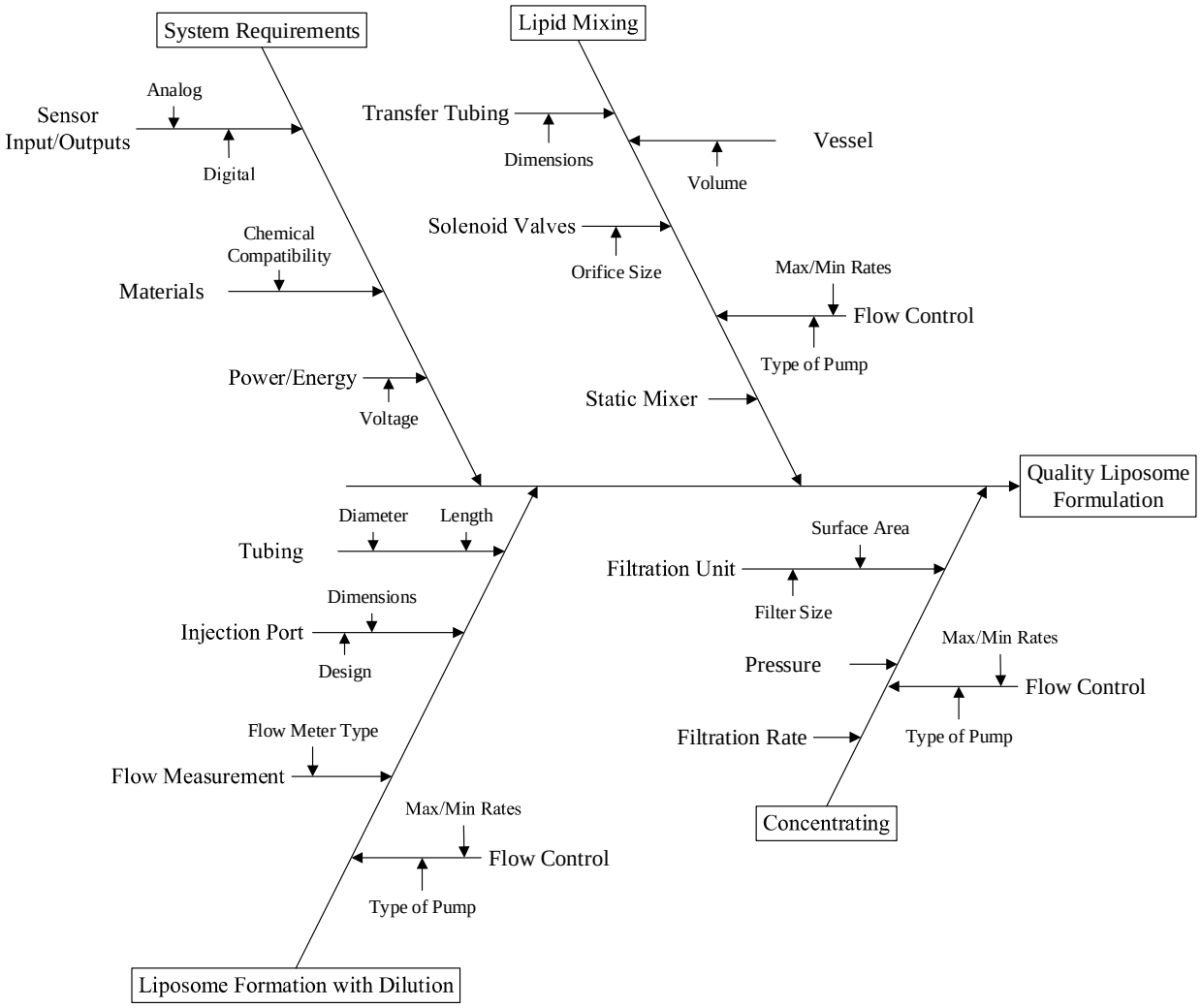

Fig 3.2: A cause and effect diagram highlighting the main stages of the continuous process with subdivisions for each main stage.

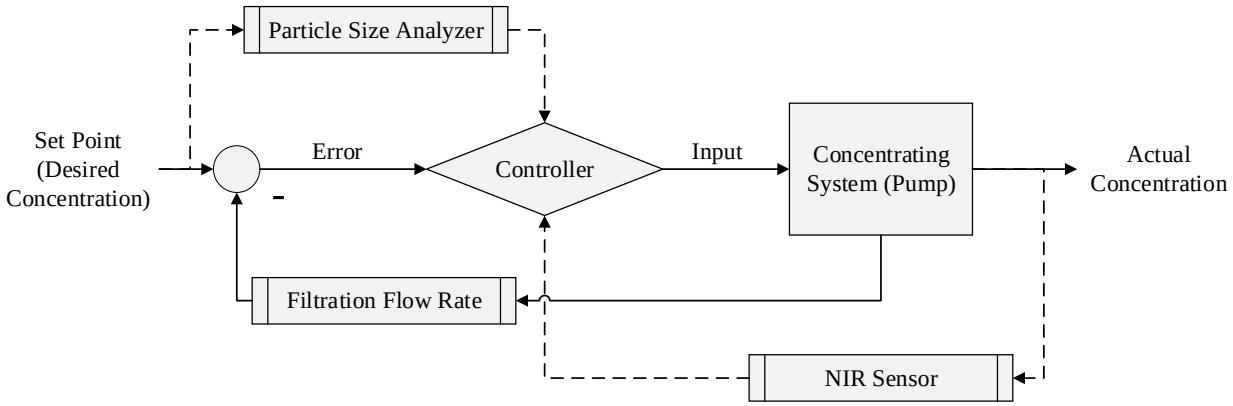

Fig 3.3: The control design for the concentrating system. This design uses feedback control (pump flow rate) and feedforward control (particle size analyzer and an NIR sensor) to determine the lipid concentration. The particle size data and data from the NIR sensor are incorporated into a mathematical model used to predict the lipid concentration.

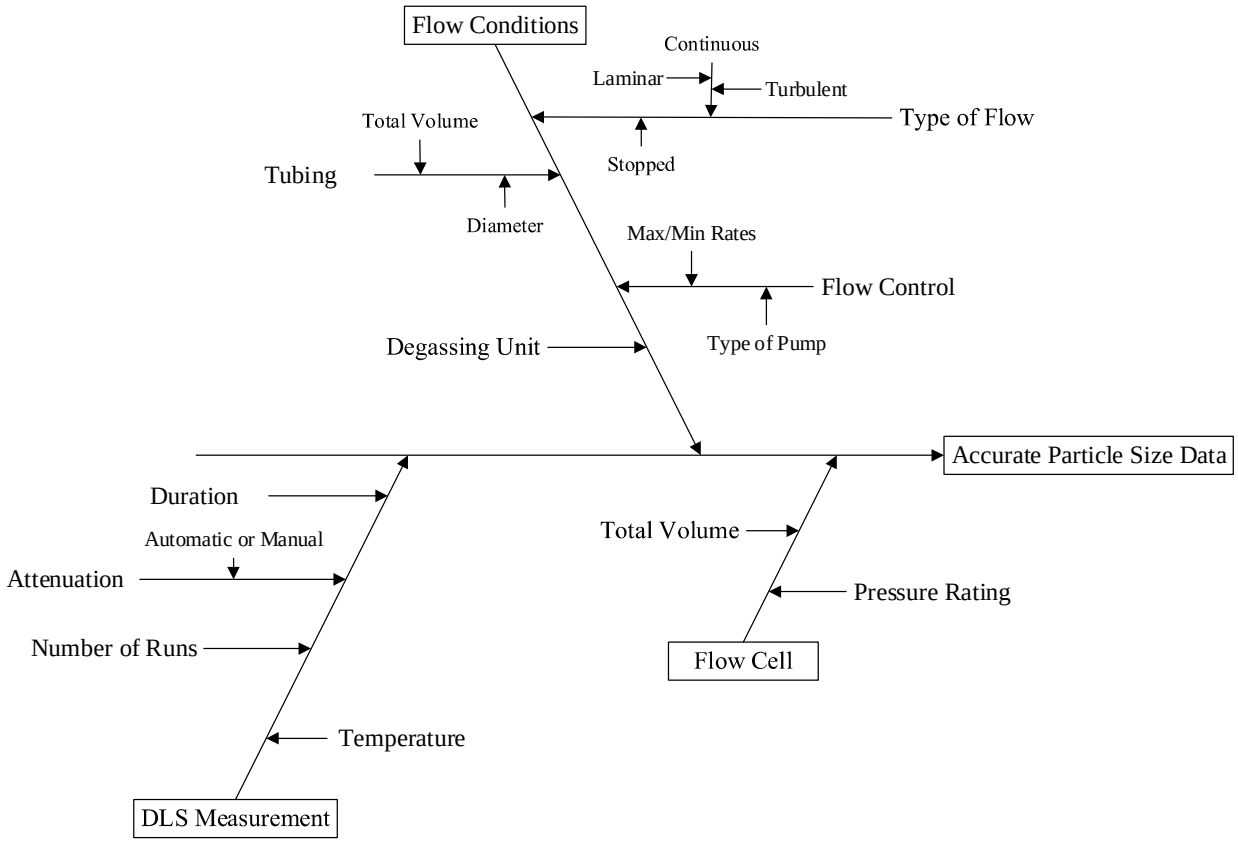

Fig 3.4: A cause and effect diagram outlining variables that result in obtaining accurate particle size data for a continuous process.

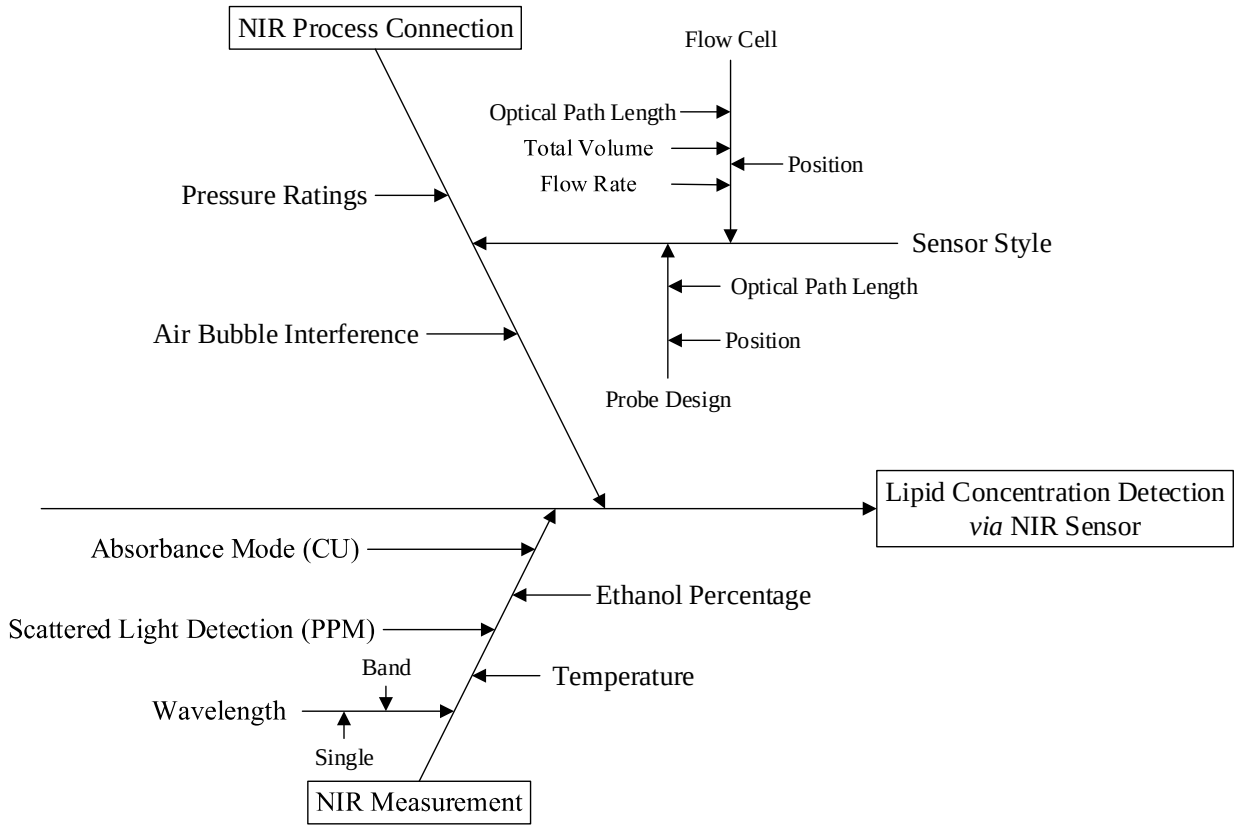

Fig 3.5: A cause and effect diagram outlining variables that affect the lipid concentration detection via a NIR sensor.

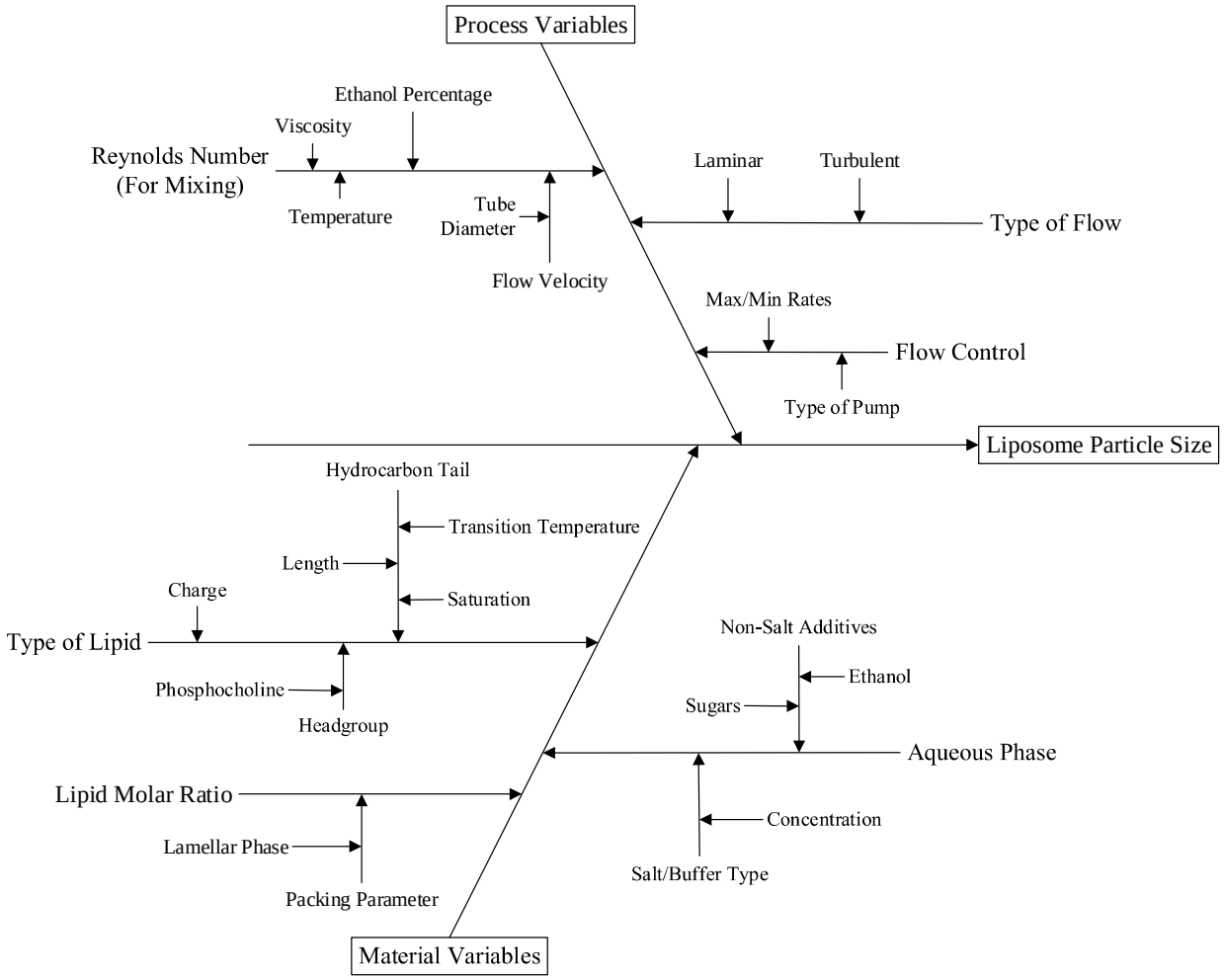

Fig 3.6: A cause and effect diagram outlining variables that affect the liposome formation process with respect to material and process variables.

Chapter 4

Liposome Formation using a Coaxial Turbulent Jet in Co-Flow

4.1 Abstract

Liposomes are robust drug delivery systems that have been developed into FDA-approved drug products for several pharmaceutical indications. Direct control in producing liposomes of a particular particle size and particle size distribution is extremely important since liposome size may impact cellular uptake and biodistribution. A device consisting of an injection-port was fabricated to form a coaxial turbulent jet in co-flow that produces liposomes *via* the ethanol injection method. By altering the injection-port dimensions and flow rates, a fluid flow profile (*i.e.* flow velocity ratio vs. Reynolds number) was plotted and associated with the polydispersity index of liposomes. Certain flow conditions produced unilamellar, monodispersed liposomes and the mean particle size was controllable from 25 nm up to >465 nm. The mean liposome size is highly dependent on the Reynolds number of the mixed ethanol/aqueous phase and independent of the flow velocity ratio. The significance of this work is that the Reynolds number is predictive of the liposome particle size, independent of the injection-port dimensions. In addition, a new model describing liposome formation is outlined. The significance of the model is that it relates fluid dynamic properties and lipid-molecule physical properties to the final liposome size.

4.2 Abbreviations

Reynolds Number – Re

Flow Velocity Ratio – FVR

Dynamic Light Scattering - DLS

Polydispersity Index - PDI

Design of Experiment - DOE

31 Phosphorous Nuclear Magnetic Resonance - ^{31}P-NMR

1,2-dimyristoyl-*sn*-glycero-3-phosphocholine - DMPC

1,2-dipalmitoyl-*sn*-glycero-3-phosphocholine - DPPC

1,2-distearoyl-sn-glycero-3-phosphocholine - DSPC

1,2-dipalmitoyl-*sn*-glycero-3-phospho-(1'-*rac*-glycerol) (sodium salt) - DPPG

1,2-dioleoyl-*sn*-glycero-3-phosphocholine – DOPC

Cholesterol – Chol

Negative Stain Transmission Electron Microscopy – NS-TEM

Cryogenic Transmission Electron Microscopy – Cryo-TEM

National Instruments – NI

International Conference on Harmonisation – ICH

Process Analytical Technology - PAT

Combined Output Flow Rate – Q

Kinematic Viscosity – v

Diameter – D

Outer Diameter – OD

Inner Diameter - ID

Cross-Sectional Area – A

4.3 Introduction

The ethanol injection method is a well-known liposome preparation method.[46] This method consists of dissolving lipid in ethanol (or a water-miscible organic solvent) and subsequently injecting this solution into an aqueous phase. Under certain conditions (*e.g.* at a low lipid concentration and processing lipids in the fluid state), the result is a dispersion of liposomes. The ethanol injection method offers the following advantages over other liposome preparation techniques: (1) the possibility to use ICH class 3 residual solvents rather than more toxic ICH class 2 solvents normally used in the thin-film hydration method (*i.e.* chloroform)[55]; (2) precise control over particle size and particle size distribution; (3) the avoidance of additional downsizing techniques such as sonication and/or extrusion; and (4) this process is a naturally continuous process. The latter is of high importance since it is of current interest to implement continuous processing in the pharmaceutical industry[36, 56] . Continuous processing introduces many benefits over batch processing. For instance, the process run-time determines the final amount of product manufactured, not the size of the reactor. Therefore, the numerous issues related to process scalability may be lessened or avoided when progressing through clinical trials to large-scale manufacturing. In addition, continuous processing may be automated, which reduces human involvement and error. An important feature of continuous processing is the ready implementation of process analytical technology (PAT) that further enhances the overall control of the system[36]. The implementation of PAT reduces energy usage, product waste and ultimately leads to a higher quality product.

There have been a number of recent reports on using the ethanol (or alcohol) injection process for the preparation of unilamellar liposomes[57-60]. There are two fundamentally different fluid mixing schemes to form monodispersed liposomes using this technique. The first scheme is based on molecular diffusion where the alcohol is hydrodynamically focused into the aqueous phase.[61] In this case, microfluidics devices are required to prepare liposomes under laminar conditions with a low Reynolds number (Re, where Re <<100)[62]. Such liposome formation appears to take place on the edges of the alcohol/aqueous flow streams as water slowly mixes with the alcohol phase[63]. The second scheme is based on inertial convective mixing or rapid mixing of the alcohol stream with the aqueous streams. This scheme has been demonstrated by creating a turbulent liquid jet either in co-flow (with the aqueous phase)[59] or in cross-flow (angled to the aqueous phase)[57]. Moreover, flow conditions based on this approach typically operate at a higher Re from 100 to >3000.

In the current work, liposomes were prepared using a coaxial turbulent jet in co-flow. The liposome formation process was investigated by relating fluid dynamic properties and lipid properties to liposomal physical properties. More specifically, it was hypothesized that under certain processing conditions, altered fluid flow profiles (*e.g.* changing volumetric flow rates to increase/decrease the Reynolds Number) combined with formulation properties (*e.g.* lipid type, hydrocarbon tail saturation, and aqueous phase additives) would result in the prediction of liposomal physical properties (*e.g*. mean particle size). In addition, a new model based on lipid hydrocarbon tail length, hydrocarbon saturation and aqueous phase additives was outlined that explains the liposome formation process using a turbulent jet in co-flow.

4.4 Materials and Methods

4.4.1. Overview of Process with Turbulent Mixer

Liposomes were prepared by a modified ethanol injection method. A schematic of this system is demonstrated in Fig. 1. Three separate 316 stainless steel tanks were fabricated to house the lipid+ethanol solution. These tanks were pressurized (at typically 20 psi) and the flow rates from these tanks were controlled by analog flow meters (McMillian) and proportioning solenoid valves (Aalborg). The flow meters were factory calibrated for water with less than 1% error. For the lipid+ethanol flow streams, these flow sensors were re-calibrated for ethanol and had an R-squared value of 0.9989, with a working range from 5-50 mL/min. The three tanks were then connected at a single point using a 4-way connector (Swagelok). A static mixer was implemented to ensure that the lipid+ethanol solutions from the three tanks were adequately mixed prior to reaching the injection port where the ethanol and aqueous streams converged. The aqueous phase volumetric flow rate was controlled by a gear pump (Micropump®). The mixed lipid+ethanol solution was then injected into the aqueous phase at various flow rates. The tubing ID of the ethanol phase was 0.508 or 1.016 mm (1.588 mm OD). The aqueous phase tubing ID was fixed at 3.175 or 4.572 mm. Typical flow rates of the lipid+ethanol phase were from 5-40 mL/min and of the aqueous phase were from 60-400 mL/min.

The entire process was controlled by a custom-made program written using National Instruments (NI) LabVIEW® software. A data acquisition system (NI PXIe-1078) was combined with multiple NI modules to accommodate various input/output signals (*e.g.* analog and digital inputs/outputs, counters, circuit switches, *etc.*). The entire system was automated and only required the user to define the final lipid concentration and molar ratios of lipid. Process

variables such as flow rates, pressure, and temperature were monitored and, for some variables, automatically adjusted using custom computer algorithms. For example, proportional-integral-derivative controls were implemented in the computer program to precisely control the flow rates of both the ethanol and aqueous phases.

4.4.2. Liposome Preparation

1,2-dimyristoyl-*sn*-glycero-3-phosphocholine (DMPC), 1,2-dipalmitoyl-*sn*-glycero-3-phosphocholine (DPPC), 1,2-distearoyl-sn-glycero-3-phosphocholine (DSPC), 1,2-dipalmitoyl-*sn*-glycero-3-phospho-(1'-*rac*-glycerol) (sodium salt) (DPPG) and 1,2-dioleoyl-*sn*-glycero-3-phosphocholine (DOPC), were purchased from Lipoid™. Cholesterol (Chol) was purchased from Sigma. The lipid (5-30 mM total lipid) was dissolved in ethanol (USP grade) and added to one of the three tanks. To dissolve the lipid in ethanol, the lipid mixture was typically heated to 60°C for 10 minutes and sonicated for 5 minutes or until all of the lipid was fully dissolved. The ethanol solution was then allowed to reach room temperature (23°C) prior to running any experiment. In some cases, the entire lipid was combined into a single tank and pure ethanol was added to the other tanks for dilution.

4.4.3 Dynamic Light Scattering for Particle Size and Zeta-Potential

Measurements were performed with a Malvern Zetasizer Nano ZS90 for zeta potential and a Malvern Zetasizer Nano S for size. The samples were placed in plastic disposable cuvettes (or a capillary cell for zeta-potential) and equilibrated to 25°C prior to measurements. Since ethanol was present in the samples, all samples were diluted to 1.64% v/v (ethanol/total solution) and the viscosity and refractive index were adjusted for in the Malvern Zetasizer software. Particle size

measurements included the z-average, PDI, volume percentage, intensity mean and intensity width. Zeta potential measurements included zeta-potential and zeta deviation. All measurements were run in triplicate.

4.4.4 Flow Visualizations

Nile Red (Sigma-Aldrich®) was used as the dye and was dissolved in ethanol. This solution was added to one of the three pressure tanks. Lipid dissolved in ethanol was added to a second tank. The lipid and Nile Red solutions were run at a 1:1 volumetric ratio under different flow conditions. As Nile Red changes color based on solution polarity[64], the solution appeared pink in ethanol, pink/orange with lipid dissolved in ethanol and purple/bluish when dissolved or mixed with water without lipid.

4.4.5 Nanoparticle Tracking Analysis

Measurements were performed with a Malvern Nanosight™ instrument. The samples were diluted down to 0.05% v/v ethanol. In some cases, additional dilution was necessary to reach acceptable conditions for particle size analysis (*e.g.* as vesicle diameter decreases, the number of vesicles increased exponentially). As for the measurements, the mean and standard deviation were recorded. All measurements were run in triplicate.

4.4.6 Negative Stain Transmission Electron Microscopy (NS-TEM)

Liposomes were prepared in 10 mM ammonium acetate-acetic acid buffer at pH 5.00. For each sample, approximately 3 µl of liposomes was placed on a plasma cleaned carbon coated grid

(Ted Pella Inc, #01840). After 1 minute incubation, the sample was flooded with several drops of 0.25% of uranyl acetate stain. The excess solution was blotted off and the sample was air dried for approximately 30 minutes. The grid was imaged at 80.0 kV in an FEI Tecnai 12 Biotwin TEM equipped with a LaB6 emitter and an Advanced Microscopy Techniques 2k XR40 CCD camera. For each sample, 7-10 images were collected and the diameter of more than 500 particles/sample were manually measured using ImageJ. The data was then collected and the mean particle size and standard deviations were determined by fitting a nonlinear analysis using a Gaussian distribution fitting function.

4.4.7 Cryo-Transmission Electron Microscopy (cryo-TEM)

Cryo-TEM was performed using cryo-transmission electron microscopy (Jeol 1400 TEM/STEM) operated at 120 kV and viewed under the Minimum Dose System. Briefly, 2 µL of liposome sample was placed on a glow-discharged Holey carbon copper grid (Quantifoil R 2/1). Using a grid plunge freezer (Leica EM GP) at 25 °C and 82% humidity, samples were blotted automatically for 2 s to remove excess liquid and plunged into a bath of liquid ethane at −175 °C. The samples were stored in liquid nitrogen until they were transferred to a cryo-TEM holder (Gatan 914) and observed in the pre-cooled cryo-TEM at 120 kV under Minimum Dose System. Images were recorded with a digital CCD Camera (Gatan ORIUS™ SC1000) at magnification of 10000 x- 20,000x.

4.4.8 Design of Experiment Study

A design of experiment was performed to analyze the lipid concentration and aqueous phase flow rates on liposome particle size. The aqueous phase flow rate range was designed to cover a

broad range of flow conditions that led to low and high Reynolds Numbers (see "Reynolds Number and Flow Velocity Ratio Calculations"). In addition, these flow rates cover the full range of the system processing capabilities (i.e. pump flow rate working range). Lipid Concentrations studied were based on reported lipid wt% that would possibly lead to the formation of liposomes[65]. A custom 2x4 full factorial design with 5 center-points, and 3 repeats was chosen as the initial design (Fig. 2). This design was chosen to support interaction and higher order terms as well as stay within constraints on the final ethanol percentage. The original design was augmented to increase the design space and to increase the statistical significance of the model (Fig. 2). With respect to model analysis, the r-squared term, analysis of variance ($p<0.05$) and lack of fit p-value ($p>>0.05$) were used to determine adequate fitting and the inclusion of model interaction terms. Only the Malvern Zetasizer Nano S was used to determine the particle size and PDI for this study. The model design and analysis was conducted using JMP by SAS.

4.4.9 Reynolds Number and Flow Velocity Ratio Calculations

The Reynolds number (Re) is defined as $Re = QD/\nu A$, where Q is the combined output flow rate, ν is the kinematic viscosity of the mixture, D is the diameter of the output tube and A is the cross-sectional area of the output tube. The kinematic viscosity was calculated for the final ethanol-water mixture based on reported dynamic viscosity and density values[66]. An equation was created using JMP by SAS to predict the kinematic viscosity with dependence on ethanol mole fraction and the output temperature (Supplemental Data Equation 1). As the enthalpy of mixing for water and ethanol mixtures is exothermic, the final output temperature varied from the initial temperatures of both phases (*i.e.* 23°C) up to ~32°C. These temperatures were

recorded for the various flow conditions and were used in the Re calculation. The flow velocity ratio (FVR) is FVR = v_i/v_o, where v_i is the inner tube velocity and v_o is the outer tube velocity. Both velocities are calculated directly from the volumetric flow rates and the geometry of the tube. For the outer tube velocity calculation, the inner tube outer diameter was subtracted from the outer tube inner diameter.

4.5. Results

4.5.1 Mixing of Ethanol and Aqueous Phase

An injection port was fabricated to accommodate the formation of a coaxial turbulent jet in co-flow. A cylindrical tube (inner tube) designed to carry the ethanol phase was positioned concentrically within second or outer cylindrical tube (Fig. 3). The second cylindrical tube (outer tube) carries the aqueous phase prior to jet formation. There are three criteria necessary to achieve suitable conditions for a stable turbulent jet. The first is that all flow rates must be pulseless to reduce flow rate fluctuations to negligible levels. The second two criteria come from non-dimensional values of fluid dynamics: (1) Reynolds number (Re) and (2) flow velocity ratio (FVR). The Re is that of the mixed ethanol/aqueous flow stream just downstream of the "jet location" (in Fig. 3) and will subsequently be referred to as the $Re_{mixture}$.

4.5.2 Relationship between Fluid Flow Properties and Liposomal Polydispersity Index

The fluid flow properties of the injection-port were related to the liposome polydispersity index. Liposomes were analyzed using dynamic light scattering (DLS) and a polydispersity index (PDI) of 0.10 was considered as the upper limit for monodispersity. The ethanol flow rate ranged from 5-40 mL/min and the aqueous phase flow rate ranged from 70-400 mL/min. The organic phase

consisted of DPPC:DPPG:Chol (4.5:0.4:3 molar ratio) dissolved in ethanol and the aqueous phase was 10 mM phosphate buffer, pH 7.4. The inner tube diameter was 0.508 mm or 1.016 mm. The outer tube diameter was 3.175 mm or 4.572 mm. In addition, the maximum final ethanol percentage was chosen to be less than 40% v/v ethanol to reduce the possibility of forming any non-liposomal structures[65]. For this lipid formulation, the average zeta-potential was -39.4 ± 6.34 mV (averaged for all samples).

The flow rates were transformed to $Re_{mixture}$ and FVR as outlined in the methods section. To achieve various $Re_{mixture}$ and FVR combinations, different inner and outer tube diameters were investigated. From Fig. 4a, it is clear that in order to achieve a monodispersed system, certain $Re_{mixture}$ and FVR combinations are required to form a stable jet. Fig. 4b depicts the fluid profiles of four locations on the FVR *vs*. $Re_{mixture}$ plot from Fig. 4a. At a $Re_{mixture} < 500$ and FVR < 7, a stratified flow is observed with the lipid+ethanol staying separated and moving to the top of the tubing (Fig. 4b-1). Limited mixing occurs in this case and the actual lipid mixing/liposome formation would occur downstream (*i.e.* possibly in the collection vessel) – leading to polydispersed liposomes. At FVR ≤ 2 and $Re_{mixture} >\sim 500$, a weak jet forms and this also leads to polydispersed liposomes (Fig. 4b-2). The other two flow conditions depicted lead to rapid mixing downstream of the injection site and stable jet formation, resulting in monodispersed liposomes (Fig. 4b-3 and Fig. 4b-4). In the case monodispersed liposomes, it is evident that liposome formation is primarily dependent on mixing and can be predicted by the $Re_{mixture}$ (Fig. 4c). At a high FVR (*i.e.* ≥ 7), the liposome particle size is monodispersed and independent of FVR and only changes according to the $Re_{mixture}$. The latter case outlines that monodispersed

liposomes may be formed under a variety of injection port dimensions that lead to the same FVR and $Re_{mixture}$ conditions.

4.5.3 Design of Experiment: Lipid Concentration vs. Particle Size

A design of experiment (DOE) study was completed to demonstrate the effects of the injected lipid concentration on liposomal particle size for a monodispersed population of liposomes. The ethanol flow rate was fixed at 40 mL/min as this flow rate corresponding to a flow region that produces monodispersed particles (Fig. 4a). The dimensions of the injection port were fixed at an aqueous phase tubing ID of 3.175 mm and an ethanol phase tubing ID of 0.508 mm. For the DOE study, the factors included: (1) aqueous phase flow rate (70-400 mL/min) and (2) injected lipid concentration (5-30 mM). The aqueous phase was 10 mM phosphate buffer. The lipid composition was fixed at DPPC:DPPG:Chol (4.5:0.4:3 molar ratio). The DOE model has a R^2-value of the actual vs. predicted values of 0.985, an analysis of variance p-value <0.0001 and a lack-of-fit p-value = 0.331 (Table I). The surface profile for this study clearly demonstrates the dependence of the mean particle size on the aqueous phase flow rate (Fig. 5). For this formulation, the smallest liposomes appeared around 58 nm and the largest around 240 nm. The PDI value averaged 0.05 ± 0.04 for all experiments, and only started to reach 0.10 at the lower aqueous phase flow rates (*e.g.* 70 mL/min). Thus, the liposomes could be considered monodispersed over the entire range of flow rates studied. The lipid concentration had a modest positive impact on the particle size. It was apparent that the aqueous phase flow rate interaction terms were dominant in controlling the z-average liposome particle size.

4.5.4 Types of Lipid on Liposome Particle Size

From the results above, it is clear that the $Re_{mixture}$ and lipid concentration play an important role in controlling liposome particle size. To determine whether lipid characteristics affect liposome particle size, four different *lipid* molecules were investigated, namely DOPC, DMPC, DPPC, DSPC and a mixture of DPPC:DSPC (1:1 molar ratio). Each formulation also contained cholesterol and DPPG. The molar ratio was held constant for *lipid*:DPPG:Chol (4.5:0.4:3.0) and 5 mM total lipid was dissolved in the ethanol phase. The z-average particle size and PDI values are plotted (Fig. 4.6). It is clear that the lipid molecule significantly altered the liposome particle size. Liposomes with a mean particle size were controllably formed from approximately 25 nm up to 465 nm and the maximum PDI value was equal to 0.18; however, the PDI was ≤ 0.05 for the majority of the samples (Fig. 4.6).

4.5.5 Aqueous Phase Additives on Liposome Particle Size

Additives to the aqueous phase were used to determine any impact on liposome formation. For this study, the lipid formulation was kept constant at DPPC:DPPG:Chol (4.5:0.4:3 molar ratio, 5 mM lipid injected) and all samples contained 10 mM phosphate buffer, pH 7.4. NaCl; glycerol; and ethanol were investigated as additives (Fig. 7). Liposomes prepared in 10 mM phosphate buffer with no additive was used as a control. For all flow conditions, the formulation containing 26 wt% glycerol was the most similar to the control. The addition of 10-30% v/v ethanol to the aqueous phase increased the particle size under most flow conditions. The 30% v/v ethanol addition caused the liposomes to be linearly dependent on the aqueous phase flow rate. The addition of 0.9 wt% NaCl dramatically increased the mean particle size under all conditions compared to the control.

4.5.6 Comparison of Particle Size and Size Distribution using Multiple Measurement Techniques

To accurately assess the mean particle size and particle size distribution, multiple techniques (*i.e.* dynamic light scattering, nanoparticle tracking and negative stain TEM) were used. Each of the three techniques can be used to determine the mean particle size and particle size distribution; however, each technique differs fundamentally. Dynamic light scattering is an intensity-based measurement, while nanoparticle tracking and negative stain TEM are number-based. Therefore, it is not desired to compare absolute values from each technique, but instead to compare trends and conclude if monomodal populations of particles are present. Samples were prepared in 10 mM ammonium-acetate-acetic acid buffer at pH=5.0 to reduce artifacts in the negative staining procedure. The lipid composition for this study was DMPC:Chol:DPPG (4.5:3.0:0.4 molar ratio) and 15 mM lipid was injected into the aqueous phase. Three samples were prepared at a constant ethanol flow rate (40 mL/min) but at different aqueous phase flow rates (*i.e.* 100, 150 and 375 mL/min). The three samples were chosen as they were estimated to produce liposomes with a mean particle size around 350, 140 and 70 nm, respectively (Fig. 6). Fig. 8 displays the mean particle size data from the three separate techniques. It is clear that nanoparticle tracking and dynamic light scattering display a monodispersed population. Negative staining produces an overall wider distribution of particles and possibly smaller particles present in the larger-sized liposome sample. However, the negative stain TEM results may not adequately represent the liposome population due to a low number count and multiple artifacts that can occur during sample preparation. Fig. 9 is a plot of the mean particle size and the standard deviation for each sample and technique. Most importantly, it was demonstrated that the mean particle size trend is the same using all three particle sizing techniques, *i.e.* for an increase in aqueous flow rates

(higher $Re_{mixture}$), the particle size decreases. For all three samples and each particle size analysis technique, the standard deviations were 15.8 ± 4.70% of the mean.

4.5.7 Negative Stain TEM Micrographs of Liposomes

Fig. 10 (a-c) are micrographs of the three different samples outlined above (Fig. 8) from the particle size technique analysis. The micrographs clearly demonstrate particle size differences between samples. Each sample set appears to be monodispersed. Fig. 10d demonstrates how liposomes are affected by the staining process. It appears that the liposomes are in one of three possible states: (1) "partially-hydrated" liposomes (these liposomes appear to be dehydrated, but partially retain the structure as in the hydrated state); (2) flattened-stacked bilayers; or (3) mixture of a flattened-stacked bilayer and/or single bilayer. The "partially- hydrated" liposomes have an appearance of dehydrated liposomes and have more uniform size, while the "flattened" states vary in size. This apparent size variation (that results from the processing required for this technique) can explain why the mean particle size and size distribution are overall greater from the NS-TEM micrographs compared to the other particle size analysis techniques.

4.5.8 Cryo-TEM Micrographs of Liposomes

The micrographs from Fig. 11 (a-c) are of the three different samples outlined above in Fig. 8 and Fig. 10. These micrographs confirm the particle size trend stated previously and that these liposomes are unilamellar. Comparing the visible black band of each liposome, the thickness of the band is very similar for the small to the large liposomes.

4.6 Discussion

4.6.1 Liposome Monodispersity via a Coaxial Turbulent Jet

Flow conditions, characterized by the FVR and the $Re_{mixture}$, lead to either polydispersed or monodispersed liposomes (Fig. 4a). Polydispersed liposomes were formed under two different flow conditions – *i.e.* an apparent stratified flow (Fig. 4b-1) and a weak jet (Fig. 4b-2). The stratified flow led to stream separation and uncontrolled mixing. The weak jet appeared to develop vortices that led to backflow along the jet – also resulting in uncontrolled mixing.

In order to achieve monodispersed liposomes, the formation of a jet was required (Fig. 3). Depending on the flow conditions, it appeared that there was the coexistence of a laminar/transitional flow followed by a jet that led to turbulent flow (Fig. 4b-3 and Fig. 4b-4). For a similar set of Reynolds numbers, Kwon *et al.* observed the same effect of a decrease in the laminar/transitional region with an increase in the Re[67]. It does not appear that the aqueous phase significantly dilutes the ethanol phase in this laminar/transitional flow region; otherwise, a color change in the fluorescent marker (Nile Red) would be observed due to the change in fluid polarity[64]. Accordingly, it may be stated that limited mixing occurs throughout the laminar/transition region. For the formation of a jet, it has been shown that the center velocity decreases[68] and the jet boundary spreads radially, resulting in a concentration gradient[69] of the injected phase (in this case, lipid+ethanol). Therefore, the majority of mixing occurs where the center velocity decreases and jet boundary spreads radially. As the spreading of the lipid+ethanol phase establishes a radial concentration gradient, it is proposed here that this promotes the controlled formation of monodispersed liposomes. Moreover, convective inertial forces are

dominant compared to viscous forces when Re >>1, which supports the reasoning that increasing Re will correspond to an increase in the extent of mixing, thus forming different sized liposomes. For the formation of monodispersed liposomes, it is clear that $Re_{mixture}$ is directly related to the liposome particle size. In addition, above a FVR of approximately 7, liposome formation is independent of FVR and dependent only on the $Re_{mixture}$. This observation is made by comparing Fig 4a with Fig 4c, where the liposomes formed at the same $Re_{mixture}$ have a similar particle size, regardless of the FVR. This latter statement is highly significant because it outlines that liposome formation from a turbulent jet is predominately a convective process and occurs at the radial spreading in the turbulent region of the jet.

Considering the phospholipid formulation as well as the $Re_{mixture}$ and FVR, the formulations containing DSPC, DPPC and DMPC formed mostly monodispersed liposomes (for an FVR $\geq$ 7). Some polydispersity was evident at lower aqueous flow rates and may have been due to higher ethanol percentages destabilizing the liposomes. However, the formulation containing DOPC formed only monodispersed liposomes at the lower aqueous flow rates. For DOPC, a higher $Re_{mixture}$ appears to destabilize the formulation, which could be due to the high curvature of the small particles (~25nm) and/or the low phase transition temperature of DOPC – making the fluid bilayer more susceptible to fusion at ambient temperature conditions.

4.6.2 Liposome Formation Model using a Coaxial Turbulent Jet

The injection of lipid dissolved in ethanol into an aqueous phase is further complicated by changes in properties such as viscosity[66], density[66], molar volume[66], heat of mixing (exothermic in this case)[70], lipid solubility[65], and lipid structure (*e.g.* lipid molecular volume). It does not

appear that any property above is solely related to the observed particle size changes of liposomes. By using the $Re_{mixture}$, the following terms are taken into account: viscosity, density and sensible heat gains.

The exact mechanism of how liposomes form is still elusive; however, a detailed model for the liposome formation process is beginning to emerge through experimental findings. The idea of mixing lipid dissolved in a water miscible solvent and injected into an aqueous phase has been around since the early 1970s.[46] Initial work in this field has outlined that bilayered phospholipid fragments (BPF)[71] form and fuse together as the volume percentage of ethanol decreases. For a turbulent jet, a model based on the formation and subsequent fusion of BPF resulting in monodispersed liposomes leads to some doubt. During the centerline velocity dissipation of a jet, multiple vortices form and subsequently shear off. Since this process is turbulent, vortices of different sizes would develop and the mixing in these micro-environments would appear to be heterogeneous. Consequently, BPFs that fused during this process would only form polydispersed particles.

A new model for liposome formation is proposed (Fig. 4.12). This model is based on the growth of a highly fluid lipid/ethanol aggregate (denoted here as a pro-liposome). Initially, lipid is dissolved in ethanol forming a solution. As outlined above, the ethanol spreads radially at the jet location resulting in a concentration gradient. At this point, water mixes with the ethanol+lipid phase and pro-liposomes begin to grow in size until a critical solubility is reached (~50-60% v/v ethanol). The final liposome size is then dependent on the following factors: (1) ethanol diffusion

out of the pro-liposome, (2) pro-liposome fluidity, (3) lipid packing, (4) pro-liposome surface charge and (5) lipid concentration.

Ethanol diffusion out of the pro-liposomes is exemplified by the addition of excess ethanol to the aqueous phase. Ethanol is known to be able to cross the lipid bilayer, *i.e.* move from the aqueous phase into one bilayer leaflet and cross from one leaflet to the other[72]. In addition, ^{31}P-NMR studies have confirmed that ethanol causes the liposome bilayer to become less packed.[73] Comparing 10-30% v/v excess ethanol to 0% v/v excess ethanol in the aqueous phase, ethanol diffusion out of the pro-liposome would be slower during the mixing process and consequently the bilayer would have higher permeability due to the larger amount of ethanol. Accordingly, there would be more time and space for lipid molecules to enter the pro-liposome – thus growing in size. Moreover, the addition of 26 wt% glycerin to the aqueous phase did not cause any major change in particle size, which indicates that the increased bulk viscosity is less essential compared to ethanol diffusion out of the pro-liposome and convective forces.

The lipid phase transition is important in assessing the fluidity of the pro-liposome. The phase transition temperatures of the phospholipids in this study are ranked in the following order: DSPC>DPPC>DMPC>DOPC (highest to lowest)[74]. By comparing only the saturated phospholipids, DSPC is the most ordered while DMPC is the most fluid over the temperature range caused by exothermic mixing in these experiments (*i.e.* 23-32°C). It appears that liposomes form when lipid molecules are in the fluid/disordered state rather than the gel/ordered state. For example, DPPC:DPPG (7.5:0.4 molar ratio) formed a viscous, gel-like structure instead of liposomes at a 5mM lipid injection (data not shown). It should be noted that adding cholesterol

increases the fluidity/disorder of the lipid membrane; thus, making it is possible to form liposomes at temperatures below the lipid phase transition temperature of the corresponding pure lipid. A more ordered structure would prevent lipid molecules from entering the pro-liposome – resulting in smaller liposomes. This reasoning explains why liposomes form in the following order of smallest to largest (DSPC<DPPC<DMPC). A more detailed analysis that includes the impact of temperature, cholesterol percentage and charged lipid percentage may be useful to thoroughly explain the above observation.

Changes in lipid packing are exemplified by DOPC, which adds an additional complexity in that this lipid is unsaturated (*i.e.* it has a double bond in each hydrocarbon tail). The geometric packing parameter of DOPC[75] is = 1.08 and, when mixed with other lipids, may support a geometrically smaller sized particle (*i.e.* as low as 25 nm in diameter). In comparison, DSPC, DPPC, and DMPC lipid molecules have a packing parameter ~1 and are more cylindrical in shape. Thus, these DOPC liposomes can support higher curvature/ smaller sized liposomes than DSPC even though the phase transition temperature of DOPC was much lower relative to the experimental conditions. Moreover, the more cylindrical shape of DSPC, DPPC and DMPC may explain why these liposomes appear to plateau at a mean particle size of ~60-70nm at a high $Re_{mixture}$. This indicates that the overall lipid packing of the lipid mixture is a geometric constraint on the liposome particle size.

In the case of the surface charge, the addition of salt to the aqueous phase (*e.g.* 0.9 wt% NaCl) would lower the surface charge of the pro-liposome and lessen the electrostatic repulsion

between the pro-liposome and the individual lipid molecules. This reduced repulsion would allow more lipid molecules to enter the pro-liposomes, thus increasing the final liposome size. Lastly, the lipid concentration led to a modest increase in liposome particle size. This increase in size further supports the pro-liposome model as more lipid molecules would be recruited into the pro-liposomes. It should be noted that only 5-30 mM lipid was injected, which is a relatively small amount of lipid compared to the other components in the system. Therefore, increasing the lipid concentration would be expected to increase the number of liposomes instead of proportionally increasing the size of the liposomes. Moreover, too high of an injection lipid concentration may cause other types of structures to form (*e.g.* stacked bilayers) and increased polydispersity[76].

Overall, the pro-liposome model appears to provide a clearer explanation on the liposome formation process using a turbulent jet. From the above discussion, $Re_{mixture}$ can be used to predict the liposome particle size for a fixed set of factors (*i.e.* lipid type, lipid concentration, aqueous phase additives, *etc.*), but will not predict particle size when changing these factors. In addition, factors not studied here such as cholesterol percentage[77], solvent/aqueous phase temperatures and type of solvent[78] will also impact liposome formation and particle size. Therefore, additional studies will need to be performed using a turbulent jet in co-flow to build on the current liposome formation model.

4.6.3 Particle Size Analysis using Multiple Measurement Techniques

Dynamic light scattering is a suitable technique to determine monodispersity by analyzing multiple parameters. These parameters include the z-average, intensity mean, volume percentage

and the PDI. The z-average is calculated from a cumulants analysis (an intensity-weighted fitting algorithm) and the intensity mean is determined directly by an intensity fitting algorithm. When both the z-average and intensity mean values are very similar, it indicates that a single population is present. In addition, a volume percentage of 100% further points to a monodispersed system since transforming the data from intensity to volume shifts the emphasis away from the mean particle size. A volume percentage other than 100% may indicate the presence of additional populations of particles. However, there was an initial uncertainty in relying only on dynamic light scattering without comparing to other techniques, as the light intensity of any larger particles will overshadow the light intensity of smaller particles. This overshadowing may prevent the smaller particles from being detected, even when transforming the raw intensity data to a volume measurement.

Comparing nanoparticle tracking and dynamic light scattering, both techniques appeared to show similar results with respect to mean particle size and size distribution. Since both of these techniques determine the particle size using completely different methods (*i.e.* individually tracking particles vs. fitting functions), the agreement in mean size and size distribution greatly supports that this liposome processing technique has the ability to controllably produce a large size range of monodispersed liposomes.

The NS-TEM micrographs were originally obtained as a way to characterize the liposomes and possibly make visible smaller particle populations that dynamic light scattering might have failed to detect. After analyzing the TEM images, it was not possible to determine an accurate mean diameter or particle size distribution. One reason is due to the processing conditions apparently

causing multiple states of liposomes present (*i.e.* partially-hydrated to flattened stacked bilayers). A second reason is that what appears to be small particles may actually be fragments of larger particles. These possible fragments may explain why the nanoparticle tracking analysis *via* Nanosight, which analyzed 30,000-90,000 particles per sample, did not show a wider particle distribution and a possible second population of particles in the 40e:100a sample (Fig. 8).

Lastly, the cryo-TEM micrographs further confirmed the mean particle size trend observed using the three particle size analysis techniques outlined above. The advantage of cryo-TEM over NS-TEM is that the samples were controllably frozen to prevent ice-crystal damage and the liposomes were imaged in a more native state. In addition, these micrographs confirmed that the liposomes are unilamellar.

4.7 Conclusion

A turbulent jet mixer can be used to form unilamellar, monodispersed liposomes with a known particle size. The unilamellar, monodispersed particles have a mean size anywhere from ~25 nm to >465 nm. The liposome mean particle size is highly dependent on the $Re_{mixture}$ and is independent of the flow velocity ratios. The monodispersity and mean particle size trend of the liposomes was analyzed using three fundamentally different particle size analysis techniques. Dynamic light scattering and nanoparticle tracking demonstrated that the liposomes were monodispersed and increased in size with a decrease in $Re_{mixture}$. Lastly, a new model outlining the liposome formation process is explained *via* a pro-liposome growth model that takes into account aqueous phase additives, types of lipid molecules, and lipid concentration.

4.8 Tables

Table 4.1 DOE on Lipid Concentration vs. Particle Size - Model Parameter Estimates Sorted by Statistical Significance[1].

Term	Estimate	Std Error	t Ratio	Prob>|t|
AFR*AFR	43.5	4.22	10.3	<.0001*
Aqueous Phase Flow Rate(AFR)	-45.6	9.16	-4.98	0.0001*
Lipid-Concentration	8.31	2.09	3.98	0.0011*
AFR * AFR * AFR	-24.2	10.2	-2.37	0.0308*
Lipid-Concentration* AFR	-2.6	2.55	-1.02	0.323

[1] The aqueous phase flow rate (AFR) and the lipid concentration terms both have statistical significance. In addition, higher order AFR terms are required due to the non-linearity of the response (*i.e.* particle size).

4.9 Figures

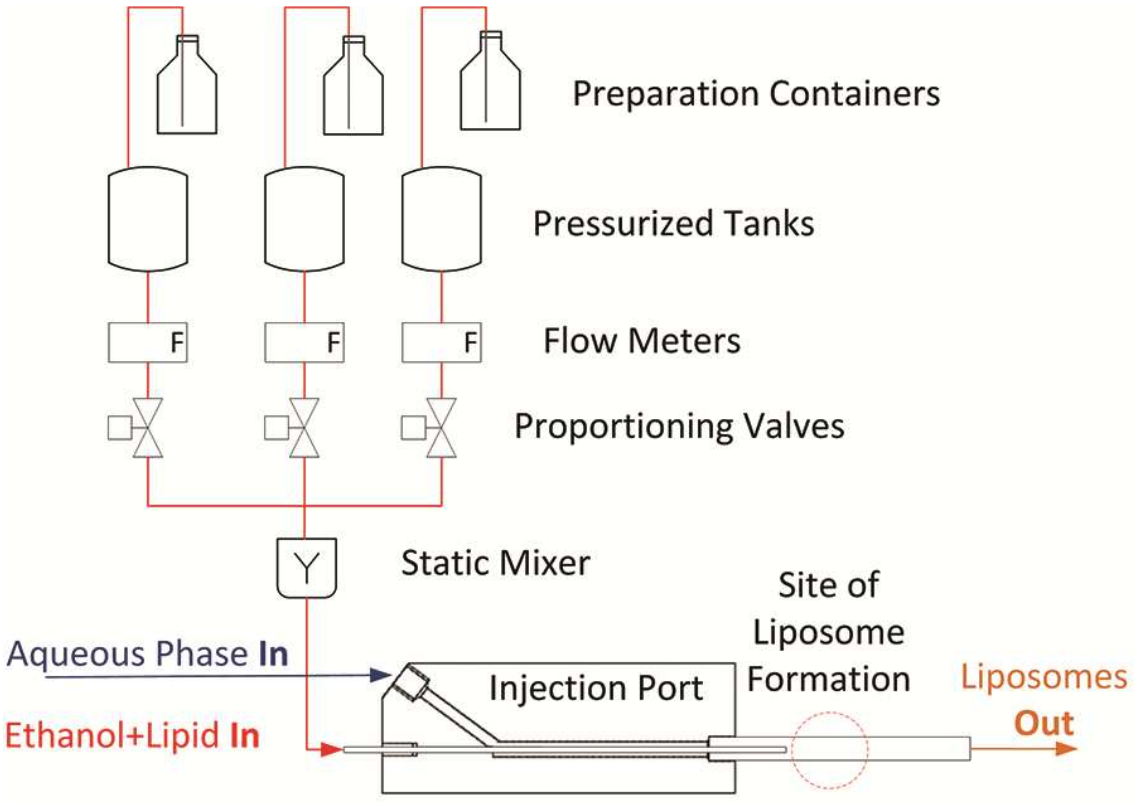

Fig. 4.1 Overall schematic of the lipid mixing process and the injection port (not shown to scale). Ethanol or lipid dissolved in ethanol is added to the pressurized tanks. NI LabVIEW is used to control the entire process and sensors such as flow meters are installed to control/monitor the flow conditions.

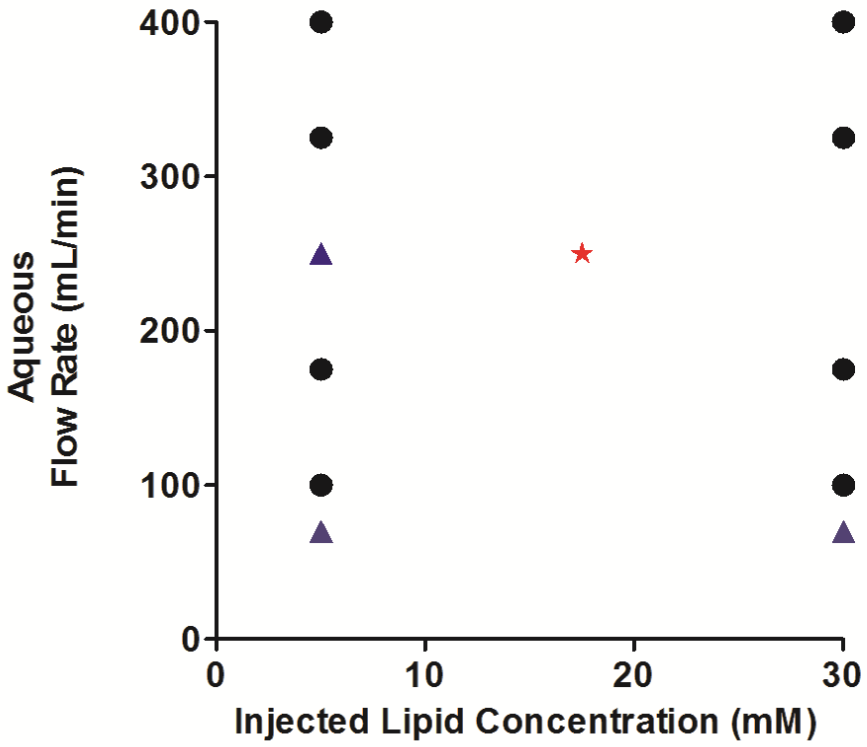

Fig. 4.2 The design space of the DOE study on the impact of lipid concentration and aqueous phase flow rate on particle size. The initial design consisted of 2 factors at 4-levels (black circles) and center points (red star). The design was augmented with additional runs to extend the model design space (blue triangles).

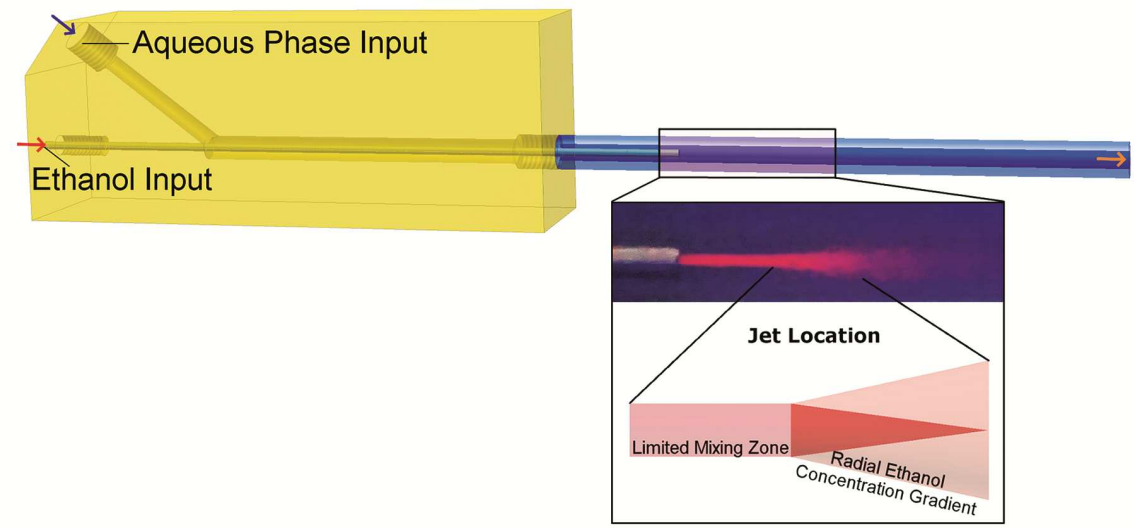

Fig. 4.3 Schematics and photographic image of the injection port that allows formation of a coaxial turbulent jet. Both the aqueous and ethanol streams are flowing in the same direction (co-flow). Arrows indicate the direction of liquid flow. The photograph is of lipid dissolved in ethanol (visualized through the use of Nile Red) that is being injected in the center of the aqueous stream. Additionally, the jet location is shown as a schematic where there is a limited mixing zone followed by a concentration gradient of the ethanol+lipid phase.

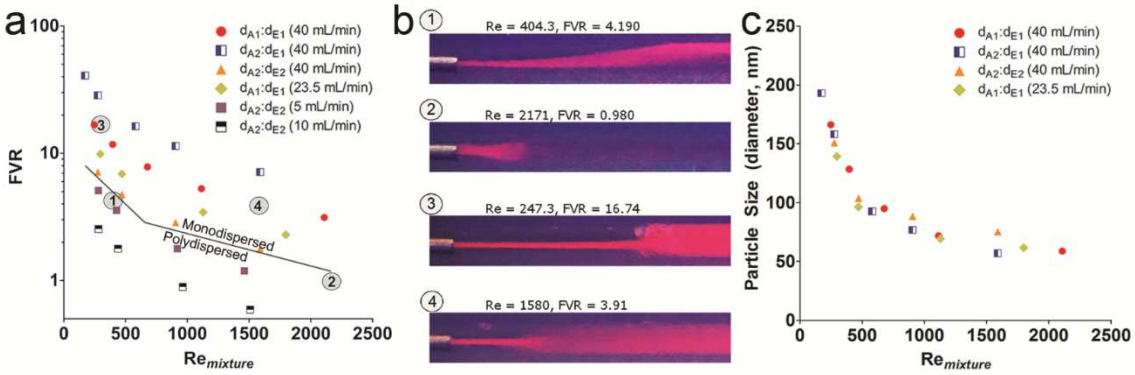

Fig. 4.4 Relationship between liposome polydispersity index and flow properties. 4a) Flow velocity ratio (FVR) *vs*. the mixture Reynolds Number ($Re_{mixture}$). The region above the solid line produced monodispersed liposomes (PDI <0.10) and the region below the solid line formed polydispersed liposomes (PDI >0.10). 4b) Flow images corresponding to locations (1, 2, 3, and 4) from Fig. 4a demonstrating flow profiles leading to monodispersed or polydispersed systems. To cover a range of FVR and $Re_{mixture}$, the ethanol containing inner tube diameter (d_E) and the aqueous containing outer tube diameter (d_A) were changed accordingly. 4c) Z-average particle size vs. $Re_{mixture}$ for only monodispersed liposomes. d_{A1} = 3.175 mm, d_{A2} = 4.572 mm, d_{E1} = 0.508 mm, d_{E2}=1.016 mm.

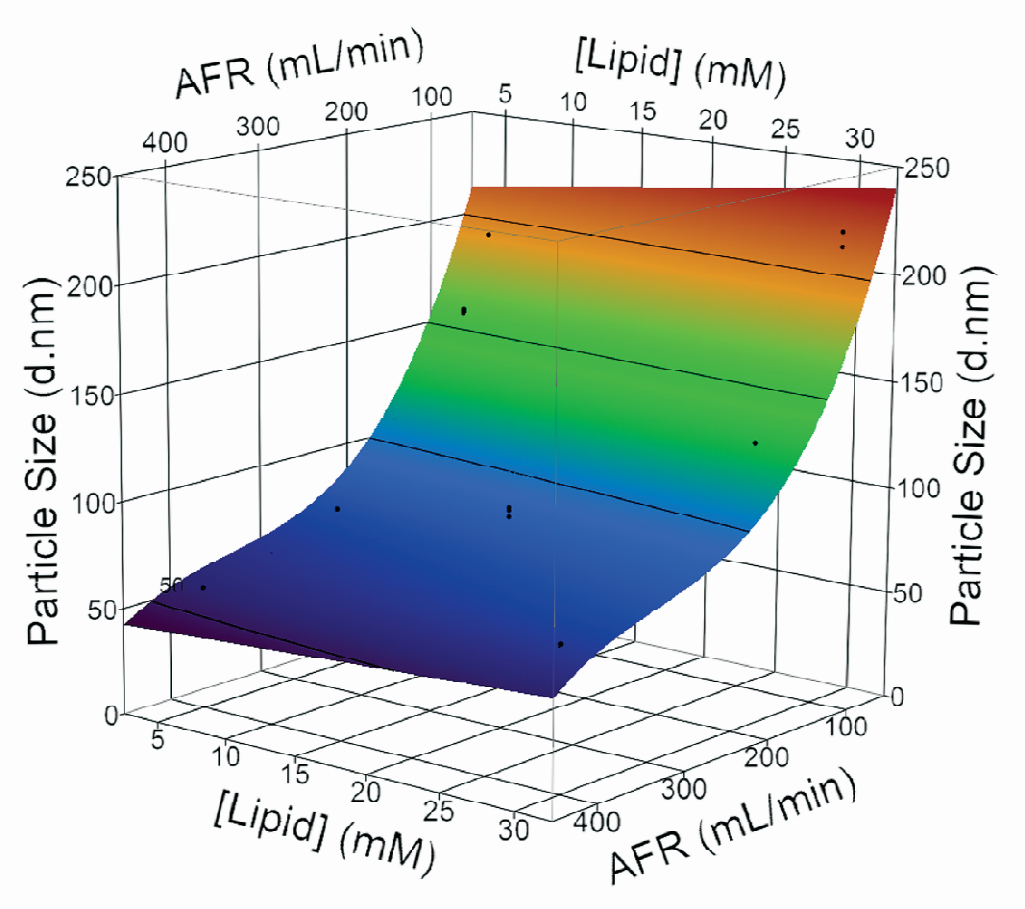

Fig. 4.5 A Surface profile plot of the Z-average particle size vs. the aqueous phase flow rate (AFR) and lipid concentration. The liposome particle size increases with an increase in the injected lipid concentration and/or a decrease in aqueous phase flow rate.

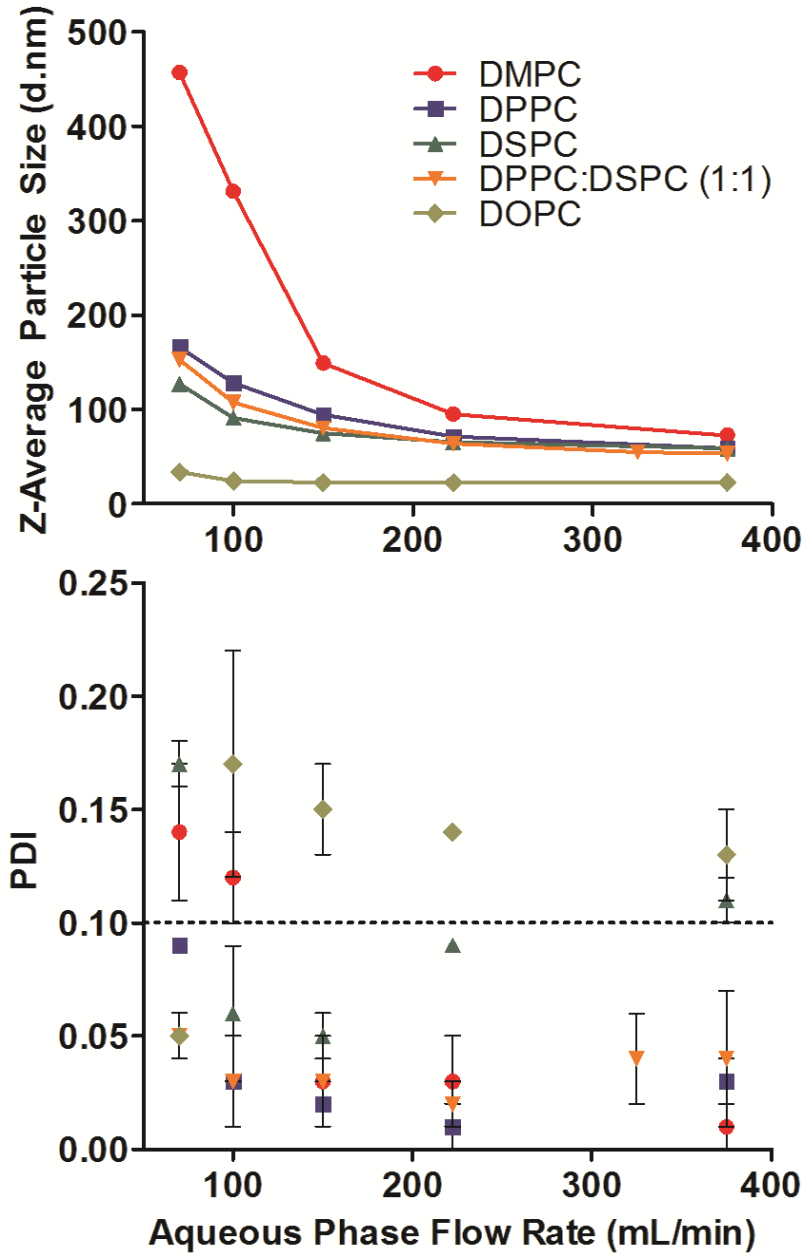

Fig. 4.6 The effect of lipid type (*i.e.* DMPC, DPPC, DSPC, DOPC) on mean particle size and PDI. The formed liposomes were mostly monodispersed with the majority of PDI values ≤ 0.05. Some polydispersity was evident for DOPC liposomes and for liposomes formed at low aqueous phase flow rates. The dotted line in the bottom plot represents the limit on monodispersity (PDI<0.10). The standard deviation from the Z-Average particle size plot was less than the symbols representing the data.

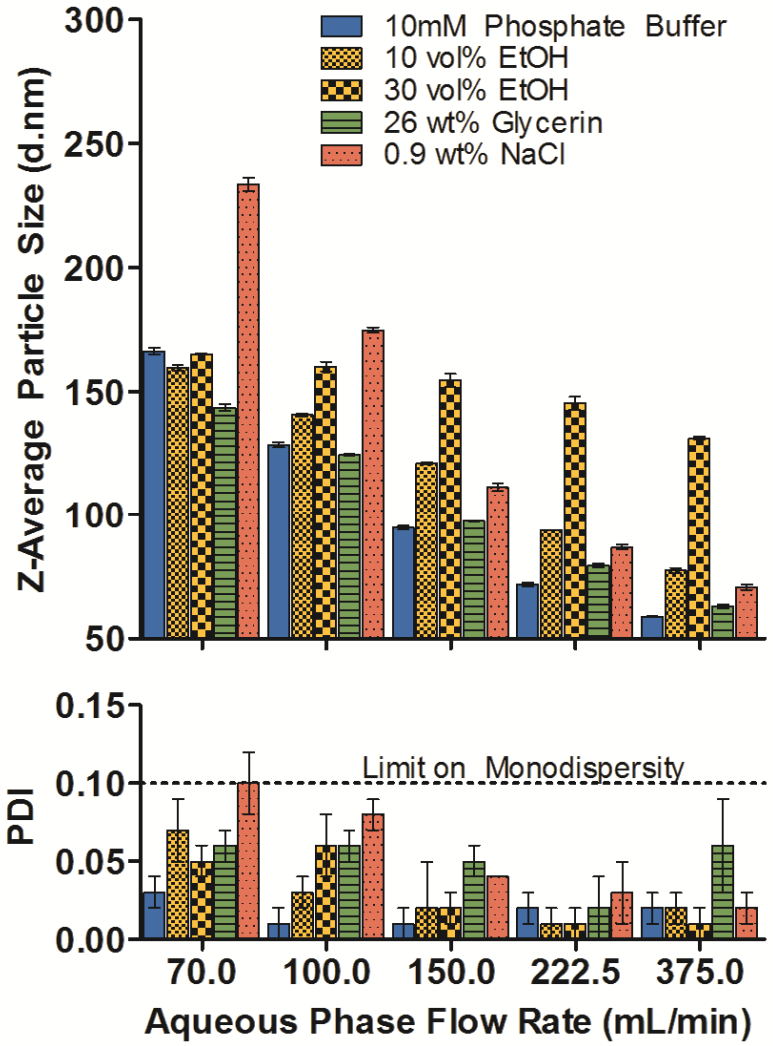

Fig. 4.7 The effect of aqueous phase additives on mean particle size. The aqueous phase consisted of 10 mM phosphate buffer plus the addition of certain additives (*i.e.* NaCl, glycerol and ethanol). All additives were pre-mixed with the aqueous phase prior to liposome formation. The 10 mM Phosphate buffer sample was used as a control. The Z-average particle size measured by DLS and PDI are plotted above.

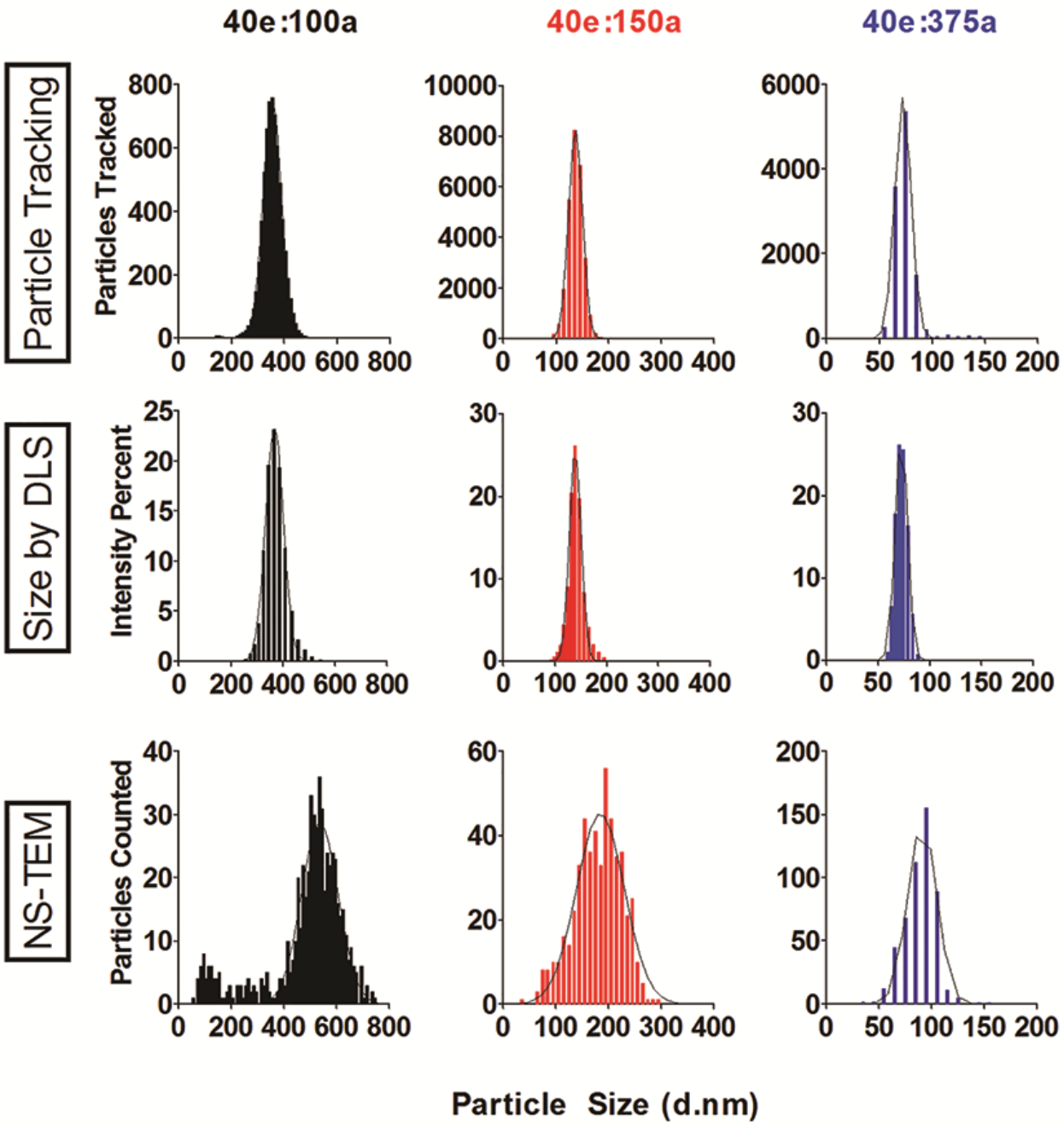

Fig. 4.8 Comparison of different particle sizing techniques (dynamic light scattering, nanoparticle tracking and particle counting *via* NS-TEM to assess liposome mean particle size and particle size distribution. DLS and nanoparticle tracking are in good agreement with both mean size and size distribution. NS-TEM produces a larger particle size and size distribution. For all three techniques, the mean particle size trend is the same, *i.e.* an increase in mean particle size for a decrease in the aqueous phase flow rate. Ethanol flow rate = e (mL/min); Aqueous flow rate = a (mL/min).

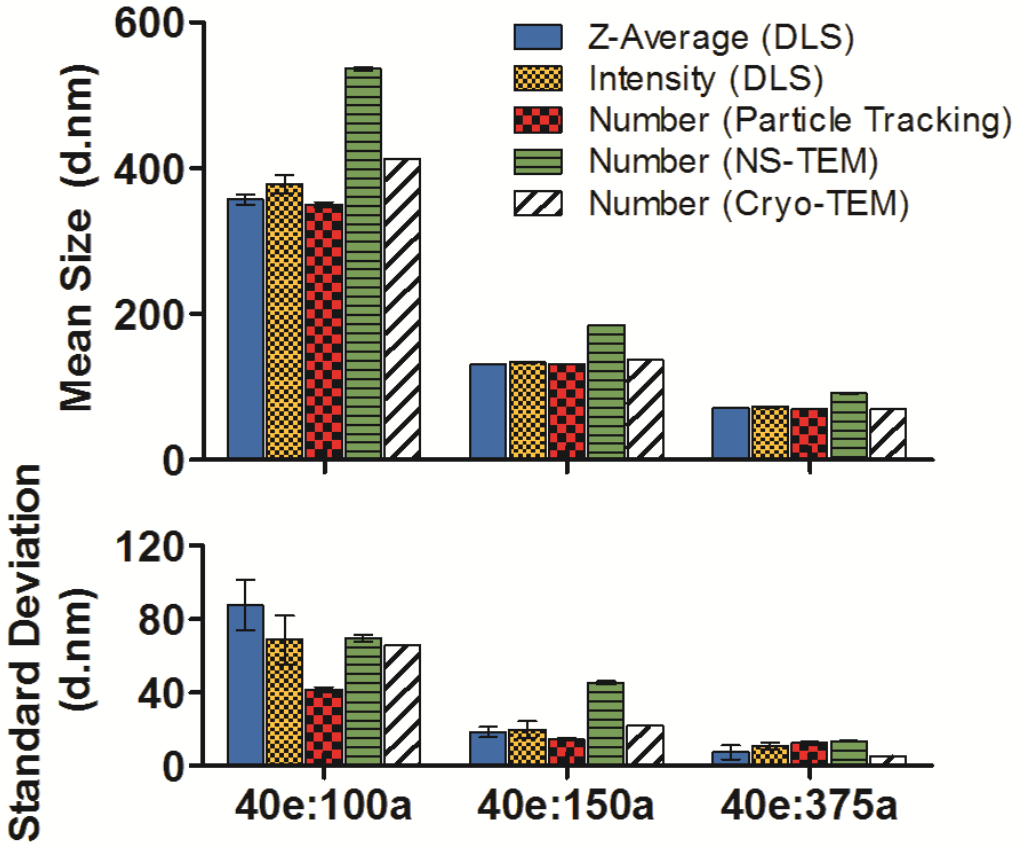

Fig. 4.9 Liposome mean particle size and standard deviations for DLS, nanoparticle tracking, NS-TEM and Cryo-TEM. The z-average standard deviation was calculated from the PDI (*i.e.* $\sigma = [\text{mean}*\text{PDI}]^{1/2}$). The intensity standard deviation was reported directly from the intensity width. The nanoparticle tracking standard deviation was reported by the Nanosight® software. The NS-TEM standard deviation was from the Gaussian distribution fit ($R^2 \geq 0.913$ for all cases). Error bars represent the standard deviation for the multiple data sets. No error bars were reported for Cryo-TEM since the particle count was limited. Ethanol flow rate = e (mL/min); Aqueous flow rate = a (mL/min).

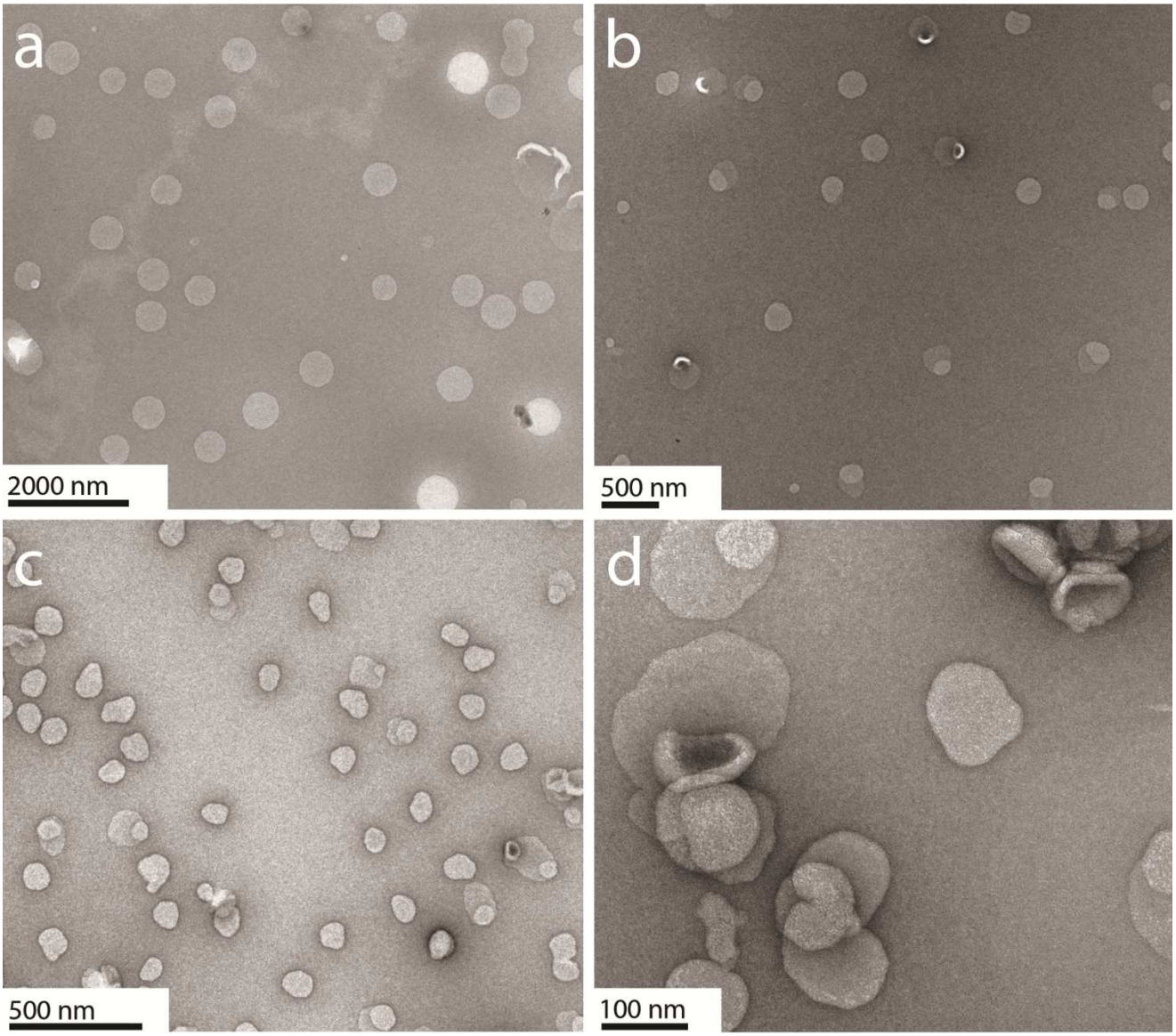

Fig. 4.10 Negative stain TEM micrographs of liposomes for three liposome samples produced using different flow conditions. a) 40e:100a sample, b) 40e:150a, c) 40e:375a and d) 40e:375a zoomed. Ethanol flow rate = e (mL/min); Aqueous flow rate = a (mL/min).

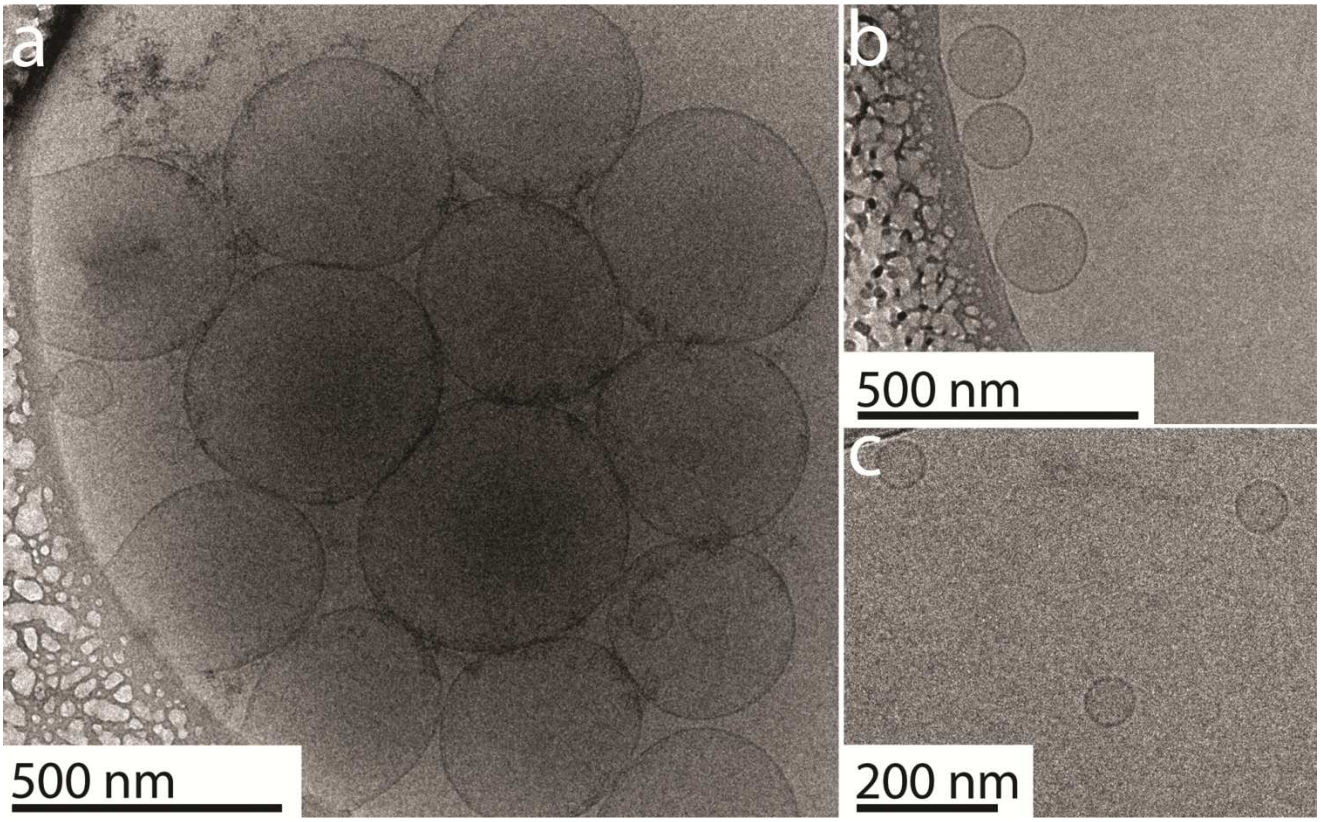

Fig. 4.11 Cryo-TEM micrographs of liposomes for three liposome samples produced using different flow conditions. a) 40e:100a sample, b) 40e:150a and c) 40e:375a. Ethanol flow rate = e (mL/min); Aqueous flow rate = a (mL/min).

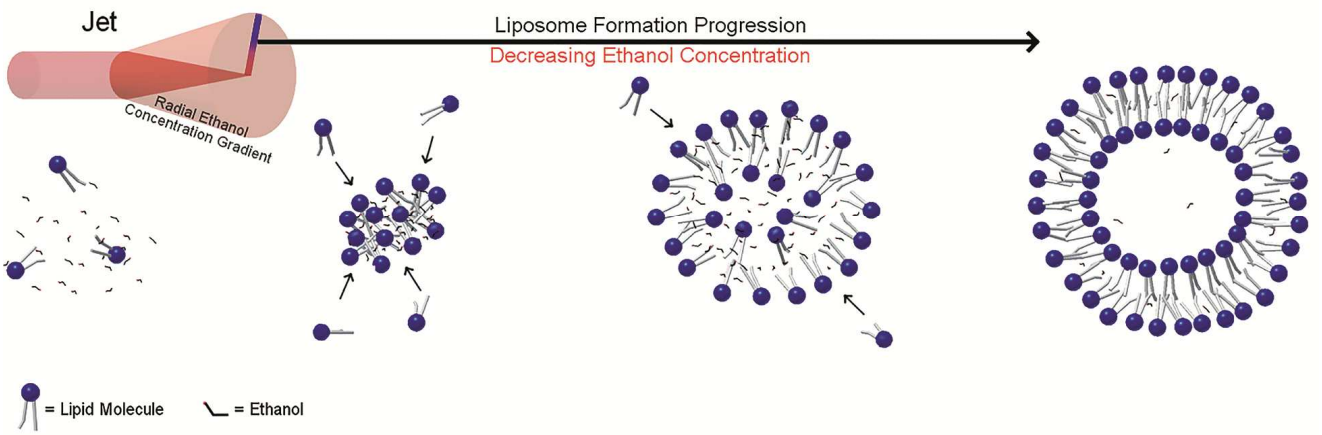

Fig. 4.12 Proposed model for liposome formation from a coaxial turbulent jet mixer in co-flow. A schematic of a turbulent jet is shown with a radial ethanol concentration gradient (top left). In the liposome formation model, lipid and ethanol molecules aggregate (forming pro-liposomes) as the ethanol concentration decreases. The pro-liposomes grow in size by "recruiting" lipid molecules. The growth continues until the ethanol concentration reduces below a critical level. Image not shown to scale.

Chapter 5

Continuous Processing of Liposomes with in-line Dilution and at-line Particle Size Analysis

5.1. Abstract

In-line dilution was added to a continuous process for forming liposomes. In-line dilution was implemented to reduce the overall amount of solvent (ethanol) in the final colloidal dispersion. In addition, at-line particle size analysis was also implemented into this process. At-line particle size analysis provided enhanced process control of the liposomal dispersions. Two techniques were compared, *i.e.* a continuous flow mode vs. a Load/Stop flow mode. The advantages and disadvantages of each technique were outlined with an explanation of limitations. Moreover, the effect of forming liposomes at different ionic strengths was investigated. Overall, the Load/Stop mode for at-line particle size analysis appeared to provide more consistent dynamic light scattering results compared to the Continuous Flow mode. Lastly, the ionic strength of the aqueous phase had a significant impact on the mean particle size of the liposomes and a brief explanation about the liposome formation mechanism was discussed.

5.2 Introduction

In the pharmaceutical industry, liposomes are used as drug delivery systems and have demonstrated clinical efficacy in anti-cancer therapies[27, 79-82], in an anti-fungal therapy[83] and in producing postsurgical analgesia[84]. Two critical quality attributes of liposomal formulations are the mean particle size and particle size distribution. The mean particle size diameter range of

liposomes is from 25 nm up to >1000 nm. For anti-cancer applications, liposomes with a diameter of around 100 nm may be considered optimal with respect to blood-to-tumor transfer and increased tumor retention times[85]. To the contrary, different types of tumors may have lower or higher pore cutoff sizes (*e.g.* 7-2000 nm)[86]. For the lower pore cutoff, smaller liposomes would be required for liposomal extravasation into the tumor.

Moreover, both the mean particle size and particle size distribution have major impacts on liposomal *in-vitro* stability as well as liposomal *in-vivo* biodistribution and cellular uptake mechanisms. For example, liposomes around 40 nm in diameter appear to be internalized by the dynamin-dependent pathway and liposomes around 98 nm are internalized by Clathrin-mediated endocytosis[87]. Additionally, it has been documented that small liposomes (~40 nm) are able to enter the lymphatic system after subcutaneous administration whereas larger liposomes remained at the site of injection.[88] With respect to *in-vitro* stability, large liposomes (micron-sized) may have a greater tendency to sediment due to gravity while smaller liposomes are not affected by gravitational forces since these particles move *via* Brownian motion and do not sediment. In addition, changes in liposomal particle size and size distribution (*i.e.* due to fusion or aggregation) are affected by the presence of ions, *e.g.* Ca^{2+} and La^{3+}.[89] Therefore, to ensure consistency of *in-vitro* and *in-vivo* performance, liposomal formulations should have a defined mean particle size and size distribution.

The mean particle size diameter and particle size distribution of liposomes can be analyzed by a variety of instruments and technologies. These technologies include but are not limited to: dynamic light scattering, static light scattering, particle tracking, various forms of electron

microscopy and acoustic spectroscopy. In order to accommodate many liposomal formulations, particle sizing technology used to measure liposomes must be capable of measuring particle diameters as low as 25 nm. Moreover, many of these technologies are only applicable to off-line measurements and cannot be implemented into a process (*i.e.* batch nor continuous). For a continuous process, the measurement must be either at/on/in-line capable. Two technologies that have this capability are dynamic light scattering and acoustic spectroscopy.

Dynamic light scattering is based on light or photon fluctuations that are correlated to the diffusion of particles, which is then related to particle size information. This technique uses two analyses in calculating the particle size data; namely, an intensity-based analysis and an intensity-weighted or cumulants analysis. The intensity analysis is based on the raw data (photon fluctuations). The cumulants analysis is based on an exponential equation and is weighted according to the intensity of the particles. For continuous measurements, this technique can be setup in a process stream by the use of a flow cell. The flow cell enables the sample to enter the cell at one end and leave the cell at the other. A pump is used to control the flow rate and/or stop the flow into the flow cell. If the flow rate is low enough to sustain laminar flow (around 1-1.5 mL/min), then the sample may constantly flow through the flow cell during measurement. For higher flow rates, turbulence develops and the higher velocities impart motion to the particles, resulting in erroneous particle size measurements. If higher flow rates are required (>1.5 mL/min), the sample can be rapidly loaded into the flow cell followed by stopping the flow prior to the particle sizing measurement.

Acoustic spectroscopy is based on the propagation of sounds waves at multiple frequencies while measuring the attenuation of the ultrasound, which is then used in calculating the particle size distribution[90]. There is a correlation between the displacement of the sound waves at multiple frequencies with the mean particle size and size distribution[85]. This technique has successfully characterized BCR silica quartz samples with precisions of 1% for particle size and 5% for distribution.[91] In a second study, microemulsions are measured from 20 nm to 100 nm up to 16.6% weight fractions.[92] These results indicate that relatively concentrated samples can still be tested with this technique, which may be problematic for dynamic light scattering. The advantage of this technique is that the particle size measurements can be taken at higher flow rates that are not constrained to the laminar flow regime as is the case with dynamic light scattering. A disadvantage of this technique is that air bubbles will interfere with the particle size measurements.

From a quality perspective, it is highly important that the mean particle size and size distribution of the liposomal formulation is within specifications. For example, these specifications could be that the mean particle size diameter is 100 nm ± 10 nm with a particle size distribution of 25 nm. For both batch and continuous processes, the particle size can be measured during or after processing. However, continuous processing has the advantage in that the particle size measurement can be performed continuously as the liposomes are being formed, and this information can be used to: divert out-of-specification liposomes to waste without compromising the entire unit or batch; and to correct the problem that caused the formation of out-of-specification liposomes. In contrast to the continuous process, the particle size measurement for a batch process would take place once all of the liposomes are formed and consequently failure

to meet the particle size specifications would result in removal of the entire batch. In this work, it is hypothesized that the mean liposome particle size diameter and particle size distribution can be quantitatively monitored during continuous processing and this information can be used in a feedback algorithm to maintain these liposomal critical quality attributes.

5.3 Materials and Methods

5.3.1 Materials

1,2-dimyristoyl-*sn*-glycero-3-phosphocholine (DMPC); 1,2-dipalmitoyl-*sn*-glycero-3-phosphocholine (DPPC); 1,2-distearoyl-sn-glycero-3-phosphocholine (DSPC); 1,2-dipalmitoyl-*sn*-glycero-3-phospho-(1'-*rac*-glycerol, sodium salt) (DPPG-Na); and Lipoid S PC-3 (HSPC) were purchased from Lipoid™. Cholesterol (Chol) was purchased from Sigma. Ethanol (200 proof, ACS/USP grade) was purchased from Pharmco-AAPER.

5.3.2 Experimental Methods

5.3.2.1. Liposome Formation and Dilution

Liposomes were prepared by a modified ethanol injection method. A schematic of this system is demonstrated in Fig. 5.1. Three separate 316 stainless steel tanks contained the lipid+ethanol solution. These tanks were pressurized (at 20 psi) and the flow rates from these tanks were controlled by analog flow meters (McMillian) and proportioning solenoid valves (Aalborg). The flow meters were factory calibrated for water with less than 1% error full-scale. For the lipid+ethanol flow streams, these flow sensors were re-calibrated for ethanol and had an R-squared value of 0.9989, with a working range from 5-50 mL/min. The three tanks were then

connected at a single point using a 4-way connector (Swagelok). A static mixer was implemented to ensure that the lipid+ethanol solutions from the three tanks were adequately mixed prior to reaching the injection port where the ethanol and aqueous phase I streams converged. The aqueous phase I volumetric flow rate was controlled by a gear pump (Micropump®). To form liposomes, the mixed lipid+ethanol solution was then injected into an aqueous phase (aqueous phase I) at various flow rates. The tubing ID of the ethanol phase was 0.508 mm (1.588 mm OD). The aqueous phase I tubing ID was fixed at 4.572 mm. Flow rates of the lipid+ethanol phase ranged from 5-40 mL/min and those of the aqueous phase I ranged from 70-300 mL/min.

After the liposomes were formed, the liposomes passed through a degassing unit (Liqui-Cel) followed by a second three-way T-port. This three-way T-port has one inlet for the liposomes, a second inlet for aqueous buffer and one outlet. A second gear pump (Micropump®) was used to control the flow of the aqueous phase into this port (aqueous phase II). The aqueous phase II flow rate was adjusted such that mixed aqueous phase would always have 5% vol. ethanol. Aqueous phase II flow rates ranged from 690-460 mL/min.

5.2.2.2. Data Acquisition System and Computer Software

The entire process was controlled by a custom-made program written using National Instruments (NI) LabVIEW® software. A data acquisition system (NI PXIe-1078) was combined with multiple NI modules to accommodate various input/output signals (*e.g.* analog and digital inputs/outputs, counters, circuit switches, *etc.*). The entire system was automated and only required the user to define the final lipid concentration and molar ratios of lipid. Process

variables such as flow rates, pressure, and temperature were monitored and some variables were automatically adjusted using custom computer algorithms. For example, proportional-integral-derivative controls were implemented in the computer program to precisely control the flow rates of both the ethanol and aqueous phases.

Communication to and from the Malvern Zetasizer was accomplished using the Malvern Link II software. Malvern Link II software was setup as an OPC server and NI LabVIEW was setup as an OPC client. The z-average particle size and PDI were recorded in the custom computer program. The custom computer program was able to send measurement instructions to the Malvern Zetasizer.

5.2.2.3. Experimental Outline for Liposomal Dilution

The impact of diluting liposomes was tested for liposome formulations consisting of *lipid*:DPPG:Chol at a molar ratio of 4.5:0.4:3, where *lipid* was either DPPC or DMPC. These lipids were chosen since each lipid was previously investigated and they produced liposomes of different sizes, *i.e.* up to ~500 nm for DMPC *vs.* up to 150 nm for DPPC. Two processing setups were investigated for the in-line dilution of liposomes. The first processing setup (setup I) was injecting the formed liposomes directly into the aqueous phase II (without the contactor in Fig 5.1). The second processing setup (setup II) consisted of incorporating a contactor (degassing unit) at the end of the liposome formation stage prior to the ethanol dilution stage (Fig. 5.1). For each processing setup, aqueous phase I flow rates ranging from 70 mL/min to 300 mL/min were tested. The aqueous phase used in this experiment was 10 mM phosphate buffer at pH = 7.4.

Each sample was analyzed for mean particle size and polydispersity index (see section 5.2.2.5).

5.2.2.4. Temperature Effects on Liposome Formation and Dilution

For the sample liposomal formulations outlined in section 5.2.2.3, these formulations were tested using the second processing setup over a range of temperatures. A chiller was connected to a custom designed heat sink and the aqueous phase I was chilled in-line to a set temperature (*e.g.* 8°C). The flow rate of the aqueous phase I was fixed at 100 mL/min. The temperature at the liposome formation stage was recorded in addition to the temperature of the aqueous phase II. Each sample was analyzed for mean particle size and polydispersity index (see section 5.2.2.5).

5.2.2.5. Particle Size Measurements

All particle size measurements were performed with a Malvern Zetasizer Nano S. Both off-line and at-line measurements were completed. Prior to measurements, the liposomes were diluted in-line to 5% vol. ethanol and the viscosity and refractive index were pre-set in the Malvern Zetasizer software. Particle size measurements included the z-average particle size and polydispersity index (PDI). For the off-line measurements, disposable plastic cuvettes were used. The samples were equilibrated at 25°C prior to each measurement. Each off-line measurement duration was set for 10 runs at 10 seconds each with n=3.

For at-line measurements, a flow cell equilibrated at 25°C was used. Prior to running at-line measurements, a population of liposomes with a low PDI was analyzed for various measurement conditions (*i.e.* attenuation, run duration, and count rate). Based on these results, the run duration was fixed (between 6-8 seconds) and the attenuation (and count rate) were adjusted to a satisfactory signal for DLS analysis. Two approaches were taken to transfer sample to the Malvern Zetasizer. The first approach (Continuous Flow Mode) was when the liposomes flowed

at a constant flow rate 1-1.5 mL/min through the flow cell while the particle size measurement was taken. The setup for this approach consisted of a miniature solenoid pump (Biochem™) that pumped the sample from the process stream to the Malvern Zetasizer. This pump operates by pumping 70 uL for each actuation and by controlling the actuation frequency, precise flow rates can be maintained.

The second approach (Load/Stop Mode) was based on loading the flow cell followed by stopping the flow prior to the measurement. A Micropump® pump was used to control the flow through the flow cell (20-25 mL/min). The pump operated at the set flow rate just prior to particle size measurements, at which point a custom computer algorithm then stopped the pump to prevent fluid flow during the measurements.

5.2.2.6. Automatic Particle Size Control

A liposome formulation consisting of HSPC:Chol:DPPG (4.5:3:0.4 molar ratio) was used to form the liposomes. The particle size was automatically controlled *via* the custom LabVIEW program. Initially, a model was established as a feedforward control using information such as salt concentration and type of lipid to reach a user defined particle size. This feedforward control provided an estimate of the aqueous phase I flow rate (ml/min) required to form liposomes of the user defined particle size. To maintain the particle size, a feedback algorithm was implemented using a proportional-integral-derivative (PID) control with the at-line particle size analysis *via* the Malvern Zetasizer as the process control input.

5.3 Results

5.3.1. Effect of Contactor prior to Ethanol Dilution

After the liposomes were formed, the liposomal dispersion was diluted to reach 5% vol. ethanol. The liposomes were diluted using the following two processing setups outline in the methods, namely: (1) setup I: without the contactor and (2) setup II: with the contactor. For DPPC liposomes, the addition of a contactor did not cause any major changes in the mean particle size nor the PDI value over the entire flow rate range. For DMPC liposomes, the contactor only appeared to cause changes at the lower aqueous phase I flow rate (*i.e.* 70 mL/min). At 70 mL/min, the mean particle size was larger and the PDI was lower compared to DMPC liposomes without the contactor. These results indicate that a larger dynamic range of particles that are more monodispersed are only obtained when the contactor is positioned at the end of the liposome formation stage.

5.3.2. Temperature Effects on Liposome Formation and Dilution

For these experiments, the temperature of the aqueous phase I and aqueous phase II were the same. When the ethanol+lipid phase was injected into the aqueous phase I, exothermic mixing caused an increase in temperature. The mean particle size and PDI for the DPPC liposomes exhibited an inverse relationship with an increase in temperature at the liposome formation stage (Fig. 5.3). This observation implies that at higher temperatures, larger liposomes form; however, at higher temperatures, the PDI also tends to increase. For DPPC liposomes, the PDI value did not exceed 0.1 even at the highest temperature, indicating that all of the liposomes, regardless of the temperature at liposome formation, were monodispersed.

Sizing data for DMPC liposomes also demonstrated an inverse relationship with an increase in temperature at the liposome formation stage (Fig. 5.4); however, significant changes in both the PDI and mean particle size occurred around 25°C. As the temperature increased from 24°C, the PDI increased from less than 0.09 ± 0.02 up to 0.24 ± 0.02. This change in PDI indicates that the particle size distribution was wider and/or multiple populations of liposomes were present as the temperature increased. In addition, the mean particle size of the liposomes increased significantly from 26°C up to 29°C, *i.e.* from 171.1 ± 1.7 nm to 333.5 ± 4.03 nm.

5.3.3. DLS Measurement Analysis

A previously prepared sample of liposomes was placed in the DLS flow cell and the DLS attenuation and cell position settings were set to automatic. These settings resulted in an optimized attenuation setting of 9 and a cell position of 4.2 – with the run duration fixed at 3 runs for 10 seconds each. The particle size information resulted in a z-average of 56.50 ± 0.03 nm, a PDI of 0.05 ± 0.02 and a count rate of 401.4 ± 2.77. Manual measurements were then taken at different attenuations (6, 7, 9 and 11) and run durations (3, 9, or 15 seconds) for a single run only. The plots from Fig 5.5a-c indicate how changing the DLS measurement settings impact the particle size analysis. From figure 5.5a, the z-average for this sample was most accurate at an attenuation of 7-9. At a higher value (*i.e.* 11), the particle size decreased. The PDI was similar to the control sample at the high attenuation (Fig. 5.5b). At a low attenuation (*i.e.* 6), the particle size was incorrect due to a very low count rate (Fig. 5.5c). In addition, the PDI increased significantly for this measurement. From these results, it is apparent that the count rate should be around or greater than 40 kcps and less than 500-1000 kcps for accurate particle size analysis. Lastly, the run duration did not appear to cause significant changes to the particle size analysis.

However, a higher value would increase the number of photons collected and would provide a more accurate particle size analysis.

5.3.4. At-line Particle Size Analysis - Approach 1: Continuous Flow Mode

The at-line particle size analysis *via* the continuous-flow mode was accomplished using a micro-solenoid pump that pumped the liposome samples at a constant flow rate (referred to as DLS flow rate) through the DLS flow cell during the particle size measurement. An initial study was conducted to determine DLS flow rates that resulted in similar particle size data to that obtained using off-line measurements. Liposomes composed of DPPC:Chol:DPPG (4.5:3:0.4 molar ratio) were formed at three aqueous phase flow rates (*i.e.* 80, 100 and 150 mL/min). The at-line particle size measurements were compared with the off-line particle size measurements. From Fig 5.6, the mean particle size was similar for both the continuous flow mode and the off-line measurements at the three different aqueous phase I flow rates and for DLS flow rates at ~ 1 and 2 mL/min. To the contrary, the PDI was only similar when the DLS flow rate was around 1 mL/min. At 2 mL/min in the continuous flow mode, the standard deviations and mean PDI were larger when compared to the off-line measurements. Therefore, the subsequent experiments for the continuous flow mode operated with a DLS flow rate around 1 mL/min.

Liposomes were then analyzed over a period of time to investigate how process changes (*i.e.* flow rate changes) impacted the mean particle size and PDI with respect to both accuracy and measurement lag time. Measurement lag time is the difference in time between a process change to the corresponding particle size data that is recorded in the custom software. This lag time is from the DLS measurement (*e.g.* run duration and temperature equilibration), delays in

software/instrument communication and time required to remove the previous sample in the DLS flow cell. The liposomal samples from Fig. 5.7 were run at 1 mL/min and showed agreement between some of the continuous particle size data and the off-line data. The mean particle sizes and PDI values for both continuous and off-line measurements were similar except for after the flow rate change. These anomalies may be explained by air bubbles entering the flow cell. In addition, there was a 58 second delay between the process changes to when the corresponding particle size data was recorded in the custom LabVIEW program.

A second analysis was conducted using for DPPC:Chol:DPPG (4.5:3:0.4 molar ratio) liposomes in 10 mM Hepes buffer (Fig 5.8). For this experiment, the liposomes flowed through a degassing unit prior to entering the DLS flow cell. The off-line particle size measurement data at the 100 mL/min aqueous 1 phase overlapped the continuous measurement data. At 150 mL/min, the particles became smaller (*i.e.* approximately 45 nm) and the particle measurement data for the off-line and continuous measurements did not correspond. The mean particle size was different by 15 nm and the continuous mode PDI ranged from 0.20 – 0.33, but was 0.05 for the off-line measurement. In addition, the measurement lag time was from 109 – 137 seconds.

5.3.5. Approach 2: Load/Stop Mode

For this approach, the liposomes were loaded into the flow cell at 20-25 mL/min prior to the DLS measurement. At 1-2 seconds before the DLS measurement, the flow was stopped. After the DLS measurement was completed, the flow began again and this process repeated for the duration of the experiments. The experiments here were designed to accommodate small and large liposomes using the same lipid formulation, *i.e.* DPPC:Chol:DPPG (4.5:3:0.4 molar ratio).

To achieve different sizes, three different aqueous phases were investigated, *i.e.* 10 mM NaCl, 75 mM NaCl and 140 mM NaCl. Liposomes prepared in 10 mM NaCl formed liposomes ranging from approximately 70 nm down to 45 nm in diameter (Fig 5.9). Slight deviations for the continuous particle size and off-line particle size were observed. The PDI was similar and less than 0.2 in all cases. The measurement lag time appeared to be consistent around 40-47 seconds. Process temperatures at both liposome formation and at the ethanol dilution stage were recorded as both of these temperatures have an impact on the mean particle size and PDI.

Liposomes prepared in 75 mM NaCl formed liposomes ranging from approximately 145 nm down to 70 nm in diameter (Fig 5.10). The mean particle size for the continuous and the off-line measurements overlapped for the majority of each flow condition. The same observation was true for the PDI values. The measurement lag time appeared to vary from 4-39 seconds; however, the 4 second may have been an anomaly. More accurately, the lag time appears to be constant around 29-39 seconds.

Liposomes prepared in 140 mM NaCl formed liposomes ranging from approximately 160 nm down to 70 nm in diameter (Fig 5.11). The mean particle size for the continuous and the off-line measurements also overlapped for the majority of each flow condition. The same observation was true for the PDI values. The measurement lag time was from 28-42 seconds, consistent with the previous two salt conditions.

5.3.5. Ionic Strength on Liposomal Physical Properties

The off-line particle size data from Fig. 5.9 to 5.11 were replotted vs. flow rate (Fig 5.12). It is clear that the mean particle size has a dependence on the amount of NaCl present in the aqueous phase. At low salt concentrations, *i.e.* 10 mM NaCl and 10 mM PB, pH 7.4, the particles were smaller compared to higher salt concentrations. There was not a large difference between the liposomes prepared in 75 mM NaCl and 140 mM NaCl. Thus, the NaCl concentration appears to have more of an impact on the particle size in between 10 to 75 mM NaCl. The 10 mM phosphate buffer had an ionic strength of 0.025 M, and the liposomes that formed under this condition had a mean particle size that was in between the 10 mM NaCl and 75 mM NaCl.

The zeta-potential was measured for the liposomes prepared in 10-140 mM NaCl and for 10 mM phosphate buffer (Fig 5.13). As the NaCl concentration increases, the zeta-potential on the particles decreases. This decrease in zeta-potential corresponds to a decrease in the particle size for the liposomes prepared in NaCl. Liposomes prepared in 10 mM phosphate buffer had a similar zeta-potential to those prepared in 10 mM NaCl; however, the particle size of the 10 mM phosphate buffer liposomes were more similar to liposomes prepared in 75 mM NaCl.

5.3.6. Automatic Particle Size Control

The feedforward model used related the flow rate to the particle size, type of lipid and salt concentration. The feedback control used a PID controller with the following settings: P = 1.5, I = 0.3 and D = 0.001. Two particle size set points were set during this experiment, i.e. 60 nm and 80 nm. Once the set point particle size was reached, the user adjusted the particle size set point to the other set point (Fig. 5.14). Initially, the feedforward algorithm was able to accurately predict

the particle size. After this initial prediction, the feedback algorithm took over to maintain the particle size at the set point. From Fig. 5.14, it was clearly demonstrated that the feedback control satisfactory maintained the mean particle size and was able to automatically adjust the flow rates to achieve the set point particle size (*i.e.* from 60nm to 80nm or vice versa). The PDI remained around 0.1 or less during the entire experiment. The DLS count rate fluctuated based on the flow rate conditions, but was within a range that was previously determined to provide satisfactory particle size analysis.

5.4. Discussion

5.4.1. In-line Liposomal Dilution

The first part of this work outlined the importance of degassing the liposomes at the end of the liposome formation stage prior to the ethanol dilution stage. As mentioned, the mixing of ethanol with an aqueous phase is exothermic and leads to sensible heat changes. These heat changes caused dissolved gas to leave the solution, forming bubbles/ an air-water interface. For DPPC liposomes, the presence of bubbles did not appear to affect the liposomal particle size distributions. For DMPC liposomes, the particle size distribution was affected at the lower aqueous phase I flow rates, but not at the higher flow rates. Moreover, it was observed that at the lower aqueous phase I flow rates (*i.e.* 70 mL/min), foam was visible for the DMPC liposomes, but not for the DPPC liposomes. This foaming may be due to a reduction in surface tension as temperature increased – subsequently causing an increase in the mobility of the lipid molecules. This analysis was further corroborated by Fig. 5.3 and Fig 5.4. In these figures, a change in temperature caused changes in liposomal mean particle size; although, to a greater extent for DMPC liposomes than for DPPC liposomes. In addition, DMPC liposomes exhibited an

increased particle size distribution (higher PDI) as temperatures exceeded 24°C and a significant change in mean particle size as temperatures exceeded 26°C. These events can be explained since the transition temperature for the DMPC phospholipid is around 24°C, which would cause this lipid to experience a more fluid-like behavior near and/or above this temperature.[2] This increased lipid mobility resulted in the formation of larger liposomes, as well as increased foaming. For the DPPC phospholipid, the phase transition temperature is closer to 41°C,[2] which explained why DPPC liposomes did not exhibit larger particle size changes compared to DMPC liposomes over the temperatures investigated.

When foam formed at the liposome formation stage and passed into the ethanol dilution stage (aqueous phase II), this dilution stage became a second stage of mixing, which caused the foam to mix back into the aqueous phase and formed a second population of liposomes. The liposomes formed at the dilution stage would then depend on the mixing at the dilution stage, *i.e.* the Reynolds number and temperature. Since the flow rates ranged from 460-660 mL/min, the Reynolds number at this stage would be >1000 and supported the formation of smaller liposomes. Therefore, with the addition of foam, a larger particle size distribution existed because essentially two populations of particles formed, one at the liposome formation stage and one at the ethanol dilution stage. By removing the foam after liposome formation, the tendency to form a second population of particles was reduced.

As previously explained, the Reynolds number may be used as a predictive measure of particle size; however, it is only suitable with fixed conditions such as lipid concentration, types of salts, salt concentrations, etc. A lower Reynolds number supports larger liposomes while a higher

Reynolds number supports smaller liposomes[37]. By lowering the temperature at the liposome formation stage, this would cause the Reynolds number to decrease, and the liposome particle size to decreases. Therefore, the Reynolds number alone is not a satisfactory measure for the liposome formation process. Instead, a more a thorough model should be established that takes into account factors such as the Reynolds number, temperature, lipid-phase transition temperature, lipid hydrocarbon saturation and buffer/salt composition.

5.4.2. Variables that Influence Particle Size Measurements

There are many important variables that influence accurate particle size measurement of liposomes for at-line measurements. These variables can be divided into processing variables and DLS measurement variables (Table 5.1). For processing variables, the first is the total dead volume, *i.e.* the volume of the tubing from the process stream to the flow cell plus the volume of the flow cell. This volume is important since this is the volume that must be replaced after each measurement; otherwise, liposomes that were formed at earlier time points will be mixed with liposomes formed at later time points. Large total dead volumes will incur a large time shift with respect to processing conditions.

A second processing variable is the process stream to flow cell velocity ratio. This ratio is the velocity of the liquid in the process stream divided by the velocity of the liquid flowing to the flow cell. In order to achieve a small time shift, this value must >>1. This variable is linked with the total dead volume since higher ratios cannot be achieved with large dead volumes, especially at flow rates around 1-1.5 mL/min. For example, the DLS flow cell volume used in these experiments is 100 µL and the total volume including the pump and tubing was approximately

220 µL. Moreover, if DLS measurements were taken every 15 seconds, then 250 µL of sample would pass through during this time. Ideally, since the flow cell has a larger volume than the tubing, it may require more volume to remove the entire previous sample (*i.e.* 2-3x the total dead volume) and longer delay times in between measurements would be required.

A third processing variable is whether laminar flow occurs. This variable is only important for the constant flow mode. For this variable, small inner diameter tubing (*e.g.* 0.01") may cause turbulence and affect the Brownian motion of the particles, thus resulting in incorrect particle size measurements. To reduce these effects, larger inner diameter tubing should be used; however, larger inner diameter tubing will increase the total dead volume.

DLS measurement variables include settings such as measurement duration, number of runs and attenuation factor. The measurement duration for each DLS run can be set in the Zetasizer software. For off-line DLS measurements, each measurement consisted of approximately 10-15 runs and each run lasted 10 seconds. The DLS data from each run was then combined to provide a single DLS result. Additionally, the mean count rate measured in kilo counts per second (kcps) should be greater than 20 kcps and less than 1000 kcps.[93] For lower photon counts, the data may not result in an accurate particle size analysis. For the at-line measurements, only a single run of 6 second duration was used for the DLS measurements, which would result in a low photon count. However, from Fig. 5.7 – Fig 5.11, the 6 second duration was adequate for determining the z-average particle size and in most cases, the PDI was similar for both off-line and at-line measurements. Shorter measurement durations (*e.g.* 3 seconds) may have also provided satisfactory results, but would lead to a lower photon count. Therefore, the at-line measurement

experiments used a longer measurement duration (*i.e.* 6 seconds) to achieve more consistent and higher quality data.

The attenuation factor is another important variable. A low attenuation factor refers to when a lesser amount of light passes through the sample and a high attenuation factor is when a greater amount of light passes through the sample (for a Malvern Zetasizer, the attenuation range is from 0-11, respectively). Changing the attenuation factor will cause the photon count rate to increase or decrease; however, very high count rates will no longer provide accurate data since the DLS detector has a maximum count rate where the response remains linear. For the off-line measurements, the count rate was set to "automatic" in the Zetasizer software. For the at-line measurements, the count rate was kept between 150-400 kcps by programmatically adjusting the attenuation factor depending on the particle size of the liposomes being tested. The advantage of a user-defined attenuation is the reduced overall time per measurement. The disadvantage is that the user-define attenuation factor may not allow for a sufficiently high photon count during measurement – resulting in lower quality data.

A fourth measurement variable is the presence of air bubbles in the sample. Air bubbles will affect the overall quality of the results since the air bubbles also scatter light. One way to circumvent this issue is to use a degassing unit between where the sample is taken and the DLS flow cell. The disadvantage of using a degassing unit is that the volume of the degassing unit adds to the total dead volume, resulting in longer measurement delays (Fig. 5.7).

5.4.3. At-line Particle Size Measurements Comparisons

By comparing the Continuous Flow mode vs. the Load/Stop Mode, the Load/Stop mode appeared to be more accurate and had a more consistent measurement time-delay. When using the Load/Stop mode, the entire sample was removed from the DLS flow cell since the flow rates were around 20-25 mL/min vs. 1-1.5 mL/min for the Continuous Flow mode. In addition, a larger inner diameter tubing was used for the Load/Stop mode and this may have reduced air bubble formation, resulting in fewer artifacts present with the DLS data. One disadvantage of the Load/Stop approach is the rapid loading of the flow cell, which does not allow for temperature equilibration. In this case, the sample temperature may be different than the temperature set in the DLS software, which could explain why the mean particle size, especially for smaller liposomes, was lower when compared to the off-line DLS measurement (Fig. 5.8). This deviation was only observed for small liposomes (*i.e.* <50 nm).

5.4.4. Ionic Strength on Liposome Formation

The ionic strength of the aqueous phase significantly affected the liposome mean particle size. From Fig. 5.12, 10 mM NaCl formed 70 nm liposomes and 140 mM NaCl formed around 160 nm liposomes at the same flow rate (*i.e.* 70 mL/min). The portion of the phospholipid molecule that is in contact with the aqueous phase is the phosphate head group. Accordingly, the head group may be changing in size (*e.g.* mean molecular area) and would influence lipid packing. Moreover, by comparing liposomes prepared in 10mM NaCl to 10 mM phosphate buffer (at pH 7.4), the liposomes prepared in 10 mM NaCl were smaller in diameter. When taking into account the ionic strength, the 10 mM phosphate buffer had an ionic strength greater than 10 mM NaCl

but less than 75 mM NaCl. Therefore, an increase in ionic strength caused an increase in liposomal mean particle size.

The ionic strength affects the electrostatic or charge repulsion of neighboring phospholipid molecules (Fig 5.12). At a low ionic strength (*e.g.* 10 mM NaCl), the repulsion would be greater than at 140 mM NaCl since a high salt concentration would lower the overall zeta-potential of the particles (Fig 5.13). This is explained by the Gouy-Chapman-Stern theory, which describes how increasing the salt concentration decreases the distance from the charged surface to the plane of shear[94]. When large amounts of charged species (*e.g.* Na^+) associate with negatively charged phospholipid membranes, the magnitude of the zeta-potential is reduced[95]. In addition, the amount of cholesterol in the lipid bilayer affects the binding of Na^+ to phospholipids and causes a reduction in the surface charge[96]. Moreover, different salt species (*e.g.* NaCl vs $NaSO_4$) will affect the overall surface charge density based on the lyotropic series[97], *i.e.* strongly hydrated anions cause a reduction in the surface charge density. According to a previously described liposome formation model, a lower zeta-potential (or surface charge density) may allow for more phospholipids to enter the pro-liposomes and hence result in the formation of larger liposomes.[37]

A second explanation for the increase in size with increase in NaCl concentration is related to local heat effects as the liposomes are initially forming. The excess enthalpy of mixing for the ternary mixture of ethanol, water and NaCl becomes more positive as the salt concentration increases[98]. Reduced enthalpy of mixing indicates more bond breaking events are occurring compared to low salt conditions, *i.e.* less water-ethanol hydrogen bond formation. This event

may suggest that more ethanol is interacting with the lipid molecules during the initial mixing stage, thus promoting larger lipid aggregates to form prior to liposomes formation. However, either explanation, *i.e.* electrostatic or changes in enthalpy of mixing would be difficult to measure directly since liposome formation is taking place at the molecular level and under turbulent flow conditions. A future study on changing the phospholipid molar ratio of the charged phospholipid may be a suitable alternative to exploring the effects of charge repulsion on the liposome formation process.

5.4.5. Automatic Particle Size Control

In the continuous manufacturing of liposomes, process changes such as pressure or temperature fluctuations will cause changes in the liposomal particle size during the liposome formation process. Using feedforward control to initially predict the process conditions (*i.e.* aqueous phase I flow rate) and a feedback control to maintain the particle size was demonstrated. By implementing these control strategies, liposomal critical quality attributes (*i.e.* mean particle size and particle size distribution) could be maintained, which supported an overall higher quality formulation.

5.5. Conclusions

In-line dilution of liposomes to reduce the ethanol concentration was implemented in this continuous process to form liposomes. Incorporating the in-line dilution stage post the liposome formation process may cause changes to the liposomal particle size distribution – depending on the liposomal formulation. Therefore, it was determined to be necessary to include a degassing unit post liposome formation and prior to the in-line dilution stage. At-line particle size analysis

was implemented into the continuous processing of liposomes. To reduce time delays between process changes (*i.e.* flow rates) and the particle size measurement data, it was determined that the Load/Stop mode provided more consistent results when compared with the Continuous flow mode. In addition, the ionic strength of the aqueous phase significantly impacted the mean particle size of the liposomes, *i.e.* an increase in ionic strength favored the formation of larger liposomes. Lastly, automatic particle size analysis was implemented using both a feedforward and a feedback control, which resulted in precise control and maintenance of the liposomal particle size and polydispersity index.

5.6. Tables

Table 5.1. Variables that Influence Continuous Particle Size Measurements

Processing Variable	DLS Measurement Variables
Total Dead Volume	Measurement Duration
Process Stream to Flow Cell Velocity Ratio	Attenuation Factor
Laminar Flow Rates[a]	Sample Temperature
	Air Bubble Presence

a = applicable only for constant flow approach

5.7. Figures

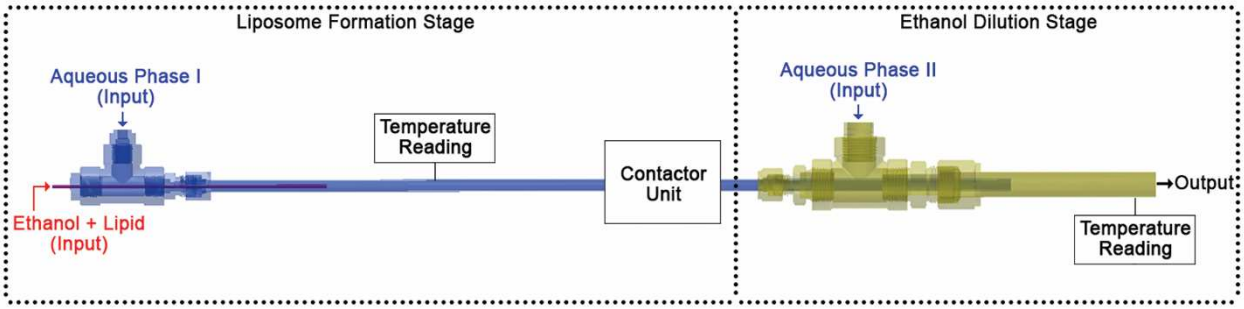

Fig. 5.1 Schematic representation of the liposome formation stage followed by the ethanol dilution stage. Two temperature readings via thermocouples are taken at each stage and a contactor (degassing unit) is positioned in some cases at the end of the liposome formation stage.

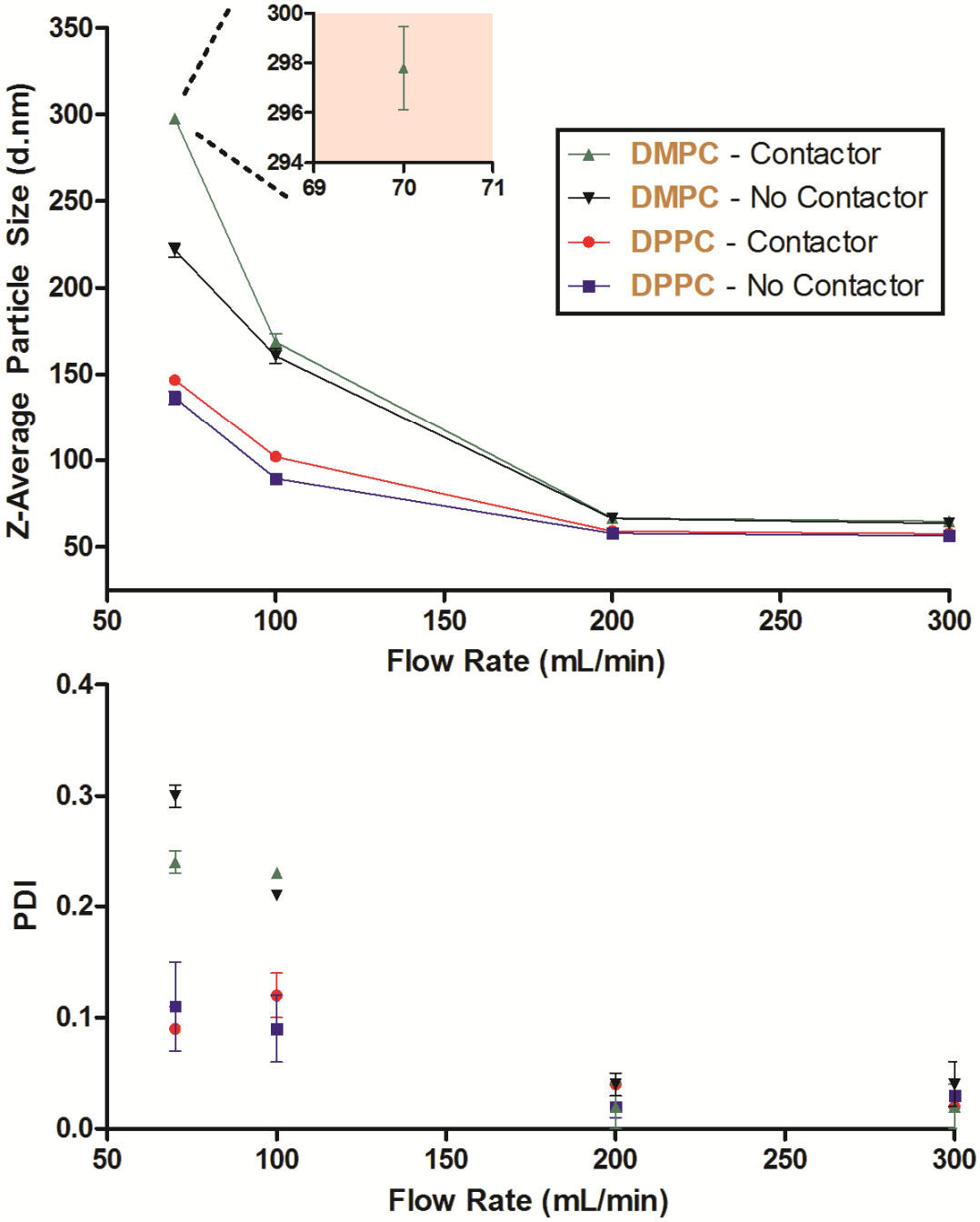

Fig 5.2 Liposome mean particle size and polydispersity index for both *lipid*:Chol:DPPG (4.5:3:0.4 molar ratio) liposomes, where *lipid* refers to either DMPC or DPPC. Both z-average particle size (top) and polydispersity index (PDI, bottom) are plotted vs. aqueous phase I flow rate (mL/min).

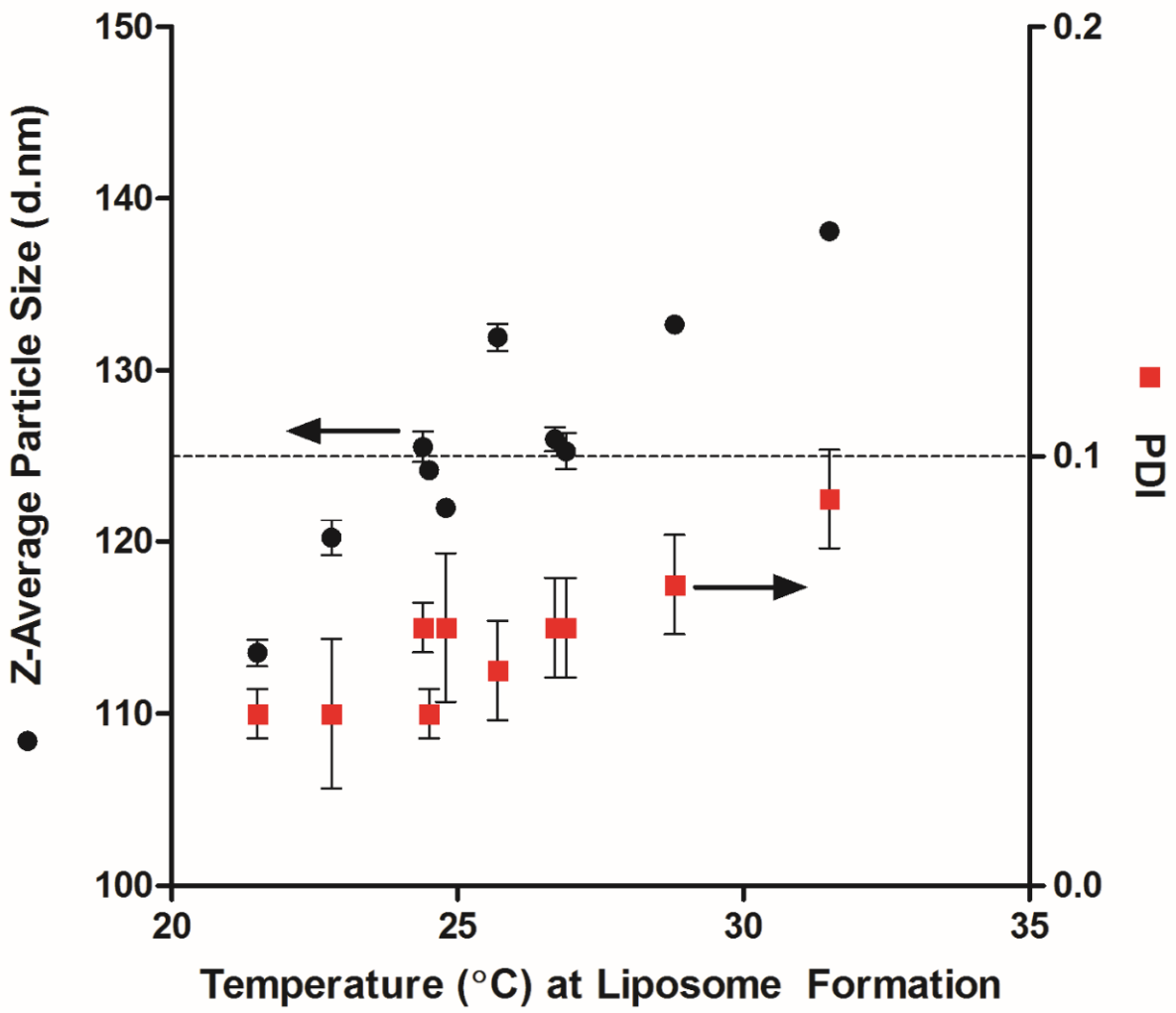

Fig 5.3 Liposome mean particle size and polydispersity index for DPPC:Chol:DPPG (4.5:3:0.4 molar ratio) liposomes. The mean particle size and PDI is plotted against the temperature (°C) at the liposome formation site (see Fig 5.1). The aqueous phase I flow rate was kept constant at 80 mL/min.

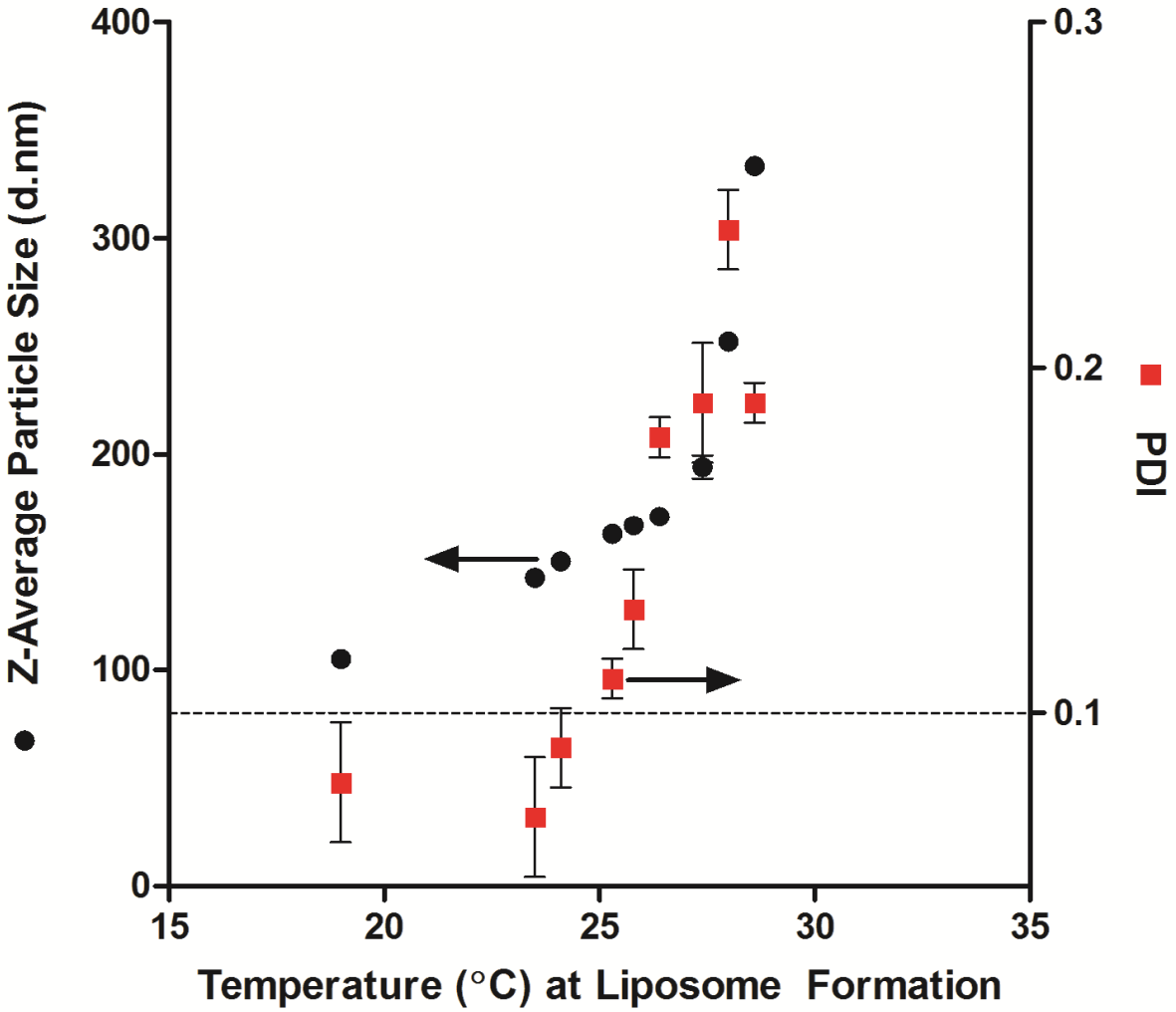

Fig 5.4 Liposome mean particle size and polydispersity index for DMPC:Chol:DPPG (4.5:3:0.4 molar ratio) liposomes. The mean particle size and PDI is plotted against the temperature (°C) at the liposome formation site (see Fig 5.1). The aqueous phase I flow rate was kept constant at 70 mL/min.

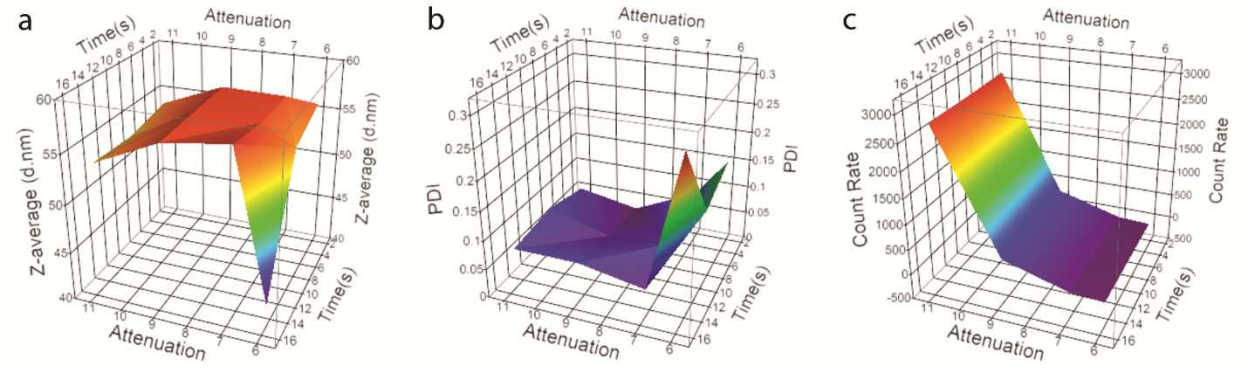

Fig 5.5 A comparison of manual DLS measurement settings on the liposome particle size (z-average), the PDI and the DLS count rate (kcps). All results were from a single run at either 3, 9 or 15 seconds. The liposome formulation was the same for all measurements and had a z-average of 56.50 ± 0.03 nm, a PDI of 0.05 ± 0.02 and a count rate of 401.4 ± 2.77.

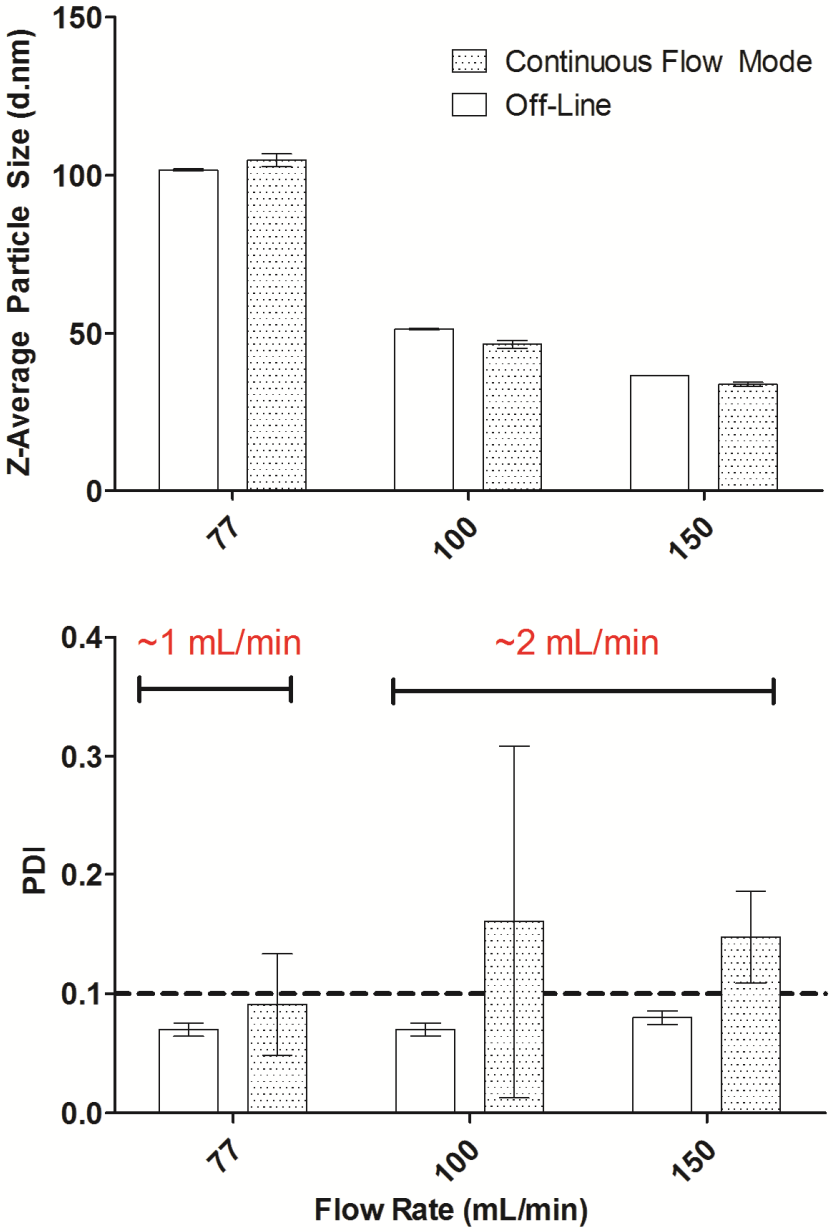

Fig 5.6 Liposome mean particle size and polydispersity index for DPPC:Chol:DPPG (4.5:3:0.4 molar ratio) liposomes. The mean particle size and PDI is plotted against aqueous phase I flow rate. The flow rates in the bottom plot in red are the DLS flow rates or the flow rate of the sample during the DLS measurement.

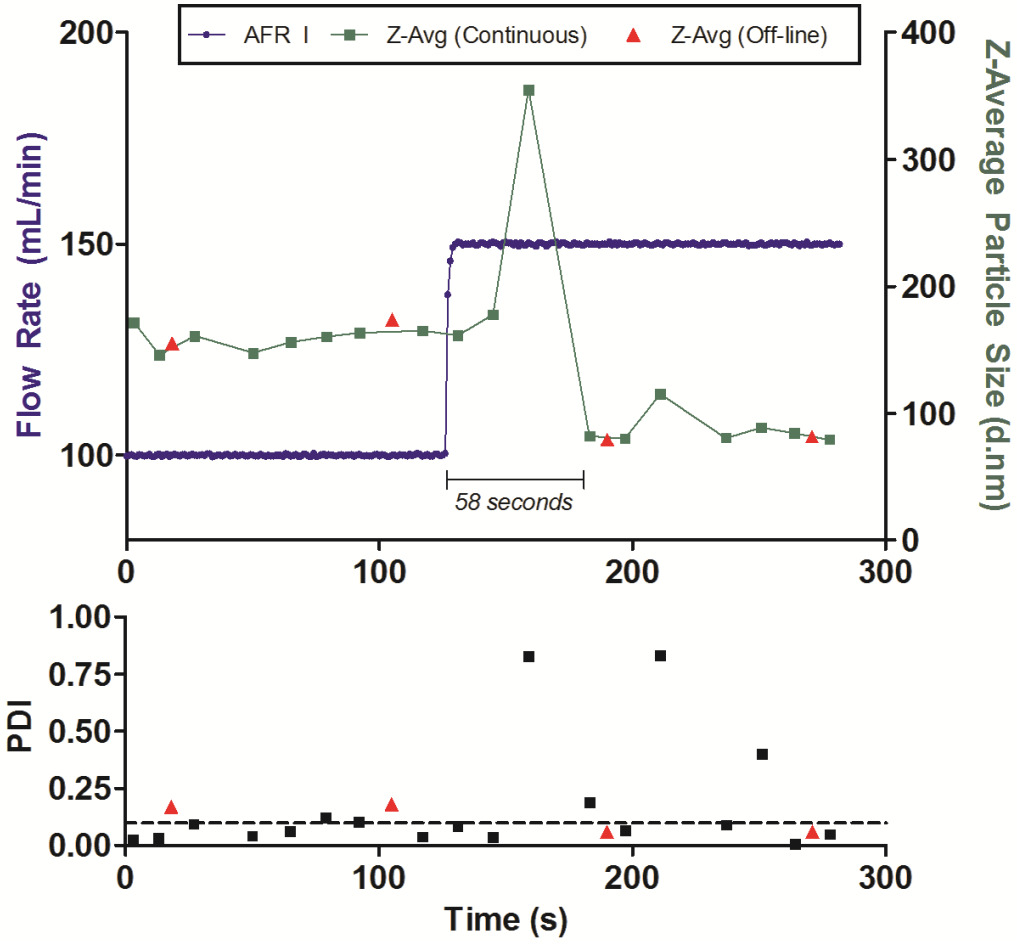

Fig 5.7 Liposome mean particle size and polydispersity index (PDI) for DMPC:Chol:DPPG (4.5:3:0.4 molar ratio) liposomes in 10 mM Phosphate Buffer. The mean particle size, PDI and aqueous phase I flow rate is plotted over a period of time. The DLS flow rate was fixed at 1 mL/min. The aqueous phase was initially at 15°C prior to liposome formation.

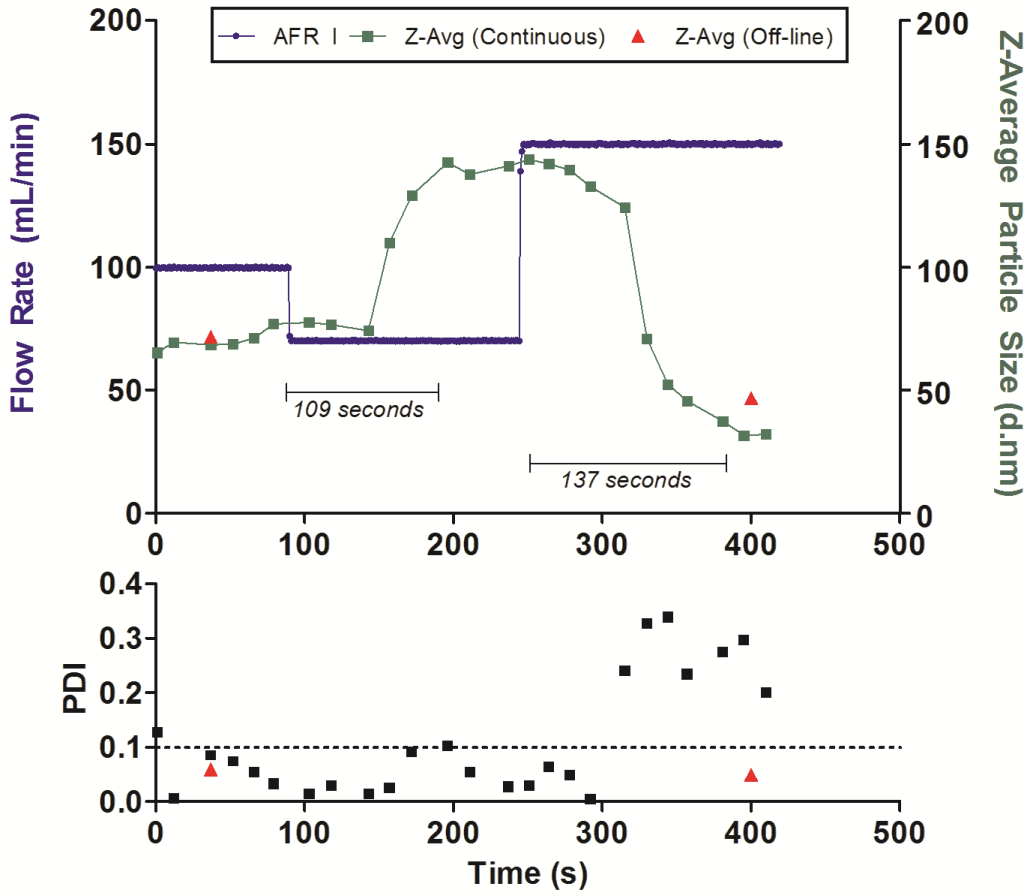

Fig 5.8 Liposome mean particle size and polydispersity index (PDI) for DPPC:Chol:DPPG (4.5:3:0.4 molar ratio) liposomes in 10 mM Hepes buffer. The mean particle size, PDI and aqueous phase I flow rate is plotted over a period of time. The DLS flow rate was fixed at 1 mL/min.

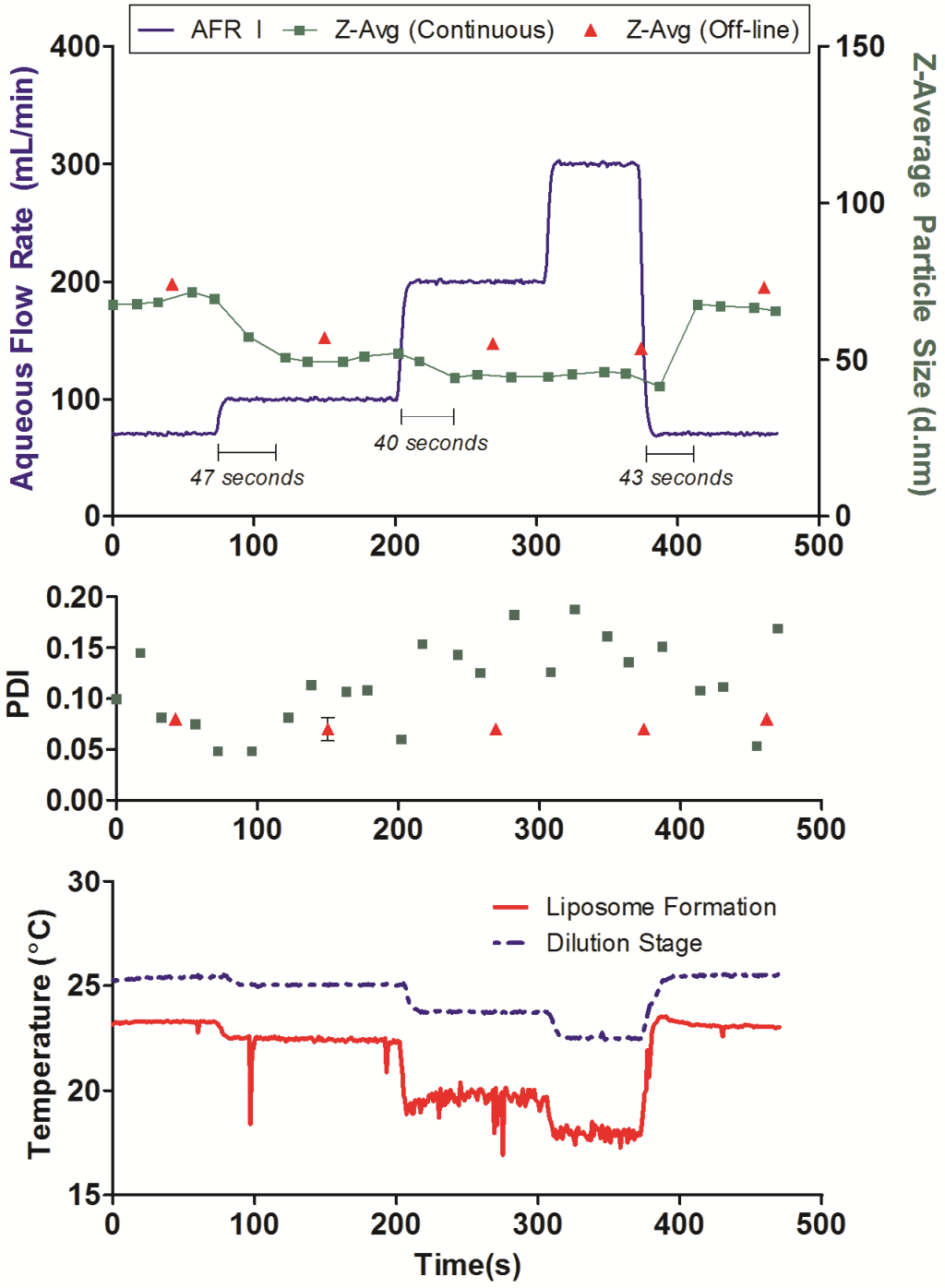

Fig 5.9 Liposome mean particle size and polydispersity index (PDI) for DPPC:Chol:DPPG (4.5:3:0.4 molar ratio) liposomes in 10 mM NaCl. The mean particle size, PDI and aqueous phase I (AFR I) flow rate is plotted over a period of time.

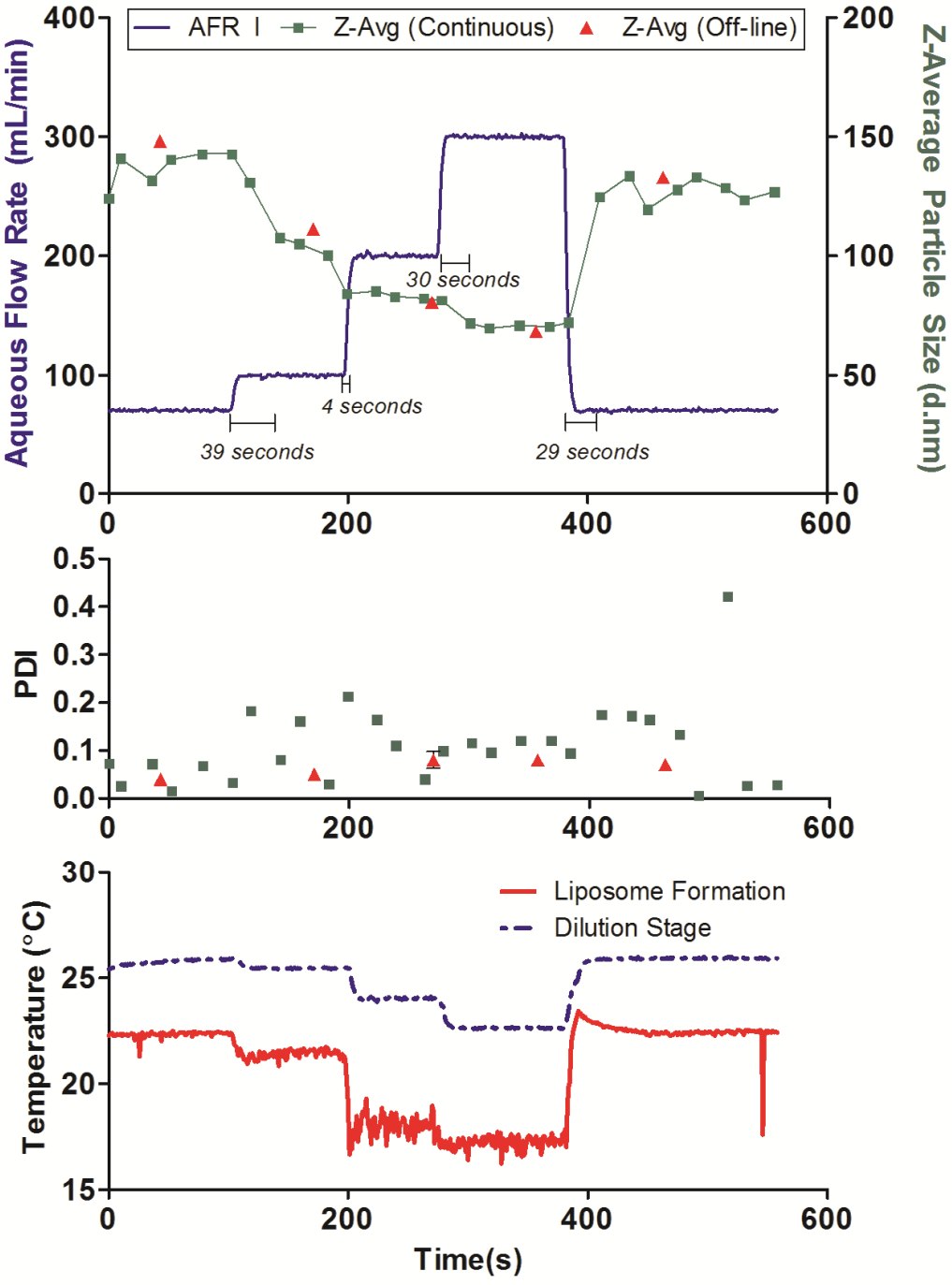

Fig 5.10 Liposome mean particle size and polydispersity index (PDI) for DPPC:Chol:DPPG (4.5:3:0.4 molar ratio) liposomes in 75 mM NaCl. The mean particle size, PDI and aqueous phase I (AFR I) flow rate is plotted over a period of time.

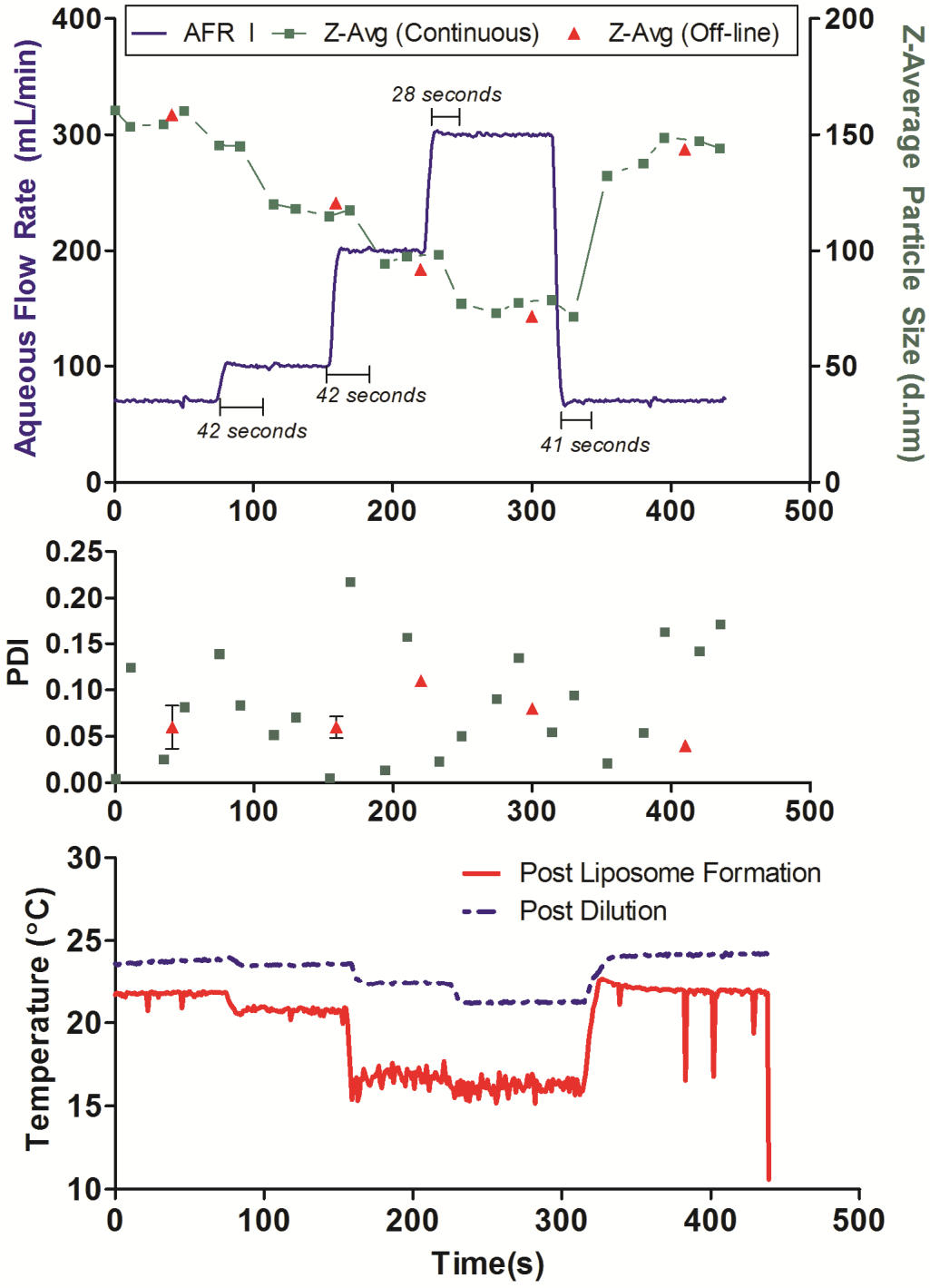

Fig 5.11 Liposome mean particle size and polydispersity index (PDI) for DPPC:Chol:DPPG (4.5:3:0.4 molar ratio) liposomes in 140 mM NaCl. The mean particle size, PDI and aqueous phase I (AFR I) flow rate is plotted over a period of time.

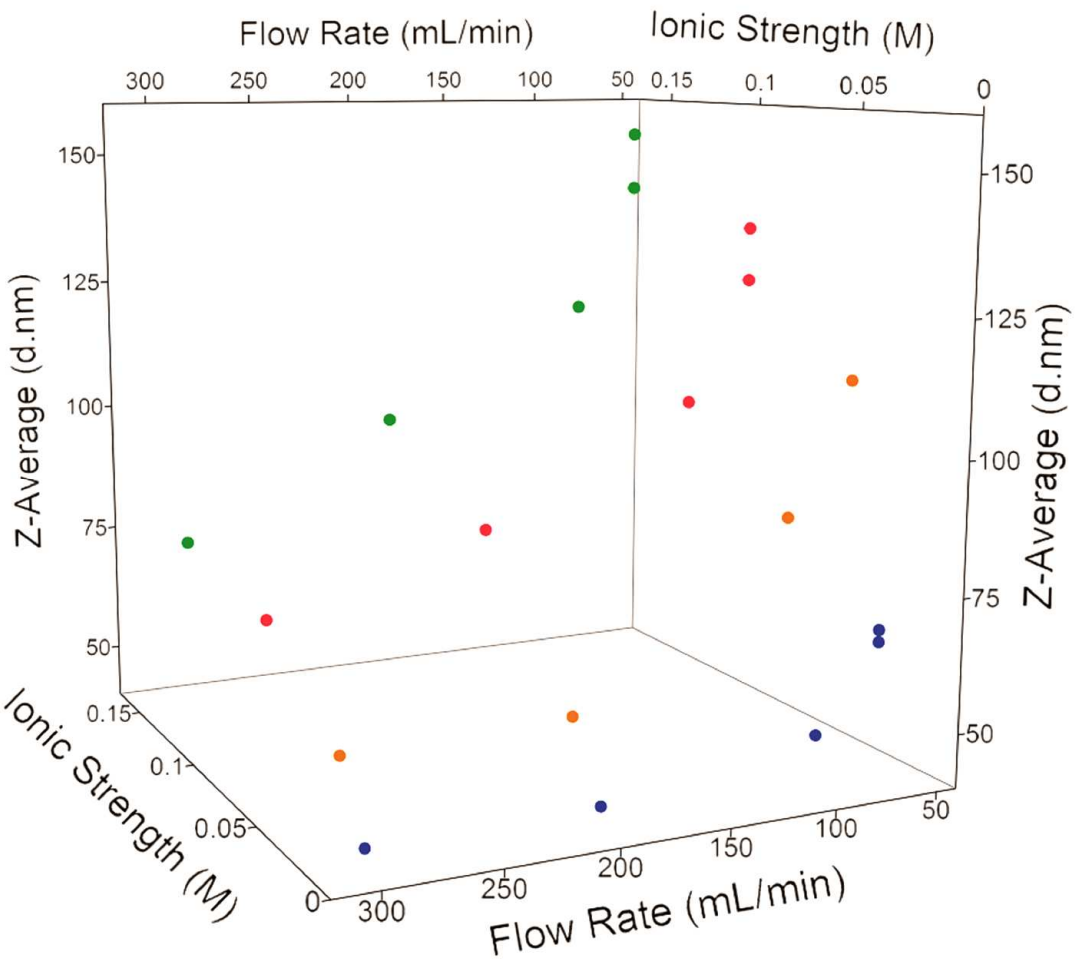

Fig 5.12 Liposome mean particle size (z-average, d.nm) for DPPC:Chol:DPPG (4.5:3:0.4 molar ratio) liposomes in 10-140 mM NaCl (green, red, blue) and 10 mM PB (orange). The mean particle size is plotted against the aqueous phase I flow rate and the ionic strength.

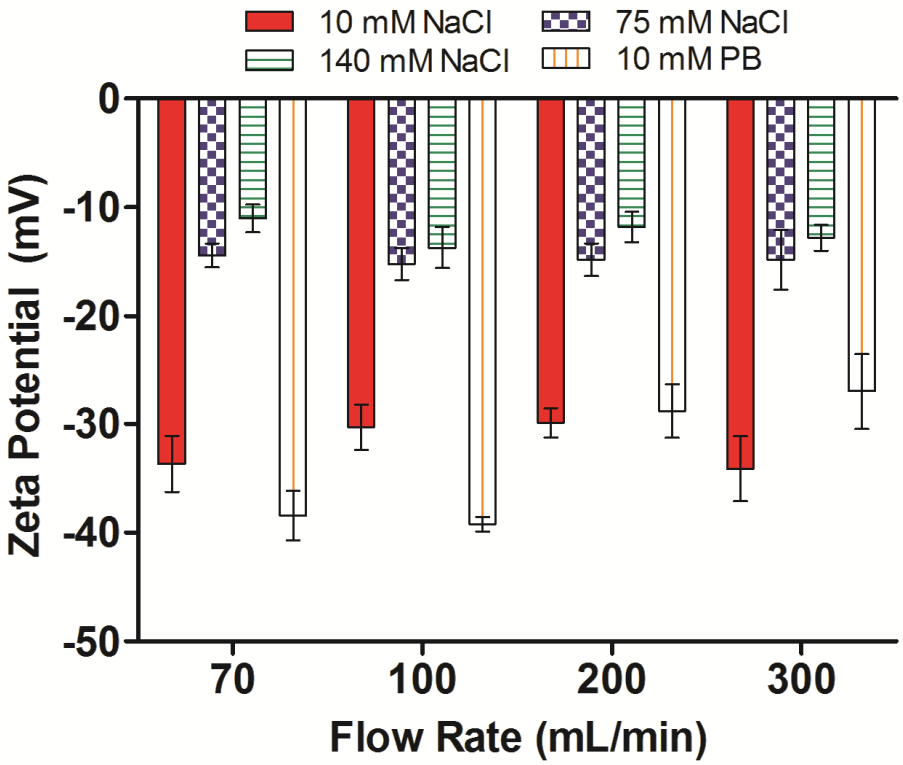

Fig 5.13 Liposome zeta potential for DPPC:Chol:DPPG (4.5:3:0.4 molar ratio) liposomes in 10-140 mM NaCl and 10 mM phosphate buffer (PB). The zeta potential is plotted against the aqueous phase I flow rate.

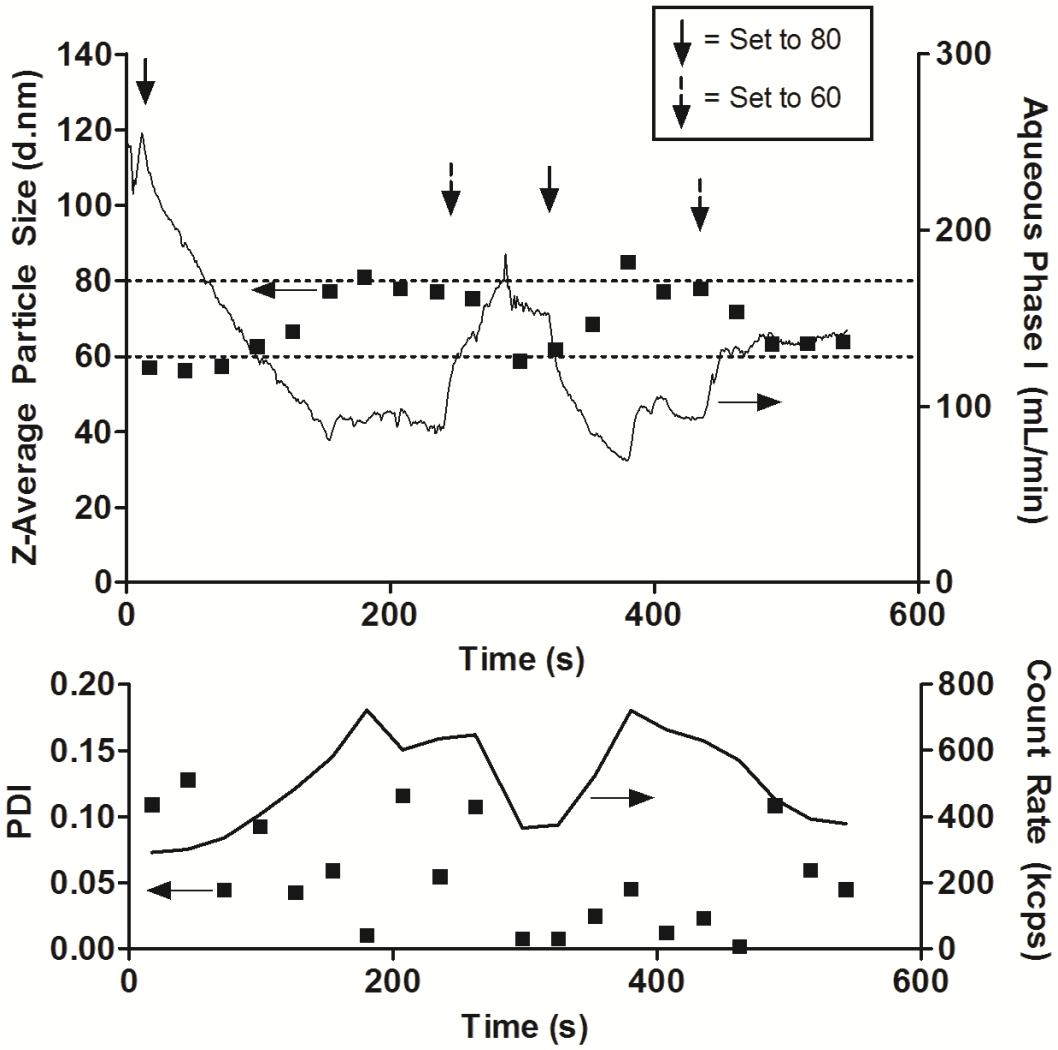

Fig 5.14 An example of automatic particle size control for HSPC:Chol:DPPG (4.5:3:0.4 molar ratio) liposomes prepared in 10 mM NaCl is shown. The mean particle size, polydispersity index (PDI), count rate (kcps) and aqueous phase I flow rate (mL/min) is plotted against time (s). The arrows indicate when the user changed the particle size set point in the software.

Chapter 6

Continuous Processing of Liposomes with In-line Concentrating

6.1 Abstract

Continuous processing is an approach that supports and ultimately leads to higher quality drug products. In the current work, a concentrating system was integrated with a previously designed continuous process for forming liposomes. The combination of both systems leads to improved control over the final liposomal formulation. Liposomes were prepared by a modified ethanol injection method. A dual channel turbidity sensor using two simultaneous channels, *i.e.* light absorption and light scattering; combined with a tangential flow filtration device, a pump and a custom developed computer program was used to control the concentration. In addition, an empirical equation was developed using the quality design approach to predict the final lipid concentration.

6.2. Introduction

Continuous processing is an approach that supports and ultimately leads to higher quality drug products. A major challenge in developing a continuous process is process control. Process control may include simple measurements such as temperature, pressure and volumetric flow rates and more advanced measurements such as particle size, particle size distribution and the concentration of excipients/active pharmaceutical ingredients. In order to continuously control a specific process in real-time, process analytical technology (PAT) under closed loop control

should be implemented. In addition, using tools related to the quality be design approach will enhance the overall process control. In the current work, a concentrating system was integrated with a previously designed continuous process for forming liposomes[37] (Chapter 4 and Chapter 5). The combination of both systems leads to improved control over the final liposomal formulation.

The total lipid concentration is a critical quality attribute for liposomal drug products. The total lipid concentration may refer to the amount of phospholipid and/or other lipid molecules such as cholesterol that form the liposomal bilayer. The lipid concentration can be used to estimate the amount of liposomal vesicles, which may further be related to either drug encapsulation[25], *i.e.* drug molecules in the aqueous compartment of the liposomes, to drug loading[99] or to the intercalation of molecules within the lipid bilayer[100]. In addition, lipid concentration is used to effectively evaluate drug-to-lipid ratios. For example, doxorubicin-to-lipid ratios of 0.3:1 led to an increase in biological activity in mice[29].

Liposomal lipid concentrations may be toxic depending on the type of lipid in the liposome composition. For example, phosphatidylglycerol and phosphatidylserine liposomes were toxic from 0.13-3.0 mM for some cultured human cell lines whereas dipalmitoylphosphatidylcholine containing liposomes were non-toxic at 4 mM.[101] In addition, certain lipid concentrations may promote cytotoxicity and can be used as a measure to determine drug effects on changes in IC_{50} – values. For example, amphotericin B containing liposomes increased the IC_{50}-value in a macrophage-like cell line (Raw 264.7) when compared to liposomes without amphotericin B.[102]

Moreover, macrophage cells are major sites of liposomal accumulation[103] and high lipid concentrations may cause macrophage cells to exhibit phospholipid overload and inhibit phagocytic function[104-105].

FDA-approved drug products are formulated with total lipid concentrations ranging from 9.15 mg/mL up to 103 mg/mL, with the majority in the range from 9.15 mg/mL – 34.88 mg/mL.[27, 79-84] This provides a pharmaceutically relevant range of lipid concentrations that are considered safe and effective. It should be noted that the lipid concentration alone is not sufficient in determining safety, as the individual lipid components may be cytotoxic, especially cationic lipids[106]. In the current study, the concentrating system should at least be capable of concentrating the liposomes to achieve a lipid concentration within the stated range – making the system pharmaceutically feasible.

6.2. Materials and Methods

6.2.1. Materials

1,2-dipalmitoyl-*sn*-glycero-3-phosphocholine (DPPC), 1,2-dipalmitoyl-*sn*-glycero-3-phospho-(1'-*rac*-glycerol) (sodium salt) (DPPG-Na) and Lipoid S PC-3 (HSPC) were purchased from Lipoid™. Cholesterol (Chol) was purchased from Sigma. Ethanol (200 proof, ACS/USP grade) was purchased from Pharmco-AAPER.

6.2.2. Experimental Methods

6.2.2.1. Liposome Formation and Dilution

Liposomes were prepared by a modified ethanol injection method. A schematic of this system is depicted in Chapter 5, Fig. 5.1. Three separate 316 stainless steel tanks contained the lipid+ethanol solution. These tanks were pressurized (at 20 psi) and the flow rates from these tanks were controlled using analog flow meters (McMillian) and proportioning solenoid valves (Aalborg). The flow meters were factory calibrated for water with less than 1% error full-scale. For the lipid+ethanol flow streams, these flow sensors were re-calibrated for ethanol and had an R-squared value of 0.9989, with a working range from 5-50 mL/min. The three tanks were then connected at a single point using a 4-way connector (Swagelok). A static mixer was implemented to ensure that the lipid+ethanol solutions from the three tanks were adequately mixed prior to reaching the injection port where the ethanol and aqueous phase 1 streams converged. The aqueous phase I volumetric flow rate was controlled by a gear pump (Micropump®). To form liposomes, the mixed lipid+ethanol solution was then injected into an aqueous phase (aqueous phase I) at various flow rates. The tubing ID of the ethanol phase was 0.508 mm (1.588 mm OD). The aqueous phase I tubing ID was fixed at 4.572 mm. Flow rates of the lipid+ethanol phase were from 5-40 mL/min and aqueous phase I were from 70-300 mL/min. After the liposomes were formed, the liposomes passed through a degassing unit (Liqui-Cel®) followed by a second three-way T-port. This three-way T-port has one inlet for the liposomes, a second inlet for aqueous buffer and one outlet. A second gear pump (Micropump®) was used to control the flow of the aqueous phase into this port (aqueous phase II). The aqueous phase II flow rate was adjusted such that mixed aqueous phase would always have 5% vol. ethanol. Aqueous phase II flow rates ranged from 690-460 mL/min.

6.2.2.2. Data Acquisition System and Computer Software

The entire process was controlled by a custom-made program written using National Instruments (NI) LabVIEW® software. A data acquisition system (NI PXIe-1078) was combined with multiple NI modules to accommodate various input/output signals (*e.g.* analog and digital inputs/outputs, counters, circuit switches, *etc.*). The entire system was automated and only required the user to define the final lipid concentration and molar ratios of lipid. Process variables such as flow rates, pressure, and temperature were monitored and, for some variables, automatically adjusted using custom computer algorithms. For example, proportional-integral-derivative controls were implemented in the computer program to precisely control the flow rates of both the ethanol and aqueous phases.

Communication to and from the Malvern Zetasizer was accomplished using the Malvern Link II software. Malvern Link II software was setup as an OPC server and NI LabVIEW was setup as an OPC client. The z-average particle size and PDI were recorded in the custom computer program. The custom computer program was able to send measurement instructions to the Malvern Zetasizer.

6.2.2.3. Particle Size Measurements

All particle size measurements were performed using a Malvern Zetasizer Nano S. Prior to measurements, the liposomes were diluted in-line to 5% vol. ethanol and the viscosity and refractive index were pre-set in the Malvern Zetasizer software. Particle size measurements included the z-average particle size and polydispersity index (PDI). For the off-line measurements, disposable plastic cuvettes were used. The samples were equilibrated at 25°C

prior to each measurement. Each off-line measurement duration was set for 10 runs at 10 seconds each with n=3.

For at-line measurements, a flow cell equilibrated at 25°C was used. The measurement duration was set to 1 run for 6 seconds. The Load/Stop Mode, based on loading the flow cell followed by stopping the flow prior to the measurement, was used in all cases (see Chapter 5). A Micropump® pump was used to control the flow through the flow cell (20-25 mL/min). The pump operated at the specified flow rate prior to the particle size measurement. Before any measurement took place, the custom computer algorithm stopped the pump to prevent fluid flow during the measurement.

6.2.2.4. NIR (Turbidity) Measurements

An Optek® TF16-N Scattered light dual channel turbidity sensor was used for the measurements. This device has two simultaneous channels, the first measures light absorption, *i.e.* this principle is based on detecting the light at 0° from the light source by a single hermetically sealed photodiode. This measurement is in concentration units (CU). The second measurement principle is based on light scattering and the scattered light is detected at 11° by eight hermetically sealed silicon photodiodes. This measurement is reported in parts per million (PPM). The measurement wavelengths are a band ranging from 730 nm to 970 nm. The optical path length of the sensor is fixed at 40 mm and is in a flow cell configuration, *i.e.* has an inlet and outlet for in-line application. The linearity of the sensor is $< \pm 1\%$ of the full scale for each measurement and has a repeatability of $< \pm 0.5\%$.

6.2.2.5. Tangential Flow Filtration System

An EMD Millipore Pellicon Mini Holder with Pellicon 2 Mini Ultrafiltration Biomax-100 modules was used as the tangential flow filtration (TFF) device. This device was connected to a peristaltic pump (Blue-White Industries, LTD) to control the flow rate. A pressure transducer and solenoid valve were connected to the output of the TFF device. The pump, pressure transducer and the solenoid valve were connected to the custom LabVIEW computer program (Fig. 6.1.).

6.2.2.6. Lipid Concentration Analysis via the Stewart Assay

The Stewart assay is a UV-spectrometric technique that determines the amount of phospholipid present. Briefly, ammonium ferrothiocyanate (AF) was prepared by dissolving 13.52 g of ferric chloride hexahydrate and 15.2 g of ammonium thiocyanate in 0.5 liters of deionized water. A calibration curve was generated by taking 10 – 70 mg of phospholipid stock solution (originally dissolved in ethanol) added to approximately 3 mg of chloroform. 2 mL of the AF solution was added to this mixture, which was then vortexed for 30 seconds followed by centrifugation at 1,500 rpm for 2 minutes. The AF was removed and the chloroform containing lipid was analyzed using a Cary 50 UV-spectrophotometer at 470 nm. The calibration curve consisted of 9 values with a quantitation limit (QL) of 0.023 µg/mL and an R-squared of 0.997.

6.2.2.6. Lipid Concentration Analysis via high pressure liquid chromatograph – Mass spectrometry

The lipid concentration was determined using a high pressure liquid chromatography (HPLC) with a mass spectrometer (MS). A Waters Xbridge C8, 3.5 um, 4.6x75 mm column heated at

30°C was used for lipid separation. The mobile phase was 2 mM ammonium formate in MS-grade methanol. The flow rate was set at 0.3 mL/min and 3 µL of sample was injected for each measurement. An ESI probe was used and the operating conditions were optimized in the TSQ software (table 6.1).

The sample was analyzed for the main phospholipid depending on the lipid formulation, *i.e.* for DPPC. The raw chromatographic data was transformed using a power function value (PFV) and the area under the curve was calculated. The tailing factor was less than 1.20 for each peak. The calibration curves had a QL of approximately 1.22 ug/mL and the R-squared value was >0.996. The PFV used for DPPC was 1.23.

6.2.2.6. Lipid Concentration Prediction Models

JMP by SAS was used to generate prediction models and equations. Two models (defined as Model 1 and Model 2) were generated that had the response as the total lipid concentration ([Lipid]) in units of mM. The possible factors for the model were the NIR measurements (both CU and ppm) the z-average particle size (d.nm) and the polydispersity index (PDI). Model 1 only included particle size and ppm as factors. Only monodispersed liposome (*i.e.* having a PDI $\leq$ 0.1) were used to generate this model. The experimental design for Model 1 is outlined in Fig 6.2. Since the ppm signal was highly dependent on the particle size, a typical experimental design (*e.g.* full factorial) was difficult to achieve. In addition, the maximum concentration reported for this model was approximately 7 mM total lipid. Higher total lipid concentrations would be required to achieve a higher ppm signal for the smaller particle sizes (*e.g.* 50 nm vs.

150 nm). Model 2 is an extension of Model 1 and included particle size, PDI, ppm and CU as factors. The experimental design of Model 2 is outlined in Fig. 6.3.

6.3. Results

6.3.1. Prediction Models

The liposomal particle size diameter ranged from 55 nm to 188 nm. For Model 1, the PDI was less than 0.10 for all sizes and concentrations tested. The total lipid concentration ranged from 0.38 mM up to 7.96 mM. The significant terms ($P<0.05$) were particle size, particle size*ppm and ppm (Table 6.2). Both the particle size and particle size*ppm negatively impacted the lipid concentration, whereas an increase in ppm related to an increase in lipid concentration. The NIR CU measurement did not correlate with the model and was omitted. The R-squared for the actual vs. prediction lipid concentration was 0.931, indicating a linear relationship. The model had 15 observations (with 3 degrees of freedom for the model), a RMSE of 0.587 and an analysis of variance <0.001.

The surface profile for Model 1 is demonstrated in Fig. 6.4. The profile is of ppm vs. particle size vs. total lipid concentration. As the particle size increases, the ppm vs. [Lipid] slope increases and higher ppm values are reached for lower lipid concentrations. The smaller sized liposomes only reached approximately 30 ppm for the same maximum [Lipid], whereas the large liposomes reached up to 70 ppm. The empirical prediction equation for the model is in Fig 6.5. This equation was implemented into the custom computer program to predict the lipid concentration based on both particle size and turbidity measurements.

For Model 2, the same particle size diameter range was used as outlined in Model 1 above. The total lipid concentration ranged from 0.38 up to 20 mM. Significant terms for Model 2 are listed in Table 6.3, with particle size*ppm and ppm as the most significant. Both the CU and PDI also had statistical significant terms in the model. The R-squared for the actual vs. prediction lipid concentration was 0.987, indicating a linear relationship. The model had 35 observations (with 11 degrees of freedom for the model), a RMSE of 0.527 and an analysis of variance <0.001. The empirical prediction equation for Model 2 is in Fig 6.6.

A validation for both Model 1 and Model 2 was included. The liposomes had a mean particle size of 167 ± 4.40 nm and a PDI of 0.05 ± 0.02 (Table 6.4). The total lipid concentration range measured was from 1.80 – 7.07 mM. As the PDI was less than 0.1, both models could be used to predict the mean particle size, with the mean error less than equal to 7.5%. When comparing the percent error of the measured [Lipid] to the predicted [Lipid], a two-tailed, paired t-test resulted in a p-value of 0.23, indicating that the differences between the sets of data are insignificant.

6.3.2. Polydispersity on the NIR Signal

A comparison was made between two sets of data for liposomes of a similar particle size but with differences in the PDI. The lower PDI (≤ 0.1) indicates a single population of particles, whereas a higher PDI indicates multiple populations of particles present. From Fig. 6.7, it is evident that the PDI is a critical factor that must be controlled. The liposomes with a mean particle size of 149 nm and a PDI of 0.18 ± 0.02 produced a PPM signal greater than those with a mean diameter of 170 nm and a PDI of 0.06 ± 0.02.

6.4. Discussion

6.4.1 Lipid Concentration Model

The relationship between scattered light and particle size are explained by Mie scattering theory. The Mie theory explains light scattering by an induced dipole moment from an incident electromagnetic wave. The induced dipole acts as a source of electromagnetic radiation and emits or scatters light at the same frequency as the source, *i.e.* elastic scattering. This theory provides an angular dependence of the scattered light based on the incident wavelength and the particle size. Relationships between liposomal particle size and light scattering and turbidity have been previously analyzed for liposomes.[107-109] The theory is based on an approximation of the Mie scattering theory, called the Rayleigh-Gans-Debye approximation. From this approximation, lipid concentration may be estimated at a fixed incident wavelength if additional properties such as the refractive index of the aqueous medium and the refractive index of the lipid bilayer are known[109]. However, this approximation may not be suitable for the current case since the incident radiation is a band of wavelengths covering 730-970 nm. In addition, the liposomes in this study were both monodispersed and polydispersed, which would further cause difficulties in using theoretical approximations to predict the total lipid concentration. For this reason, an empirical model was developed to relate liposomal particle size, PDI and the NIR signals (ppm and CU) to the total lipid concentration.

As expected, smaller particles scatter less light compared to larger particles. For this reason, the ppm/CU increases as the particle size increases. Two predictive models were generated; the first for only monodispersed liposomes (*i.e.* liposomes with a PDI $\leq$ 0.10) and the second included liposomal formulations with a higher PDI (PDI > 0.10). For the monodispersed liposomal model,

detection at 0° (measured in CU) did not appear to have any correlation with particle size and concentration at the concentrations measured. The CU did increase linearly with an increase in lipid concentration, but did not form a correlation when comparing different particle size liposomes. In contrast, the scattered light at 11° (*i.e.* the ppm) demonstrated a correlation with both liposomal particle size and total lipid concentration. For this reason, only the scattered light was used in the prediction model for monodispersed liposomes. Moreover, since the ppm signal is referenced to the medium, the NIR sensor was able to measure low lipid concentrations and the detection was not affected by additions to the aqueous phase (*e.g.* ethanol).

For the second model (Model 2), the CU signal and the particle size PDI were added to Model 1. This addition to the model enabled the total lipid concentration to be predicted for both monodispersed and polydispersed liposomal formulations. The addition of a polydispersity term into the model enhances the overall predictability of the total lipid concentration for both monodispersed and polydispersed systems. The validation sample set demonstrated the robustness of both models. By comparing the mean error for each model, the error was insignificant, indicating that each model could be used for low PDI formulations. However, Model 1 could not be used for higher PDI formulations. These results demonstrated that a empirical model with only 3 degrees of freedom could predict the particle size of monodispersed liposomes; whereas an empirical model with 11 degrees of freedom was required for polydispersed samples. Therefore, when liposomes are formed with a low polydispersity, a relatively simple and low degree of freedom model may be used to predict the total lipid concentration of the liposomes.

6.4.2 Polydispersity on NIR Detection

To emphasize how the polydispersity of the sample negatively impacted the prediction model, two data sets were plotted. The result that a high PDI sample increased the scattered light was expected as multiple populations of liposomes in the same sample will cause large variations in the scattered light. From the Mie theory, large particles will scatter more light in the forward direction than smaller particles. In addition, larger diameter particles scatter more light. The combination of a change in the angular scattering and scattering intensity prevented this model from predicting the lipid concentration. Therefore, a limitation to Model 1 is that it is only applicable to monodispersed liposomes. For polydispersed liposomes, Model 2 should be used to predict the total lipid concentration.

6.5. Conclusions

A tangential flow filtration system was implemented with a continuous liposome formation process to continuously concentrate liposomes in-line. Empirical models were developed for both monodispersed and polydispersed liposomes that had the total lipid concentration as the model response. These models can predict the lipid concentration from 0.38 up to 20 mM total lipid for particle size diameters from approximately 50 nm up to 200 nm. One limitation for Model 1 is that it is only applicable to monodispersed liposomes. Model 2 has predictive power for both monodispersed and polydispersed, but requires a model with 11 degrees of freedom. The implementation of the concentrating system and predictive models into a continuous process for liposomes enhances process control. Moreover, this system results in effectively controlling an important critical quality attribute (*i.e.* lipid concentration) of liposomal drug products.

6.5. Tables

Table 6.1: TSQ HPLC-MS ESI Operating Conditions used in the Analysis of Lipid Concentration Quantitation.

Spray Voltage	4000
Sheath Gas Pressure	20
Ion Sweep Gas Pressure	8
Aux. Gas Pressure	5
Capillary Temperature	350
Tube Lense Offset	131
Skimmer Offset	0

Table 6.2: Sorted parameter estimates and model terms for Model 1.

Term	Estimate	Std Error	t Ratio	Prob>|t|
Particle Size (d.nm)	-49.1	11.2	-4.4	0.0011*
Particle Size (d.nm)*ppm	-46.9	11.9	-3.9	0.0023*
ppm	10.7	6.0	1.8	0.1046

Table 6.3: Sorted parameter estimates and model terms for Model 2.

Term	Estimate	Std Error	t Ratio	Prob>|t|
Particle Size (d.nm)*ppm	-97.0	9.6	-10.2	<.0001*
ppm	-66.0	7.9	-8.4	<.0001*
Particle Size (d.nm)*Particle Size (d.nm)	29.9	4.6	6.6	<.0001*
Particle Size (d.nm)	-58.7	9.4	-6.3	<.0001*
Particle Size (d.nm)*(PDI-0.102)	86.0	14.6	5.9	<.0001*
CU	53.5	12.0	4.5	0.0002*
PDI	76.0	26.5	2.9	0.0087*
CU*(PDI-0.102)*(PDI-0.102)	1285.5	673.8	1.9	0.069
(PDI-0.102)*(PDI-0.102)	1071.4	608.5	1.8	0.0916
ppm*CU	11.6	9.1	1.3	0.2141
CU*(PDI-0.102)	22.0	29.5	0.8	0.4638

Table 6.4: Validation data points for both lipid concentration ([Lipid]) models. Model 1 is based on particle size and ppm, whereas Model 2 includes particle size, polydispersity index (PDI), ppm and CU.

Measured Value	Model Factors				Model 1 Prediction		Model 2 Prediction	
Total [Lipid] mM	ppm	CU	Particle Size (d.nm)	PDI	Total [Lipid] mM	%Error	Total [Lipid] mM	%Error
1.80	16.5	0.206	167	0.05	1.81	0.3%	1.78	0.9%
2.62	24.6	0.294	167	0.05	2.77	5.5%	2.56	2.3%
2.78	27.6	0.333	167	0.05	3.12	12.5%	3.00	8.2%
7.07	67.8	0.789	167	0.05	7.89	11.7%	7.88	11.4%
					Average	7.5%	**Average**	5.7%
					StDEV	5.7%	**StDEV**	4.9%

6.6. Figures

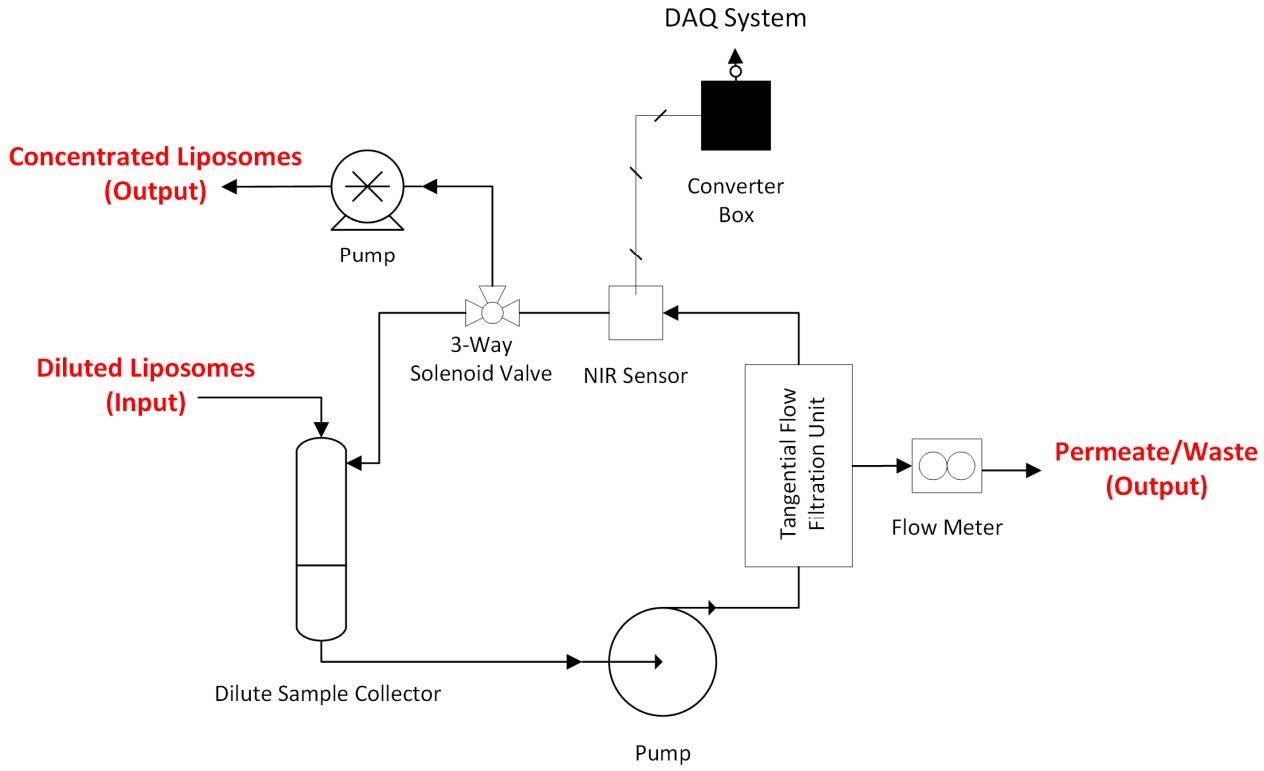

Fig 6.1: Schematic of the lipid concentration stage consisting of multiple components such as pumps, a tangential flow filtration unit, a flow meter and an NIR turbidity sensor.

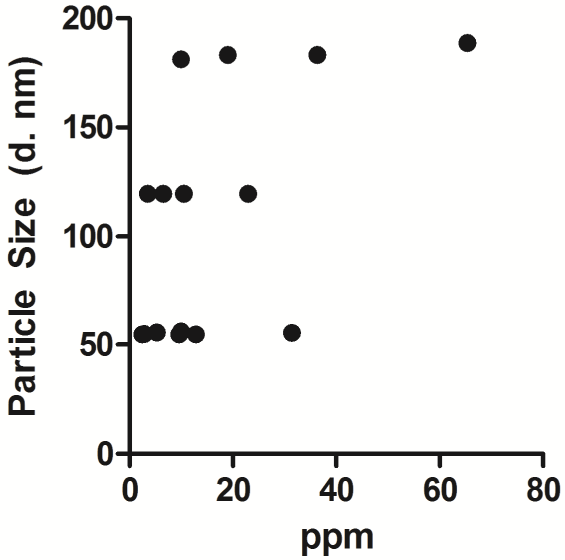

Fig 6.2: Experimental design of the lipid concentration prediction model based on scattered light from an NIR turbidity sensor.

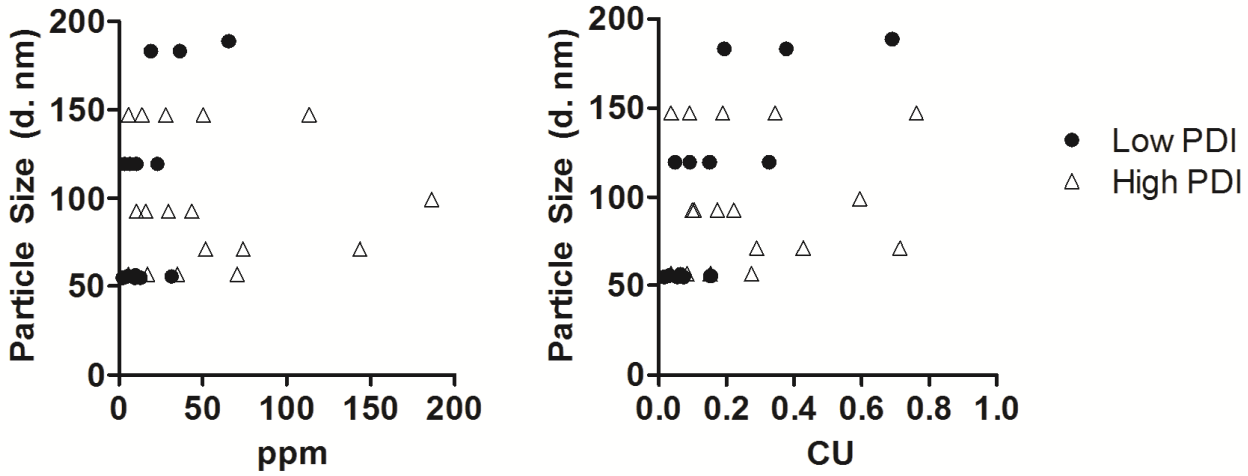

Fig 6.3: Model 2 experimental design for the lipid concentration with factors including particle size (d.nm), polydispersity index (PDI), ppm and CU. The PDI was from 0.03 – 0.21, with "low PDI" as PDI $\leq$ 0.1 and "high PDI" as PDI > 0.1.

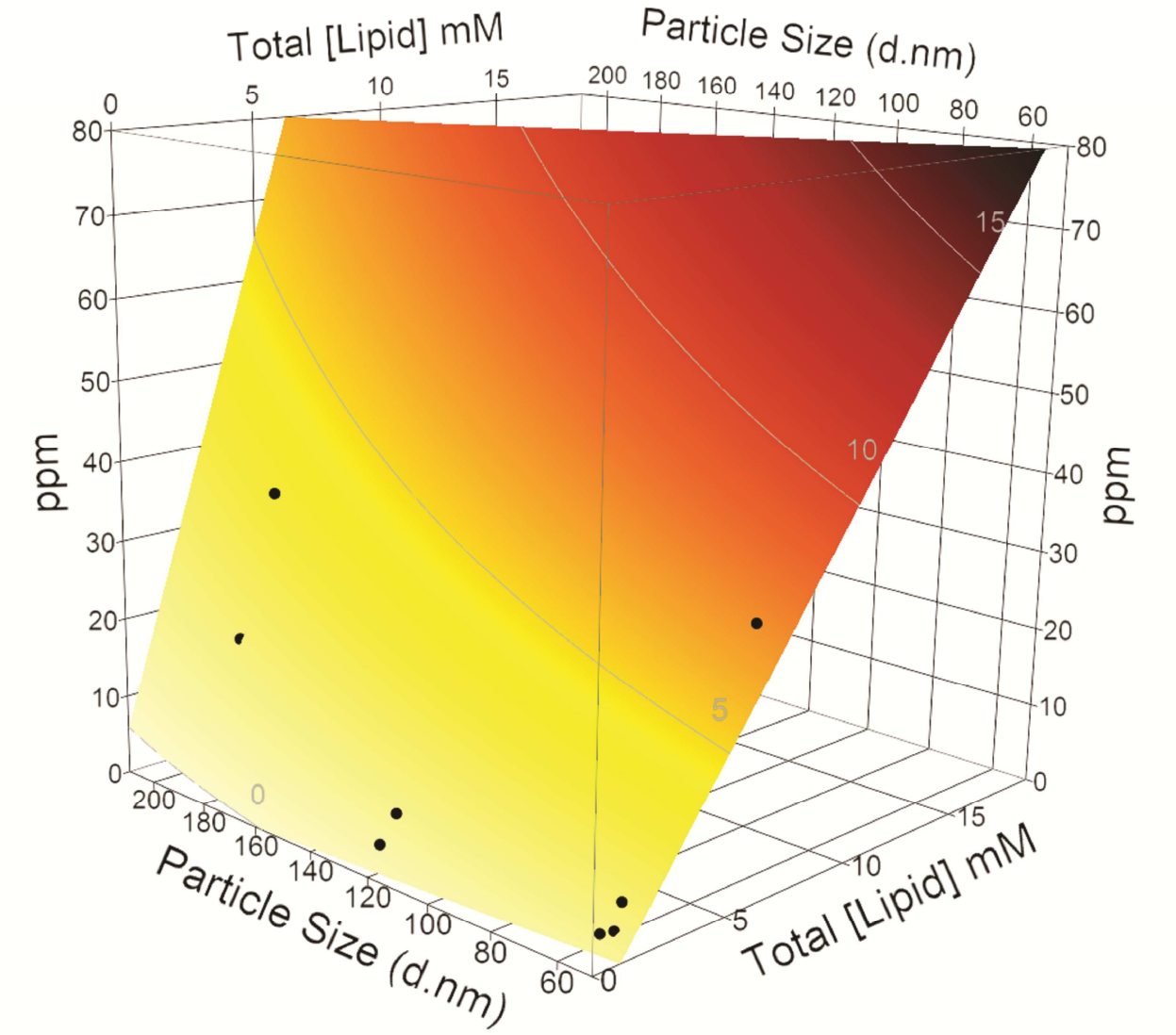

Fig 6.4: Surface Profile plot for the lipid concentration [Lipid] prediction model. The scattered light from the NIR turbidity detector was measured in units of ppm. ppm vs. particle size (d.nm) vs. the total lipid concentration (mM) was plotted.

$$[\boldsymbol{Lipid}] = 9.66 - 49.1 * \left(\frac{Particle\ Size - 263}{238}\right) + 10.7 * \left(\frac{ppm - 250}{250}\right) + (-46.9) * \left(\frac{Particle\ Size\ - 263}{238}\right) * \left(\frac{ppm - 250}{250}\right)$$

Fig 6.5: The Lipid Concentration prediction model equation based on the study outlined in Fig. 6.2 and Fig. 6.4.

$$\begin{aligned}[\boldsymbol{Lipid}] = {} & -20.1 - 58.7 * \left(\frac{Particle\ Size - 263}{238}\right) - 66.0 * \left(\frac{ppm - 250}{250}\right) + 53.5 * \left(\frac{CU - 2}{2}\right) \\ & + 76.0 * PDI + 29.9 * \left(\frac{Particle\ Size\ - 263}{238}\right) * \left(\frac{Particle\ Size - 263}{238}\right) \\ & - 97.0 * \left(\frac{Particle\ Size\ - 263}{238}\right) * \left(\frac{ppm - 250}{250}\right) + 11.6 * \left(\frac{ppm - 250}{250}\right) \\ & * \left(\frac{CU - 2}{2}\right) + 86.0 \left(\frac{Particle\ Size\ - 263}{238}\right) * (PDI - 0.102) + 22.0 \\ & * \left(\frac{CU - 2}{2}\right) * (PDI - 0.102) + 1290 * \left(\frac{CU - 2}{2}\right) * (PDI - 0.102) \\ & * (PDI - 0.102) + 1070 * (PDI - 0.102) * (PDI - 0.102)\end{aligned}$$

Fig 6.6: The Lipid Concentration prediction model equation for Model 2 as outlined in Fig 6.3. The response for the model is the total lipid concentration denoted as [Lipid] and has four factors: particle size (d.nm), polydispersity (PDI), ppm and CU. Both ppm and CU are detected by an NIR turbidity meter.

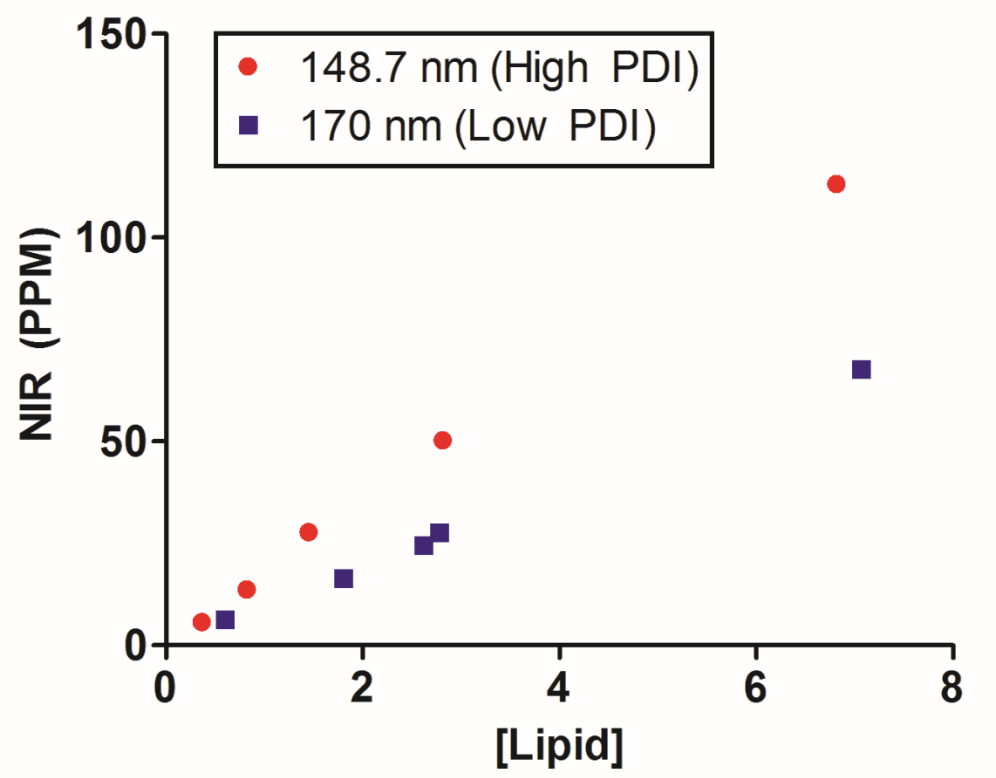

Fig 6.7: An example of how the NIR signal output in PPM is affected by the polydispersity of a liposomal formation. The polydispersity index (PDI) was approximately 0.16 for the high PDI sample and was <0.1 for the low PDI sample. In the case of larger liposomes, the NIR scattered light signal should be greater.

Chapter 7

Freeze-Anneal-Thaw Cycling of Unilamellar Liposomes: Effect on Encapsulation Efficiency

7.1 Abstract

Freeze-thaw cycling is an important processing step in the preparation of liposomes that leads to the encapsulation of drug molecules. There is considerable variability in the number of freeze-thaw cycles reported in the literature. This work is designed to aid in liposomal formulation design by gaining an insight into the drug encapsulation process and an understanding of liposome stabilization during various thawing conditions. The effects of different thawing temperatures, as well as "annealing" at subzero temperatures on a liposome formulation, are reported here. Two freeze-anneal-thaw ($FA_{NN}T$) cycles (freezing to -196°C, annealing at -1.4°C for ~30 minutes, thawing at 65°C) resulted in the maximum predicted encapsulation efficiency without causing any significant change in particle size or zeta potential. Annealing at -22°C was shown to be destabilizing due to limited hydration of the liposomes in the frozen state. It was shown that two important processes are occurring during the $FA_{NN}T$ cycling that affect liposome encapsulation efficiency. The first is drug diffusion in the frozen state and the second is fusion/destabilization of the liposomes. This is the first report on the annealing of liposomes and understanding the mechanism of drug encapsulation using the freeze-thaw cycling method.

7.2 Abbreviations

FT	Freeze-Thaw
$FA_{NN}T$	Freeze-Anneal-Thaw
PFE	Pre-formed Empty
PDI	Polydispersity Index
EE%	Encapsulation Efficiency Percentage
DSC	Differential Scanning Calorimetry
DSPC	1,2-distearoyl-*sn*-glycero-3-phosphocholine
DPPC	1,2-dipalmitoyl-*sn*-glycero-3-phosphocholine
DSPG	1,2-dioctadecanoyl-sn-glycero-3-phospho-(1'-rac-glycerol)
Chol	Cholesterol
Cryo-SEM	Cryogenic Scanning Electron Microscopy

7.3 Introduction

Freeze-thaw (FT) cycling is a technique often used in the preparation of liposomes to increase encapsulation efficiency[110-111]. A common procedure is freezing the liposomes with liquid nitrogen (-196°C) and thawing at a temperature above the phase transition temperature of the lipids[24-25, 112]. In the preparation of liposomes, freeze-thaw cycling is implemented to reduce the lamellarity of liposomes[20], form a less polydispersed system and/or disrupt the liposomal bilayer[21] to allow drug molecules to diffuse into the liposome, promoting encapsulation[22-24]. The number of freeze-thaw cycles needed to encapsulate drug molecules varies greatly in the literature, with some papers reporting up to 10 cycles[113-114]. The reason for using multiple freeze-thaw cycles is to achieve equilibrium drug concentration conditions (*i.e.* concentration inside the liposomes is equal to the concentration outside of the liposomes). Prior to this study, the mechanism for drug encapsulation was considered to be due to physical disruption of the lipid-bilayer as a result of ice crystal formation[22]. Disruption of the lipid-bilayer typically results in vesicle fusion[115] and increased polydispersity. In this study a second mechanism for drug encapsulation is reported based on cryo-concentration (the phenomenon when water freezes and excludes molecules into concentrated zones). Cryo-concentration of the liposome and drug will increase drug diffusion into the liposome while the dispersion is in a semi-frozen state. Unilamellar, pre-formed empty (PFE) liposomes of a monodispersed population were chosen to eliminate any effects related to polydispersity and/or multiple lipid lamellae. The factors that are studied include thawing and annealing temperatures as well as annealing duration, where annealing refers to holding the samples at constant sub-zero temperatures for a certain duration. The freezing procedure was kept constant.

To study the effects of drug diffusion in the frozen state, stable DSPC:Chol:DSPG (6:3:1) liposomes were prepared and the EE% was calculated. Similar DSPC liposomes have previously exhibited minimal particle size changes after freeze-thaw cycling[23]. This minimal size change will allow drug diffusion to be studied while avoiding the effects on EE% from changes in particle size/ polydispersity. The EE% for this liposome system was then compared to a theoretical maximum EE% based on a mathematical model for the entrapped volume of unilamellar liposomes.[25] Briefly, this theoretical EE% is based on parameters such as liposome size, size distribution, bilayer thickness, average molecular area of a lipid at an interface, and the lipid molarity. By supplying these parameters, this mathematical model is able to predict the encapsulation efficiency for any unilamellar, monodispersed liposomal system.

As a model drug, Tenofovir was chosen due to its high polarity (LogP= -1.71)[116] and low membrane permeability. Tenofovir has a pKa of 4.11 ± 0.5 and is negatively charged at the studied pH of 7.4. Since the liposomes were also negatively charged, electrostatic interactions between the drug and liposome surface were avoided. The significance of this research is that it offers physical insight into the behavior of liposomes in the frozen state and provides a method to achieve efficient drug encapsulation into unilamellar, PFE liposomes without the need for multiple freeze-thaw cycling steps and additional downsizing techniques.

7.4 Materials and Methods

7.4.1 Preformed Empty Liposomes Preparation

1,2-distearoyl-*sn*-glycero-3-phosphocholine, cholesterol and 1,2-dioctadecanoyl-sn-glycero-3-phospho-(1'-rac-glycerol) were purchased from Avanti Polar Lipids. DSPC:Chol:DSPG (6:3:1

molar ratio, 60mM) PFE liposomes were prepared by the film-hydration method. Briefly, lipid was mixed with chloroform:methanol (2:1 v/v) and evaporated using a Büchi Rotavapor at an elevated temperature (50°C). During evaporation, a low vacuum was applied initially to avoid bursting of the lipid solution. Chloroform and methanol were purchased from Fisher Scientific. The dried lipid was placed under vacuum overnight to remove residual solvent. The lipid was hydrated at 65°C in 10 mM HEPES buffer, pH 7.4 for approximately two hours. The liposomes were then sonicated at 80W for 1 minute followed by two freeze-thaw cycles (-196°C for 5 minutes, 65°C for 10 minutes). The liposomes were then extruded 8x through a single stack of one 400 nm and two 200 nm polycarbonate membranes using a LIPEX™ Extruder (Northern Lipids Inc.). The extruder was brought to 65°C prior to extrusion.

7.4.2 Drug Encapsulation Process

Tenofovir (CAS# 147127-20-6) was prepared in 10 mM HEPES buffer, pH 7.4 at approximately 8.7 mg/ml. This solution was added to the PFE liposomes. The mixture was frozen in liquid nitrogen (-196°C) for 3 minutes. The samples were transferred to a temperature controlled water bath at various temperatures (Table 7.2). For samples thawed above 0°C, the thawing time was determined by measuring the temperature of a duplicate sample until the thaw temperature was reached. All samples were placed in a water bath at 65°C prior to extrusion. Extruded samples were extruded 6x through a single stack of one 400 nm and two 200 nm polycarbonate membranes. Before extrusion, particle size and zeta potential were monitored for most samples. After extrusion, particle size, zeta potential and EE% were measured for all samples.

7.4.3 Encapsulation Efficiency (EE%)

Encapsulation efficiency was determined by the following equation: $EE\% = 1-C_{free}/C_{total}$, where C_{free} is the free drug concentration and C_{total} is the total drug concentration. The free drug was separated from encapsulated drug by ultra-centrifugation using Amicon 50 kd filters at 4,000 g for 12 minutes. Free drug did not interact with the filter membrane and > 99% of the free drug passed through the filter. The total drug was determined by lysing the liposomes in a 6% v/v TX-100 solution. The free drug from the filtrate and total drug was then analyzed using a previously developed HPLC analysis[117]. All measurements were run in triplicate.

7.4.4 Particle Size and Zeta-Potential

All measurements were performed using a Malvern Zetasizer Nano ZS90. For both particle size and zeta-potential, samples were placed in plastic disposable cuvettes and equilibrated at 25°C. The viscosity of water was assumed since liposome dispersions were below 0.5 mg/ml. Particle size measurements included z-average, PDI, and PDI width. Zeta potential measurements included zeta-potential and zeta deviation. All measurements were run in triplicate.

7.4.5 Cryo-SEM Imaging

In order to determine how annealing can destabilize liposomes in the frozen state, cryo-SEM was performed for samples, (1) frozen to -196°C; and (2) frozen to -196°C then annealed at -20°C. Both samples were immersed in liquid nitrogen before further processing. The -20°C sample was stored in the freezer overnight (~16 hrs). The samples were then fractured using a Leica EM MED020 with an attached cryo-transfer system (Leica EM VCT100). During fracturing, the sample was held at -140°C and sputter coated with platinum (5 nm thickness). The sample was

then transferred at -140°C under vacuum to the scanning electron microscope (FEI Nova™ NanoSEM 450). The accelerating voltage was set to 2.0 kV with a working distance of 5.1 nm and viewed at -140°C.

7.4.6 Differential Scanning Calorimetry

Measurements were carried out using a Q1000 DSC with a Refrigerated Cooling System 90 (TA Instruments). Empty liposome samples with Tenofovir (~20 mg total) were pipetted onto an open aluminum plate, immersed in liquid nitrogen and then transferred to the DSC holder equilibrated at -60°C. The sample was then heated at 50°C/min to either -22°C or -1.4°C. The samples were held at this temperature for 10 minutes and subsequently cooled to -60°C at 10°C/min. Only the latter thermogram was analyzed. The fast heating rate was used to mimic the thawing conditions of the liposome samples used in the EE% tests.

7.5 Results

7.5.1 Particle Size

Particle size analysis was performed to compare the average size and distribution of the particles before and after processing. The PFE liposomes that were used in all the following cases had a particle size diameter of 166.77± 39.75 nm (PDI = 0.07). As a control, the common procedure of freeze-thaw cycling (in this case, freezing at -196°C and thawing at 65°C for up to ten freeze-thaw cycles) was performed. Since the liposomes were subsequently extruded, the mean particle size diameter for all cycles was 153.3± 3.99 nm (PDI = 0.06± 0.02, PDI width = 36.82± 7.47). For the test samples, the pre-extrusion particle size and size distribution of FT (thawed at temperatures below 65°C) and freeze-anneal-thaw ($FA_{NN}T$) liposomes frozen at -196°C,

annealed at -1.4°C for 16 hours and thawed at 65°C [$FA_{NN}T(-196/-1.4_{16hrs}/65)$] did not change significantly (Fig. 7.1). The PDI did increase slightly for $FA_{NN}T$ samples held longer than 90 minutes, but was still ≤ 0.1 in all cases, which suggests a monodispersed system. The $FA_{NN}T(-196/-22_{16hrs}/65)$ liposomes had a pre-extrusion particle size of 373.20± 263.20 nm and a PDI of 0.5, which indicates high polydispersity. After extrusion, the particle size was similar to all other formulations.

7.5.2 Zeta-Potential

In addition to particle size measurements, zeta-potential was compared to pre- and post-extrusion conditions. Pre-extrusion mean zeta potentials were lower than the post-extrusion mean zeta-potentials; however, these values were still within the reported zeta-deviation (Fig. 7.2). The only sample that did show a major difference in zeta potential was the $FA_{NN}T(-196/-22_{16hrs}/65)$ liposome sample. This difference is due to the particle size and particle size distribution increase noted in Fig. 7.1. In all cases, the zeta-potential did not drop to low levels that would cause instability; however, instability may arise from sample polydispersity[23] (Fig. 7.2).

7.5.3 Encapsulation Efficiency (Post-Extrusion)

Fig 7.3 reports on the difference in encapsulation efficiency post-extrusion for all samples. For thawing at 65°C, the first freeze-thaw cycle had an EE% of 3.71± 0.23, whereas the EE% was 7.22± 0.21 after 10 freeze-thaw cycles. Thawing at various temperatures below 65°C followed a trend in that lowering the thawing temperature increased the encapsulation efficiency. In all cases, annealing increased the EE%. A single $FA_{NN}T(-196/-1.4_{36min}/65)$ cycle had an encapsulation efficiency of 9.83± 0.23%, roughly 2.6 times greater than the FT(-196/65) sample.

By increasing the annealing duration, slight increases in EE% were observed but reached a plateau around 12%. Lastly, annealing at -22°C increased the EE% into the theoretical maximum EE% range.

7.5.4 Two Freeze-Anneal-Thaw Cycles (Pre-Extrusion)

Another sample was prepared to determine whether the maximum EE% could be reached without the need for extrusion while maintaining the particle size characteristics of the extruded liposomes. In order to achieve this, two cycles of $FA_{NN}T(-196/-1.4_{36min}/65)$ were performed (Table 7.2). After two cycles, the particle size characteristics were not significantly different than the post-extruded samples. The EE% increased to values within the maximum EE% range for this formulation. A direct comparison of these results to the EE% results for two freeze-thaw cycles (thawed at 65°C without annealing, Fig. 7.3) suggests that sub-zero temperatures near the freezing point of the solution allows for increased drug encapsulation.

7.5.5 Cryo-SEM Imaging

It can be seen from Fig. 7.4 that ice formation (darker, solid regions) causes the liposomes to be excluded from regions occupied by ice crystals thus forming concentrated clusters (lighter regions). The samples that were only frozen (not annealed) appear to have well-defined liposomes with larger clusters of liposomes (Fig. 7.4A, B). For the -20°C annealed sample, the liposomes were more difficult to find and either had an overall less-defined/fused structure and/or were within narrow bands between the ice-phase (Fig. 7.4C, D). Moreover, for the -20°C annealed samples, there were some locations in the sample that did have clusters of moderately-defined liposomes. The existence of both clusters of moderately-defined liposomes and large

regions of fused liposomes would contribute to the increase in polydispersity as shown in Fig. 7.1 for the -22°C annealed sample.

7.5.6 Differential Scanning Calorimetry Thermogram

DSC was performed to determine whether water melted during the annealing process. Heating from -196°C to either -1.4°C or -22°C and annealing for 10 minutes before re-cooling to -60°C, a peak only appears for the -1.4°C sample (Fig. 7.5). This indicates a portion of the water in the -1.4°C sample melted and then refroze. HEPES buffer without liposomes was measured as a control. The increase in enthalpy for liposomes -1.4°C vs. HEPES -1.4°C suggests additional water melted and froze upon re-cooling for the liposome samples.

7.6 Discussion

For the liposome formulation investigated here, the theoretical maximum EE% is 16.3±2% [25]. Accordingly, it would appear that more than half of the predicted drug amount was not encapsulated even after 10 freeze-thaw cycles. In order to understand how freeze-thaw cycling influenced liposome EE%, all of the liposome samples [except for $FA_{NN}T(-196/-1.4_{36min}/65)$] underwent a single freeze-thaw cycle. Liposomes were immersed in liquid nitrogen and thawed at various temperatures to determine whether the thawing temperature influenced liposome physical characteristics. As seen above, thawing at temperatures above 0°C did not significantly alter liposome particle size both pre- and post-extrusion (Fig. 7.1), which indicates liposome stability. Additionally, the physical characteristics of the samples that underwent $FA_{NN}T$ cycles did not change significantly except for the $FA_{NN}T(-196/-22_{16hrs}/65)$ sample. The reason for the

liposome stability at -1.4°C and at temperatures above 0°C may be due to the hydration of the liposomes as discussed later.

The EE% was analyzed to determine whether drug molecules entered the liposomes during the frozen state. As compared to the control freeze-thaw cycles, adjusting the thawing temperatures to less than 65°C showed an increase in EE% as the thawing temperature was lowered. An explanation is that at lower temperatures, it takes more time for ice to melt, thus ice growth and subsequent cryo-concentration of drug and liposomes increases the amount of drug entrapped once the liposomes become rehydrated. Furthermore, complete thawing at 1°C took about 55 minutes, and the EE% is comparable to annealing at -1.4°C for both 36 and 90 minutes (Fig. 7.3). As for the annealed samples, increased drug diffusion was evident (EE% > 9% after 1 cycle). However, the maximum encapsulation (~16.3%) was still not reached, which indicates that there was either limited drug diffusion into the liposomes or that only a percentage of the liposomes had drug encapsulated. A possible explanation is that under these freezing conditions, densely populated liposome phases (Fig. 7.4A, B) are present. These dense phases may inhibit the diffusion of the water-soluble drug within the liposome phase. Liposomes located more towards the center of this phase and/or liposomes entrapped in the bulk ice would have limited contact with the drug. It is suggested that two $FA_{NN}T$ cycles are necessary since a second cycle redistributes the liposomes, facilitating contact of the drug with all liposomes. After the two $FA_{NN}T$ cycles, the EE% was similar to the theoretical maximum and the physical characteristics did not change.

In addition to increased drug diffusion, liposomal disruption/fusion is another mechanism of drug encapsulation. This is evident from the $FA_{NN}T(-196/-22_{16hrs}/65)$ sample, which had high polydispersity pre-extrusion. The post-extrusion polydispersity returned to a monodispersed system and the EE% was near the theoretical maximum value. This is due to the complete disruption and fusion of the liposomes during the thaw process –after extrusion, the drug is equally dispersed between the intraliposomal and extraliposomal space. As suggested by Talsma *et al*. and supported by cryo-SEM imaging (Fig. 7.4C, D), ice crystal growth may be destabilizing to the liposomes[118] by forcing the vesicles into close contact. At such close distances between liposomes, electrostatic repulsive forces and hydration forces[95] are no longer sufficient to prevent particle fusion. Thus, particle size, size distribution and polydispersity increased for the $FA_{NN}T(-196/-22_{16hrs}/65)$ samples. For the $FA_{NN}T(-196/-1.4/65)$ and FT samples, it may be that the high concentrations of drug, liposomes and buffer between the ice-phase is allowing for intra-liposomal and/or extra-liposomal ice within the vicinity of the liposomes to melt, thus keeping the liposomes hydrated and preventing them from fusing. Thus, at temperatures close to 0°C, such high concentrations would result in a freezing point depression causing the ice to melt.

To further investigate whether ice is melting and possibly hydrating/stabilizing the liposomes at subzero temperatures, DSC was used to detect exothermic peaks that indicate water refreezing after annealing. Reported DSC measurements for DPPC liposomes demonstrates that heating a sample from -50°C to -15°C and re-cooling to -50°C does not show the intra-liposomal water freezing peak (at -43°C) in the DSC profile[119], thus intra-liposomal and extra-liposomal ice is not melting upon heating to moderate temperatures above the intra-liposomal freezing temperature.

In the current case, the DSC thermogram from Fig. 7.5 shows that ice melted and refroze for the -1.4°C sample. This suggests that melted water is hydrating the liposomes and preventing liposome fusion. In the case of the -22°C sample, no exothermic peak was visible, which indicated water did not melt during the annealing stage and did not stabilize the liposomes.

Lastly, the results reported here were only for encapsulating a single hydrophilic molecule. As previously mentioned, we avoided lipid-drug interactions by choosing a model drug that was hydrophilic and exhibited low permeability, and by choosing lipid of the same charge as the drug. Therefore, these results can be extended to other small molecules and/or proteins (depending on protein stability during freezing/thawing). Moreover, further testing needs to be done on lipid composition (*e.g.* mixing lipids of various hydrocarbon chain lengths, that are saturated vs. unsaturated and/or that have different lipid head groups). All of these adjustments in the lipid composition may form voids in the lipid bilayer, causing the liposomes to fuse during the thawing cycle and resulting in a polydispersed system rather than a monodispersed system after freeze-thaw cycling.

7.7 Conclusion

The significance of this work is that the results provide further insight into conditions that destabilize liposomes and induce fusion (due to dehydration and ice growth). The results also suggest a second mechanism for drug encapsulation (*i.e.*, cryo-concentration of drug and liposomes in the frozen state) that increases the EE% of the drug. Moreover, for this DSPC:Chol:DSPG liposome formulation, it is possible to encapsulate drug into pre-formed empty liposomes without the need for extrusion or other downsizing techniques. As for other

applications, such as freeze-drying of liposomes, this mechanistic insight provides an understanding of why liposomes become destabilized under various different conditions.

7.8 Disclaimer

The views expressed are those of authors and do not necessarily represent the official position of the Agency (FDA).

7.9 Acknowledgement

We express our gratitude to Dr. Marie Cantino and Stephen Daniels from the Biosciences Electron Microscope Laboratory of the Physiology and Neurobiology Department at the University of Connecticut for their work on the cryo-SEM images.

7.10 Tables

Table 7.1: Experimental outline for 60 mM DSPC:Chol:DSPG (6:3:1 molar ratio) liposomes.[2]

Sample ID	Annealed Temperature (°C)	Thaw/annealing time (min)	Thawing temperature (°C)	Time at 65°C following thawing (min)
FT(65°C)	n/a	10	65	--
FT(1°C)	n/a	90	1	10
FT(4°C)	n/a	45	4	10
FT(23°C)	n/a	20	23	10
$FA_{NN}T$(-1.4°C/65°C)	-1.4	36, 90, 360 and 960	65	10
$FA_{NN}T$ (-22°C/65°C)	-22	960	65	10

[2] A single freeze-thaw cycle was performed in all cases, with differences in the thawing temperature. The difference in thawing time was needed to accommodate complete thawing. Liposomes were held at 65°C for 10 minutes before extrusion to prevent membrane fouling.

Table 7.2. Pre-Extrusion Results for Two $FA_{NN}T(-196/-1.4_{36min}/65)$ Cycles (n=3)

Particle Size ± PDI Width (d. nm)	151.90± 34.97
PDI	0.05
Zeta-Potential± Deviation (mV)	-56.77± 10.17
Encapsulation Efficiency	15.42± 0.08%

7.11 Figures

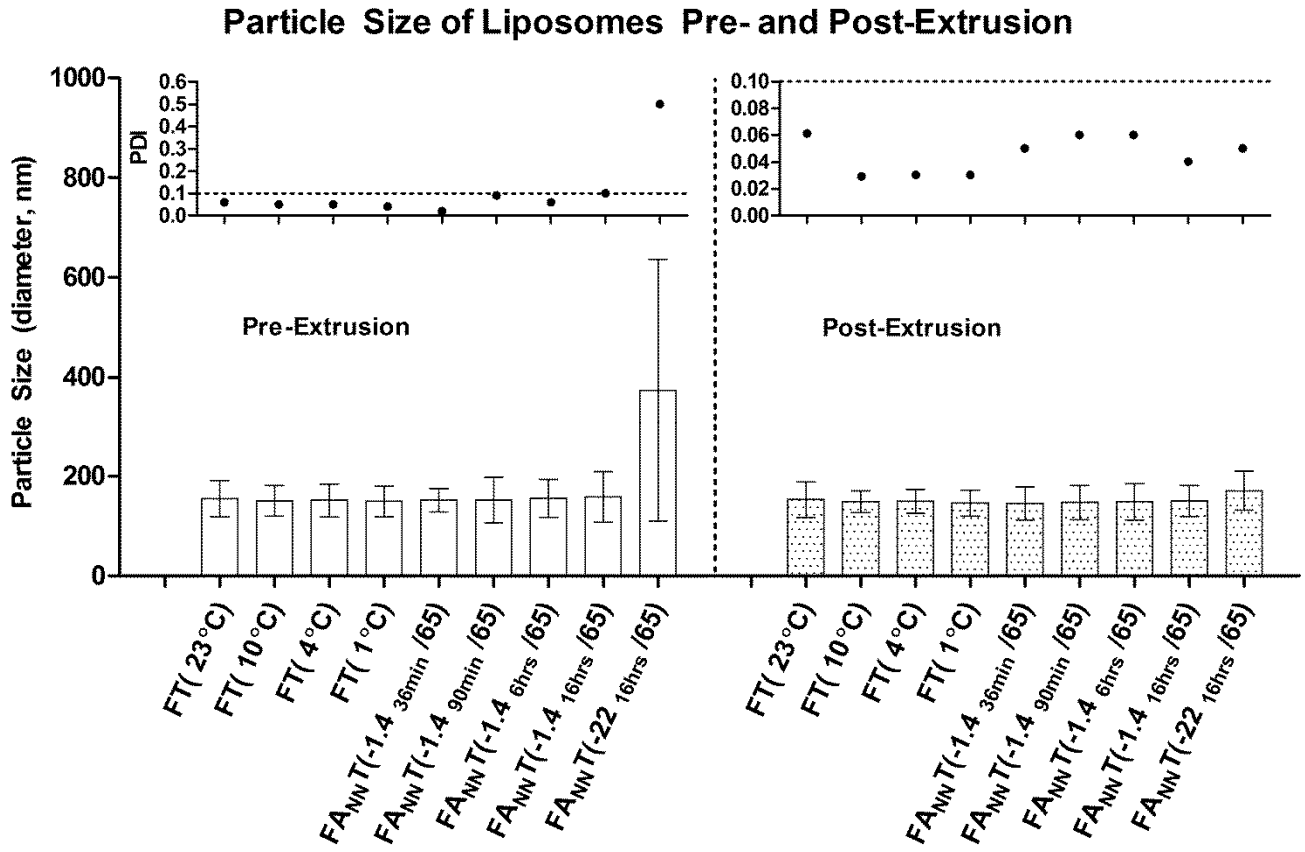

Fig. 7.1. Particle size of liposomes under various conditions. Samples either underwent a freeze-thaw (FT) cycle or a freeze-anneal-thaw ($FA_{NN}T$) cycle. All liposomes were frozen in liquid nitrogen (-196°C). All $FA_{NN}T$ samples were thawed at 65°C. Both pre-extrusion and post-extrusion particle size properties are detailed above. The error bar represents the PDI distribution width. The inset above each group of data represents the PDI of the samples for pre- and post-extrusion.

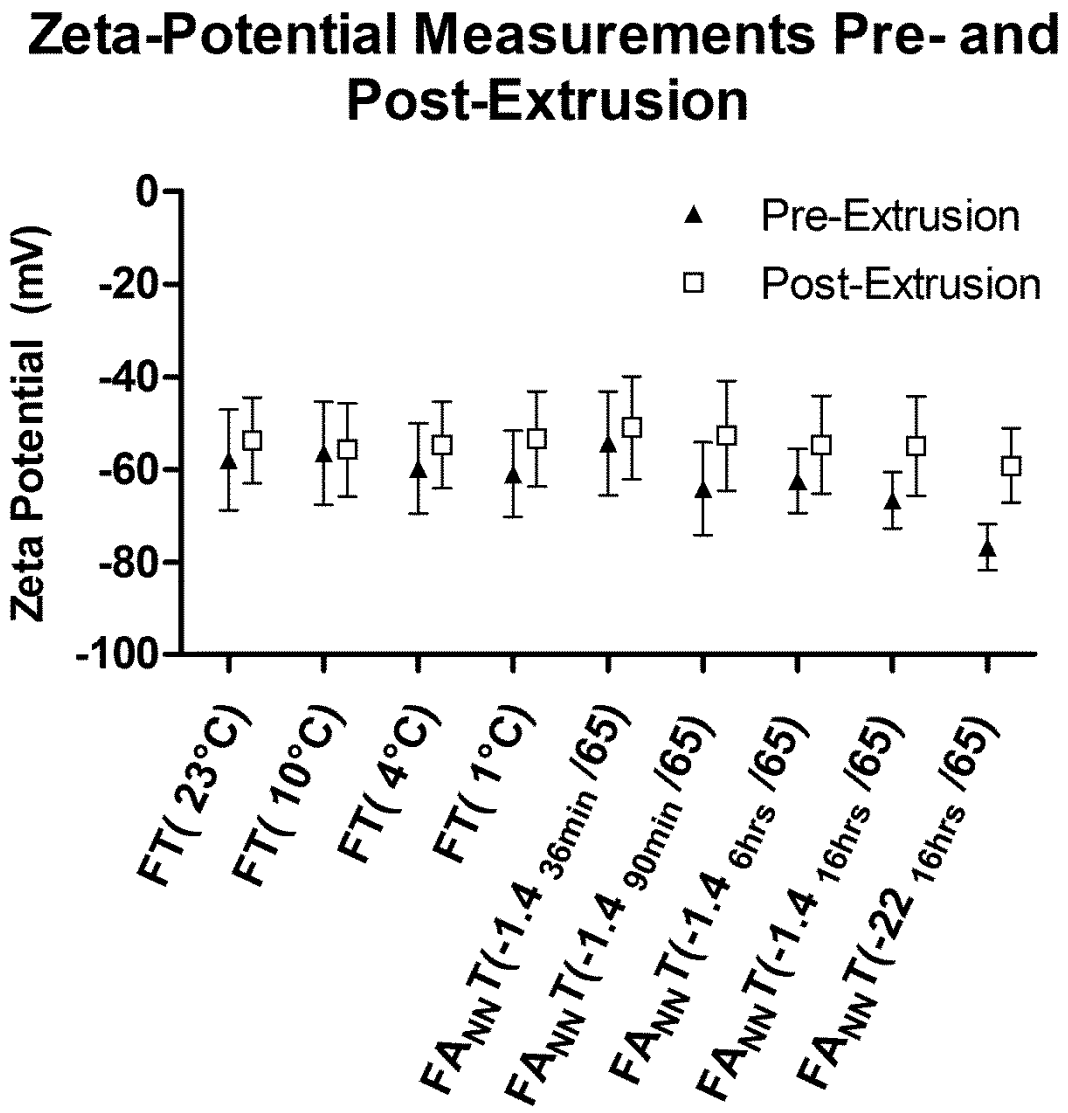

Fig. 7.2. Zeta-potential of the liposome formulation. The zeta-potential is provided for both pre- and post-extrusion for the samples listed in Fig. 7.1.

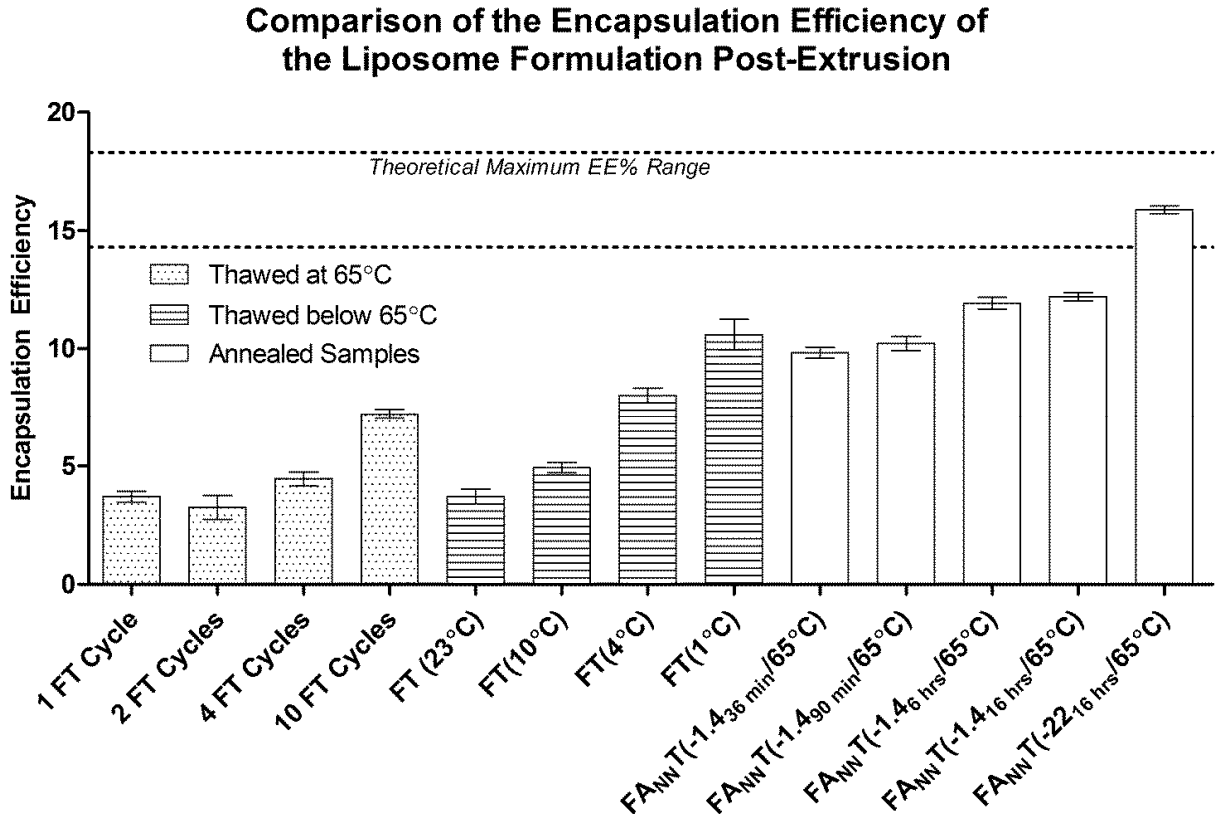

Fig. 7.3. Encapsulation efficiency for samples thawed under various conditions. All samples were frozen in liquid nitrogen at -196°C. The samples thawed directly at 65°C represent normal freeze-thaw cycling. All other samples underwent a single freeze-thaw or freeze-anneal-thaw cycle. The effects on EE% of thawing at temperatures above 0°C and annealing at subzero temperatures is demonstrated (n=3).

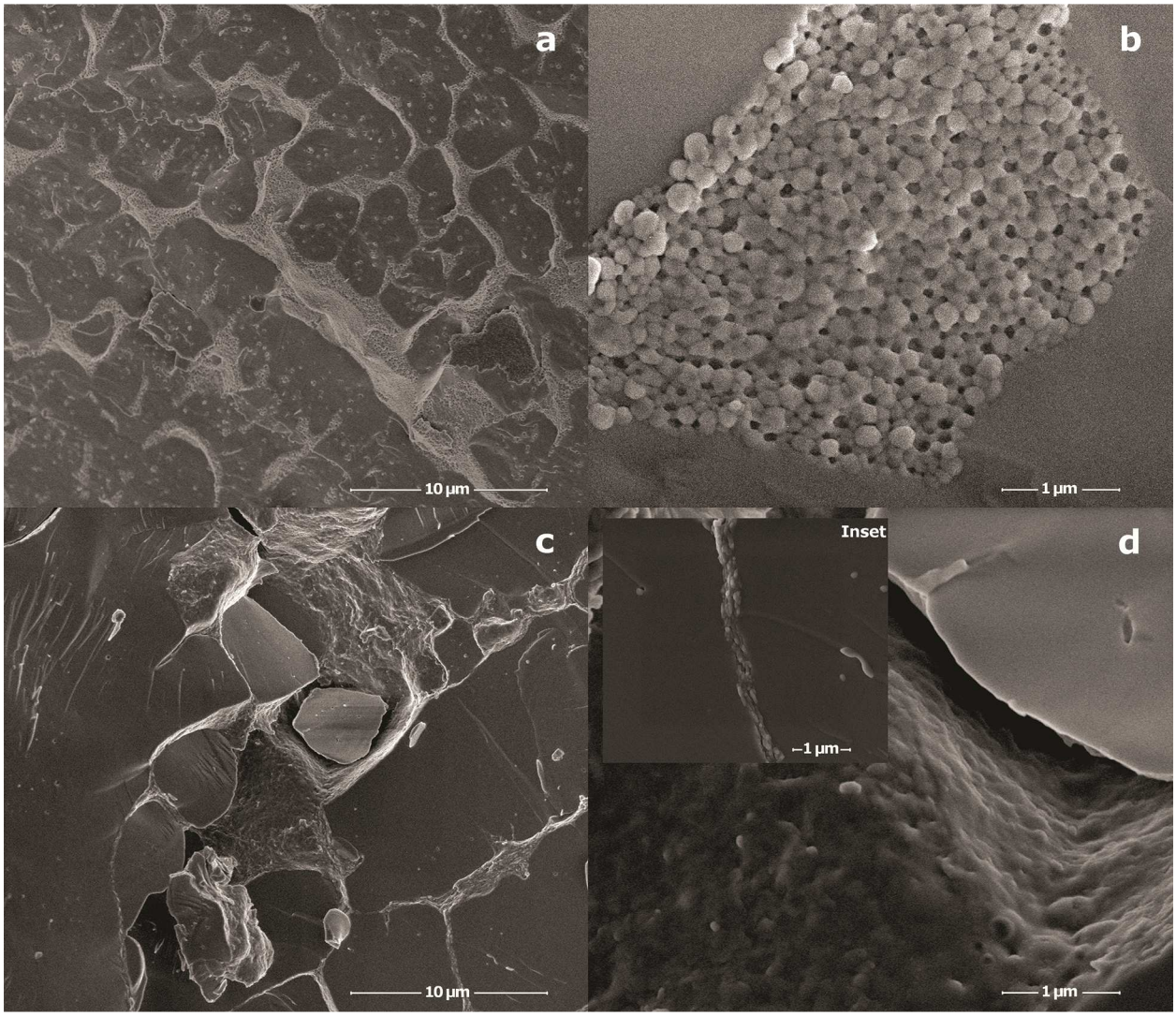

Fig. 7.4. Cryo-SEM images of PFE-liposomes with tenofovir. In all the images, the smooth/darker areas represent the ice phase while the non-smooth/lighter regions are liposomes. (A) Sample frozen to -196°C, magnification (mag.) 5,000x. (B) 30,000x mag. of sample from A with liposomes clearly visible. (C) Sample frozen to -196°C, annealed at -20°C overnight, and then refrozen to -196°C prior to imaging, mag. 5,000x. (D) 30,000x mag. of sample from C. In D, the top right hand corner is ice while the rest of the image is of liposomes in an apparent fused state. (D Inset) 30,000x mag. of a thin channel of liposomes between the ice-phases.

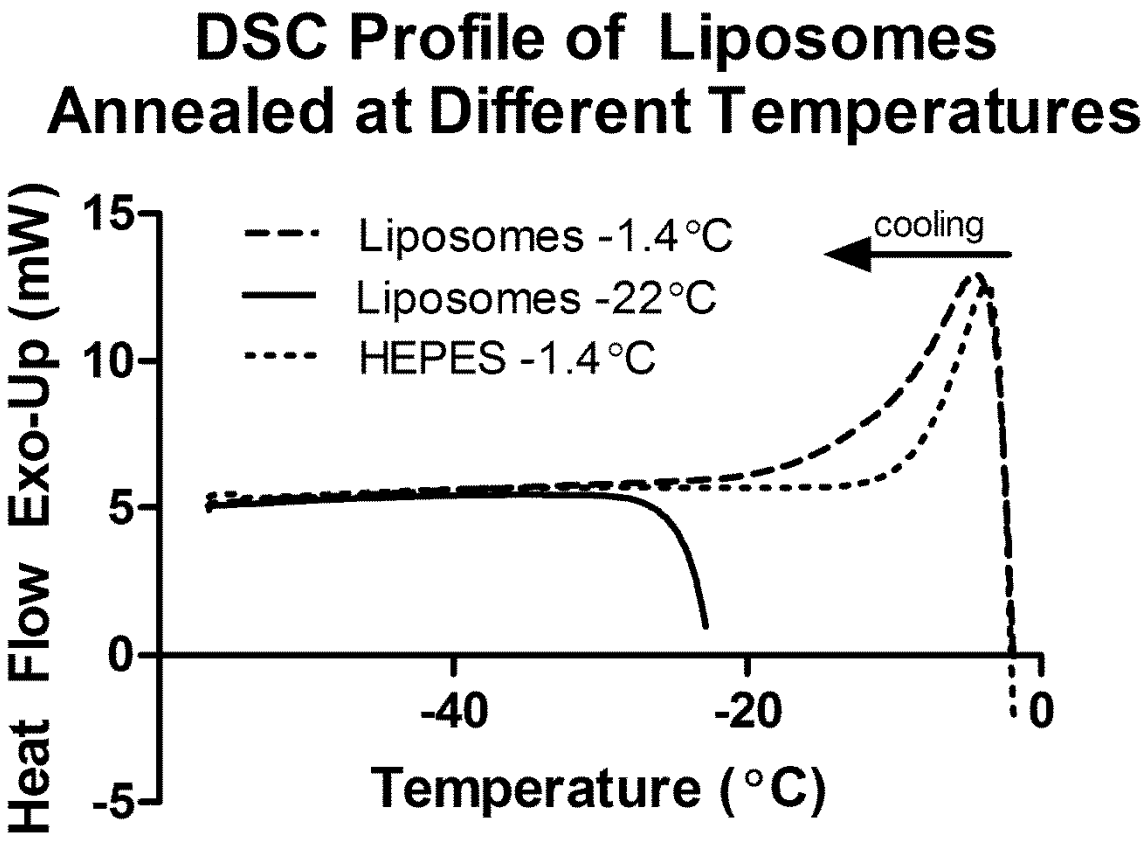

Fig. 7.5. DSC profile of annealed liposomes. Samples were first frozen in liquid nitrogen (-196°C) and heated to the annealing temperature (-22°C or -1.4°C) and held at that temperature for 10 min (not shown). The sample was then re-cooled to -60°C (shown above). HEPES buffer without liposomes was shown as a control. All samples were run in triplicate and the average standard deviation was <0.4 in all cases.

Chapter 8

Conclusions and Suggested Studies

8.1 Conclusions

The implementation of the quality by design approach at the onset of this work provided valuable insight required for the system design and for an understanding of the liposomal formation process. From Chapter 3, risk analyses were performed for various "effects" associated with this work, such as "the formation of quality liposomes" and "in-line particle size analysis". From Chapter 4, a turbulent jet mixer was fabricated and investigated in detail. The turbulent jet mixer established flow conditions that formed unilamellar, monodispersed liposomes. The particle size of these liposomes was controllable from ~25 nm to >465 nm. It was determined that the mean particle size of the liposomes had a significant dependence on the Reynolds Number of the mixture (*i.e.* ethanol and aqueous phase) and was independent of flow velocity ratios above a flow velocity ratio of approximately 7. The mean particle size and particle size distribution of these liposomes was measured using multiple techniques such as dynamic light scattering, nanoparticle tracking and two electron microscopy techniques. Each technique concluded that the liposomes increased in size with a decrease in Reynolds Number of the mixture, and three of these techniques confirmed the monodispersity of these liposomes. In addition, a novel model on the liposome formation process was explained. From analyzing aqueous phase additives, types of lipid molecules, and lipid concentration on the liposome

formation process, it was determined that it is likely that pro-liposomes initially form and grow in size depending on process conditions and the lipid formulation.

From chapter 5, an in-line dilution stage was added to the liposome formation process to reduce the total amount of ethanol down to 5 % vol. It was determined that the in-line dilution stage causes changes to the mean particle size and particle size distribution. This indicates that the liposomes may not be fully formed or unstable at the liposome formation site. One major finding was that air bubbles caused multiple populations of liposomes to form at the in-line dilution site. This phenomenon was thought to occur since lipid molecules would align at the air-water interface and then mix back into solution at the in-line dilution stage. When the lipid molecules mixed back into the aqueous phase, the liposomes formed at a different Reynolds number and possibly temperature, thus forming liposomes of a different size. The combined effects led to polydispersity in the system. To prevent liposomal polydispersity, a degassing unit post the liposome formation site was implemented. It was determined that low phase transition temperature lipids (*e.g.* DMPC) exhibited a larger polydispersity than higher phase transition temperature lipids (*e.g.* DPPC); however, this polydispersity was reduced for the low phase transition temperature lipids when the degassing unit was implemented.

In addition, at-line particle size analysis was implemented into the continuous processing of liposomes. Dynamic light scattering was the particle size analysis technique implemented in the process. Two modes were investigated to transfer the liposomal dispersion to the instrument for analysis. The first was the continuous flow mode and the second was the load/stop mode. The load/stop mode provided more consistent results in measuring the particle size of the liposomes

For example, this mode exhibited a reduced lag time between process changes and particle size measurements and the mean particle size data was similar to off-line particle size measurements. Moreover, the amount of NaCl dissolved in the aqueous phase was investigated. It was determined that the ionic strength of the aqueous phase significantly impacted the mean particle size of the liposomes during the liposomal formation process, *i.e.* an increase in ionic strength formed larger liposomes.

From chapter 6, a tangential flow filtration system was implemented in the continuous processing of liposomes. Two empirical models that related factors such as particle size, scattered light (ppm) and absorbance (CU) to the total lipid concentration were established. The first model (Model I) predicted the lipid concentration from 0.5 to 7 mM total lipid for particle size diameters from approximately 50 nm up to 200 nm with an RMSE of 0.587 mM. As explained, one of the limitations for this model is that the liposomes must be monodispersed. The second model took into account the polydispersity index (PDI) of the liposome formulation. This addition allowed for the prediction of both monodispersed and polydispersed liposomal formulations, but at a cost of increased model degrees of freedom.

Lastly, from chapter 7, freeze-thaw-anneal cycling on liposomal dispersions was investigated. This work provided insight into conditions that destabilized liposomes and induced fusion (*i.e.* due to dehydration and ice growth). In addition, a mechanism to encapsulate drug was suggested that was based on the cryo-concentration of the drug and liposomes while in the frozen state. This cryo-concentration effect led to an increase in the encapsulation efficiency per freeze-anneal-thaw cycle. Moreover, the stability of different lipid formulations was assessed. It was

determined that high phase transition lipids such as DSPC formed highly stable liposomes that were able to withstand freeze-anneal-thaw cycling without change in the physical properties (*e.g.* particle size and size distribution). In this case, drug could be encapsulated during this process without the need for extrusion or other downsizing techniques. Lastly, this mechanistic insight provides an understanding of liposomal stability during freezing and thawing conditions.

8.2 Suggested Studies

8.2.1 Continuous Processing of Liposomes

From the current work, the liposome formation process was dependent on many factors such as temperature, ionic strength, the extent of mixing (predicted by the Reynolds Number), aqueous phase additives and the lipid formulation. Additional studies may include investigating different types of buffers (*e.g.* phosphate, hepes or tris buffers), enthalpy of mixing and lipid packing. The combination of the previous work with these additional studies may support an empirical model to explain and predict the formation of liposomes. This model could then be further investigated to establish a theoretical model based on first principles.

In addition, the continuous processing of liposomes has multiple stages and different drugs may be intercalated with the lipid bilayer, loaded into the liposomes and/or encapsulated. Additional stages could be incorporated into the continuous process to accommodate high loading/encapsulation efficiencies of different drugs. Moreover, additional process analytical technology (*e.g.* Raman spectroscopy) could be incorporated into the system to monitor and control the drug loading/encapsulation from the beginning of the process to the end.

8.2.2 Freeze-Anneal-Thaw Cycling

This work could be enhanced by developing a method to precisely cryo-concentrate the drug and liposomes to achieve high encapsulation efficiency. Future work on developing a freezing protocol or an apparatus that forms a highly concentrated liposomal region with drug in the frozen state, followed by thawing, may achieve higher encapsulation efficiencies. In addition, this technique could be implemented in the continuous processing of liposomes to support the encapsulation of compounds that cannot undergo remote loading such as proteins.

9. References

1. Dopico, A.; Tigyi, G., A Glance at the Structural and Functional Diversity of Membrane Lipids. In *Methods in Membrane Lipids*, Dopico, A., Ed. Humana Press: 2007; Vol. 400, pp 1-13.
2. Koynova, R.; Caffrey, M., Phases and phase transitions of the phosphatidylcholines. *Biochimica et Biophysica Acta (BBA) - Reviews on Biomembranes* 1998, *1376* (1), 91-145.
3. Lewis, R. N. A. H.; Mak, N.; McElhaney, R. N., A differential scanning calorimetric study of the thermotropic phase behavior of model membranes composed of phosphatidylcholines containing linear saturated fatty acyl chains. *Biochemistry* 1987, *26* (19), 6118-6126.
4. Jain, M.; Wu, N., Effect of small molecules on the dipalmitoyl lecithin liposomal bilayer: III. Phase transition in lipid bilayer. *J. Membrain Biol.* 1977, *34* (1), 157-201.
5. Papahadjopoulos, D.; Nir, S.; Ohki, S., Permeability properties of phospholipid membranes: Effect of cholesterol and temperature. *Biochimica et Biophysica Acta (BBA) - Biomembranes* 1972, *266* (3), 561-583.
6. Blicher, A.; Wodzinska, K.; Fidorra, M.; Winterhalter, M.; Heimburg, T., The Temperature Dependence of Lipid Membrane Permeability, its Quantized Nature, and the Influence of Anesthetics. *Biophysical Journal* 2009, *96* (11), 4581-4591.
7. McIntosh, T. J., The effect of cholesterol on the structure of phosphatidylcholine bilayers. *Biochim. Biophys. Acta: Biomembranes* 1978, *513* (1), 43-58.
8. Sułkowski, W. W.; Pentak, D.; Nowak, K.; Sułkowska, A., The influence of temperature, cholesterol content and pH on liposome stability. *Journal of Molecular Structure* 2005, *744–747*, 737-747.
9. Mortensen, K.; Pfeiffer, W.; Sackmann, E.; Knoll, W., Structural properties of a phosphatidylcholine-cholesterol system as studied by small-angle neutron scattering: ripple structure and phase diagram. *Biochimica et Biophysica Acta (BBA) - Biomembranes* 1988, *945* (2), 221-245.
10. Lasic, D. D., *Liposomes : from physics to applications*. Elsevier: Amsterdam; New York, 1993.
11. Kunisawa, J.; Masuda, T.; Katayama, K.; Yoshikawa, T.; Tsutsumi, Y.; Akashi, M.; Mayumi, T.; Nakagawa, S., Fusogenic liposome delivers encapsulated nanoparticles for cytosolic controlled gene release. *Journal of Controlled Release* 2005, *105* (3), 344-353.
12. Martin, F. J.; Zalipsky, S., Fusogenic liposome compositions and method. Google Patents: 1999.
13. Simões, S.; Moreira, J. N.; Fonseca, C.; Düzgüneş, N.; Pedroso de Lima, M. C., On the formulation of pH-sensitive liposomes with long circulation times. *Advanced Drug Delivery Reviews* 2004, *56* (7), 947-965.
14. Collins, D., pH-sensitive liposomes as tools for cytoplasmic delivery. *Liposomes as tools in basic research and industry* 1994, *13*, 201-214.
15. Moghimi, S. M.; Szebeni, J., Stealth liposomes and long circulating nanoparticles: critical issues in pharmacokinetics, opsonization and protein-binding properties. *Progress in Lipid Research* 2003, *42* (6), 463-478.
16. Heurtault, B.; Saulnier, P.; Pech, B.; Proust, J.-E.; Benoit, J.-P., Physico-chemical stability of colloidal lipid particles. *Biomaterials* 2003, *24* (23), 4283-4300.

17. Gabizon, A.; Catane, R.; Uziely, B.; Kaufman, B.; Safra, T.; Cohen, R.; Martin, F.; Huang, A.; Barenholz, Y., Prolonged circulation time and enhanced accumulation in malignant exudates of doxorubicin encapsulated in polyethylene-glycol coated liposomes. *Cancer research* 1994, *54* (4), 987-92.
18. Gabizon, A.; Martin, F., Polyethylene Glycol-Coated (Pegylated) Liposomal Doxorubicin. *Drugs* 1997, *54* (4), 15-21.
19. *United States Pharmacopeia 33- National Formulary 28*. The United States Pharmacopeial Convention: 12601 Twinbrook Parkway, Rockville, MD 20852, 2010; Vol. 1, p 188-190.
20. Traïkia, M.; Warschawski, D. E.; Recouvreur, M.; Cartaud, J.; Devaux, P. F., Formation of unilamellar vesicles by repetitive freeze-thaw cycles: characterization by electron microscopy and 31P-nuclear magnetic resonance. *Eur. Biophys. J.* 2000, *29* (3), 184-195.
21. MacDonald, R. C.; Jones, F. D.; Qui, R., Fragmentation into small vesicles of dioleoylphosphatidylcholine bilayers during freezing and thawing. *Biochim. Biophys. Acta - Biomembranes* 1994, *1191* (2), 362-370.
22. Hope, M. J.; Bally, M. B.; Mayer, L. D.; Janoff, A. S.; Cullis, P. R., Generation of multilamellar and unilamellar phospholipid vesicles. *Chem. Phys. Lipids* 1986, *40* (2-4), 89-107.
23. Xu, X.; Costa, A.; Burgess, D., Protein Encapsulation in Unilamellar Liposomes: High Encapsulation Efficiency and A Novel Technique to Assess Lipid-Protein Interaction. *Pharm. Res.* 2012, *Springer Netherlands*, 1-13.
24. Aliño, S. F.; García, M.; Lejarreta, M.; Bobadilla, M.; Pérez-Yarza, G.; Unda, F. J., Trapping drug efficiency in liposomes produced by extrusion of freeze-thaw multilamellar vesicles. *Biochem. Soc. Trans.* 1989, *17* (6), 1000-1001.
25. Xu, X., Khan, M.A., Burgess, D.J., Predicting hydrophilic drug encapsulation inside unilamellar liposomes. *Int. J. Pharm.* 2012, *423*, 410-418.
26. Costa, A. P.; Xu, X.; Burgess, D. J., Freeze-Anneal-Thaw Cycling of Unilamellar Liposomes: Effect on Encapsulation Efficiency. *Pharm Res* 2013, 1-7.
27. Doxil (R) [package insert]. Horsham, PA: Janssen Products, LP; 2014.
28. Fritze, A.; Hens, F.; Kimpfler, A.; Schubert, R.; Peschka-Süss, R., Remote loading of doxorubicin into liposomes driven by a transmembrane phosphate gradient. *Biochimica et Biophysica Acta (BBA) - Biomembranes* 2006, *1758* (10), 1633-1640.
29. Mayer, L. D.; Tai, L. C. L.; Ko, D. S. C.; Masin, D.; Ginsberg, R. S.; Cullis, P. R.; Bally, M. B., Influence of Vesicle Size, Lipid Composition, and Drug-to-Lipid Ratio on the Biological Activity of Liposomal Doxorubicin in Mice. *Cancer Research* 1989, *49* (21), 5922-5930.
30. Harrigan, P. R.; Wong, K. F.; Redelmeier, T. E.; Wheeler, J. J.; Cullis, P. R., Accumulation of doxorubicin and other lipophilic amines into large unilamellar vesicles in response to transmembrane pH gradients. *BBA - Biomembranes* 1993, *1149* (2), 329-338.
31. Li, X.; Hirsh, D. J.; Cabral-Lilly, D.; Zirkel, A.; Gruner, S. M.; Janoff, A. S.; Perkins, W. R., Doxorubicin physical state in solution and inside liposomes loaded via a pH gradient. *Biochimica et biophysica acta* 1998, *1415* (1), 23-40.
32. Haran, G.; Cohen, R.; Bar, L. K.; Barenholz, Y., Transmembrane ammonium sulfate gradients in liposomes produce efficient and stable entrapment of amphipathic weak bases. *Biochimica et Biophysica Acta (BBA) - Biomembranes* 1993, *1151* (2), 201-215.
33. Himanshu Anwekar; Sitasharan Patel; Singhai, A. K., Liposome- as drug carriers. *Int. J. of Pharm. & Life Sci.* 2011, *2* (7), 945-951.

34. In: ClinicalTrials.gov [Internet]. Bethesda (MD): National Library of Medicine (US). 2000-2015.
Available from:. https://clinicaltrials.gov/ct2/results?term=liposomal&recr=Open&no_unk=Y.
35. Allison, G.; Cain, Y. T.; Cooney, C.; Garcia, T.; Bizjak, T. G.; Holte, O.; Jagota, N.; Komas, B.; Korakianiti, E.; Kourti, D.; Madurawe, R.; Morefield, E.; Montgomery, F.; Nasr, M.; Randolph, W.; Robert, J. L.; Rudd, D.; Zezza, D., Regulatory and quality considerations for continuous manufacturing. May 20-21, 2014 Continuous Manufacturing Symposium. *Journal of pharmaceutical sciences* 2015, *104* (3), 803-12.
36. FDA, Guidance for Industry PAT — A Framework for Innovative Pharmaceutical Development, Manufacturing, and Quality Assurance. 2004, 1-19.
37. Costa, A.; Xu, X.; Khan, M.; Burgess, D., Liposome Formation Using a Coaxial Turbulent Jet in Co-Flow. *Pharm Res* 2015, 1-13.
38. Wartewig, S.; Neubert, R. H. H., Pharmaceutical applications of Mid-IR and Raman spectroscopy. *Advanced Drug Delivery Reviews* 2005, *57* (8), 1144-1170.
39. Saerens, L.; Dierickx, L.; Lenain, B.; Vervaet, C.; Remon, J. P.; Beer, T. D., Raman spectroscopy for the in-line polymer–drug quantification and solid state characterization during a pharmaceutical hot-melt extrusion process. *European Journal of Pharmaceutics and Biopharmaceutics* 2011, *77* (1), 158-163.
40. Guo, J.; Cai, W.; Du, B.; Qian, M.; Sun, Z., Raman spectroscopic investigation on the interaction of malignanthepatocytes with doxorubicin. *Biophysical Chemistry* 2009, *140* (1–3), 57-61.
41. Taylor, L.; Zografi, G., The Quantitative Analysis of Crystallinity Using FT-Raman Spectroscopy. *Pharm Res* 1998, *15* (5), 755-761.
42. . Food and Drug Administration, Process Analytical Technology Initiative, Guidance for Industry PAT – A Framework for Innovative Pharmaceutical development, Manufacturing and Quality Assurance 2004.
43. FDA. Guidance for Industry: Q8(R2) Pharmaceutical Development 2009. http://www.fda.gov/Drugs/GuidanceComplianceRegulatoryInformation/Guidances/default.htm (accessed 11/28/2015).
44. Bangham, A. D.; Horne, R. W., Negative Staining of Phospholipids and their Structural Modification by Surface-Active Agents as Observed in the Electron Micropscope. *J. Mol. Biol.* 1964, *8*, 660-668.
45. Pons, M.; Foradada, M.; Estelrich, J., Liposomes obtained by the ethanol injection method. *International Journal of Pharmaceutics* 1993, *95* (1–3), 51-56.
46. Batzri, S.; Korn, E. D., Single Bilayer Liposomes Prepared Without Sonication. *Biochimica et Biophysica Acta (BBA) - Biomembranes* 1973, *298* (4), 1015-1019.
47. Perrett, S.; Golding, M.; Williams, W. P., A Simple Method for the Preparation of Liposomes for Pharmaceutical Applications: Characterization of the Liposomes. *Journal of Pharmacy and Pharmacology* 1991, *43* (3), 154-161.
48. Schätzel, K., Correlation techniques in dynamic light scattering. *Appl. Phys. B* 1987, *42* (4), 193-213.
49. Schmitz, K. S., *An introduction to dynamic light scattering of macromolecules*. 1990; p Medium: X; Size: Pages: (472 p).
50. Dukhin, A. S.; Goetz, P. J., Acoustic and Electroacoustic Spectroscopy. *Langmuir* 1996, *12* (18), 4336-4344.

51. Bibi, S.; Kaur, R.; Henriksen-Lacey, M.; McNeil, S. E.; Wilkhu, J.; Lattmann, E.; Christensen, D.; Mohammed, A. R.; Perrie, Y., Microscopy imaging of liposomes: From coverslips to environmental SEM. *International Journal of Pharmaceutics* 2011, *417* (1–2), 138-150.
52. Almgren, M.; Edwards, K.; Karlsson, G., Cryo transmission electron microscopy of liposomes and related structures. *Colloids and Surfaces A: Physicochemical and Engineering Aspects* 2000, *174* (1–2), 3-21.
53. Bouwstra, J. A.; Gooris, G. S.; Bras, W.; Talsma, H., Small angle X-ray scattering: possibilities and limitations in characterization of vesicles. *Chemistry and Physics of Lipids* 1993, *64* (1–3), 83-98.
54. Pabst, G.; Rappolt, M.; Amenitsch, H.; Laggner, P., Structural information from multilamellar liposomes at full hydration: Full \textit{q} -range fitting with high quality x-ray data. *Physical Review E* 2000, *62* (3), 4000-4009.
55. ICH Harmonised Tripartite Guideline. Impurities: Guideline For Residual Solvents Q3C(R4), Current Step 4 version. 2009, 1-25.
56. Buchholz, S., Future Manufacturing Approaches in the Chemical and Pharmaceutical Industry. *Chem. Eng. Process.* 2010, *49*, 993-995.
57. Wagner, A.; Vorauer-Uhl, K.; Kreismayr, G.; Katinger, H., The crossflow injection technique: An improvement of the ethanol injection method. *Journal of Liposome Research* 2002, *12* (3), 259-270.
58. Jahn, A.; Vreeland, W. N.; Gaitan, M.; Locascio, L. E., Controlled Vesicle Self-Assembly in Microfluidic Channels with Hydrodynamic Focusing. *J. Am. Chem. Soc.* 2004, *126*, 2674-2675.
59. Lim, J.-M.; Swami, A.; Gilson, L. M.; Chopra, S.; Choi, S.; Wu, J.; Langer, R.; Karnik, R.; Farokhzad, O. C., Ultra-High Throughput Synthesis of Nanoparticles with Homogeneous Size Distribution using a Coaxial Turbulent Jet Mixer. *ACS Nano* 2014, *8*, 6056-6065.
60. Jaafar-Maalej, C.; Charcosset, C.; Fessi, H., A New Method for Liposome Preparation using a Membrane Contactor. *J. Liposome Res.* 2011, *21*, 213-220.
61. Jahn, A.; Vreeland, W. N.; DeVoe, D. L.; Locascio, L. E.; Gaitan, M., Microfluidic Directed Formation of Liposomes of Controlled Size. *Langmuir* 2007, *23*, 6289-6293.
62. Hood, R. R.; DeVoe, D. L.; Atencia, J.; Vreeland, W. N.; Omiatek, D. M., A Facile Route to the Synthesis of Monodisperse Nanoscale Liposomes Using 3D Microfluidic Hydrodynamic Focusing in a Concentric Capillary Array. *Lab on a Chip* 2014, *14*, 2403-2409.
63. Jahn, A.; Lucas, F.; Wepf, R. A.; Dittrich, P. S., Freezing Continuous-Flow Self-Assembly in a Microfluidic Device: Toward Imaging of Liposome Formation. *Langmuir* 2013, *29*, 1717-1723.
64. Greenspan, P.; Fowler, S. D., Spectrofluorometric Studies of the Lipid Probe, Nile Red. *J. Lipid Res.* 1985, *26*, 781-9.
65. Perrett, S.; Golding, M.; Williams, W. P., A Simple Method for the Preparation of Liposomes for Pharmaceutical Applications: Characterization of the Liposomes. *J. Pharm. Pharmacol.* 1991, *43*, 154-161.
66. Khattab, I. S.; Bandarkar, F.; Fakhree, M. A. A.; Jouyban, A., Density, Viscosity, and Surface Tension of Water+Ethanol Mixtures from 293 to 323K. *Korean J. Chem. Eng.* 2012, *29*, 812-817.
67. Kwon, S.; Seo, I., Reynolds Number Effects on the Behavior of a Non-Buoyant Round Jet. *Exp. Fluids* 2005, *38*, 801-812.

68. Or, C. M.; Lam, K. M.; Liu, P., Potential Core Lengths of Round Jets in Stagnant and Moving Environments. *J. Hydro-Environment Res.* 2011, *5*, 81-91.
69. Chu, P.; Lee, J.; Chu, V., Spreading of Turbulent Round Jet in Coflow. *J. Hydraul. Eng.* 1999, *125*, 193-204.
70. Zhao, E.; Benson, G. C.; Lu, B. C. Y., Excess Enthalpies of Ternary Mixtures of Ethanol + Water + Sodium Chloride or Zinc Chloride at 298.15 K. *J. Chem. Eng. Data* 1995, *40*, 665-668.
71. Lasic, D. D., The Mechanism of Vesicle Formation. *Biochem. J.* 1988, *256*, 1-11.
72. Patra, M.; Salonen, E.; Terama, E.; Vattulainen, I.; Faller, R.; Lee, B. W.; Holopainen, J.; Karttunen, M., Under the Influence of Alcohol: The Effect of Ethanol and Methanol on Lipid Bilayers. *Biophys. J.* 2006, *90*, 1121-1135.
73. Touitou, E.; Dayan, N.; Bergelson, L.; Godin, B.; Eliaz, M., Ethosomes — Novel Vesicular Carriers for Enhanced Delivery: Characterization and Skin Penetration Properties. *J. Controlled Release* 2000, *65*, 403-418.
74. Szoka, F.; Papahadjopoulos, D., Comparative Properties and Methods of Preparation of Lipid Vesicles (Liposomes). *Annu. Rev. Biophys. Bioeng.* 1980, *9*, 467-508.
75. Marsh, D., Intrinsic curvature in normal and inverted lipid structures and in membranes. *Biophys. J.* 1996, *70* (5), 2248-2255.
76. Pons, M.; Foradada, M.; Estelrich, J., Liposomes Obtained by the Ethanol Injection Method. *Int. J. Pharm.* 1993, *95*, 51-56.
77. Jaafar-Maalej, C.; Diab, R.; Andrieu, V.; Elaissari, A.; Fessi, H., Ethanol Injection Method for Hydrophilic and Lipophilic Drug-Loaded Liposome Preparation. *J. Liposome Res.* 2010, *20*, 228-243.
78. Schubert, M. A.; Müller-Goymann, C. C., Solvent Injection as a New Approach for Manufacturing Lipid Nanoparticles – Evaluation of the Method and Process Parameters. *Eur. J. Pharm. Biopharm.* 2003, *55*, 125-131.
79. DaunoXome (R) [package Insert]. Souderton, PA: Galen US Inc; 2011.
80. Depocyt (R) [package insert]. San Diego, CA; Pacira Pharmaceuticals, Inc; 2011.
81. Marqibo Kit (R) [package insert]. South San Francisco, CA; Talon Therapeutics, Inc; 2012.
82. ONIVYDE (TM) [package insert]. Cambridge, MA; Merrimack Pharmaceuticals, Inc; 2015.
83. Ambisome(R) [package insert]. Northbrook, IL: Astellas Pharma US, Inc; 2012.
84. Exparel(R) [package insert]. San Diego, CA: Pacira Pharmaceuticals, Inc; 2012.
85. Nagayasu, A.; Uchiyama, K.; Kiwada, H., The size of liposomes: a factor which affects their targeting efficiency to tumors and therapeutic activity of liposomal antitumor drugs. *Advanced Drug Delivery Reviews* 1999, *40* (1–2), 75-87.
86. Hobbs, S. K.; Monsky, W. L.; Yuan, F.; Roberts, W. G.; Griffith, L.; Torchilin, V. P.; Jain, R. K., Regulation of transport pathways in tumor vessels: Role of tumor type and microenvironment. *Proceedings of the National Academy of Sciences* 1998, *95* (8), 4607-4612.
87. Andar, A.; Hood, R.; Vreeland, W.; DeVoe, D.; Swaan, P., Microfluidic Preparation of Liposomes to Determine Particle Size Influence on Cellular Uptake Mechanisms. *Pharm Res* 2014, *31* (2), 401-413.
88. Oussoren, C.; Zuidema, J.; Crommelin, D. J. A.; Storm, G., Lymphatic uptake and biodistribution of liposomes after subcutaneous injection.: II. Influence of liposomal size, lipid

composition and lipid dose. *Biochimica et Biophysica Acta (BBA) - Biomembranes* 1997, *1328* (2), 261-272.
89. Sabín, J.; Prieto, G.; Messina, P. V.; Ruso, J. M.; Hidalgo-Alvarez, R.; Sarmiento, F., On the Effect of Ca^{2+} and La^{3+} on the Colloidal Stability of Liposomes. *Langmuir* 2005, *21* (24), 10968-10975.
90. Dukhin, A. S.; Goetz, P. J., Chapter 4 - Acoustic Theory for Particulates. In *Studies in Interface Science*, Andrei, S. D.; Philip, J. G., Eds. Elsevier: 2010; Vol. Volume 24, pp 127-185.
91. Dukhin, A. S., and Goetz, P. J., *in "Handbook of Ultrasonic and Dielectric Characterization Techniques for Suspended Particles"* American Ceramic Society: Westerville, 1998.
92. Wines, T. H.; Dukhin, A. S.; Somasundaran, P., Acoustic Spectroscopy for Characterizing Heptane/H2O/AOT Reverse Microemulsions. *Journal of Colloid and Interface Science* 1999, *216* (2), 303-308.
93. Technical Note: The Zetasizer Nano Expert Advice System for Aiding Data and Result Interpretation. Worcestershire, UK: Malvern Instruments Worldwide; 2014.
94. McLaughlin, S., The Electrostatic Properties of Membranes. *Annual Review of Biophysics and Biophysical Chemistry* 1989, *18* (1), 113-136.
95. Sabín, J.; Prieto, G.; Ruso, J. M.; Hidalgo-Alvarez, R.; Sarmiento, F., Size and stability of liposomes: A possible role of hydration and osmotic forces. *Eur. Phys. J. E* 2006, *20* (4), 401-408.
96. Magarkar, A.; Dhawan, V.; Kallinteri, P.; Viitala, T.; Elmowafy, M.; Róg, T.; Bunker, A., Cholesterol level affects surface charge of lipid membranes in saline solution. *Scientific Reports* 2014, *4*, 5005.
97. Carrión, F. J.; De La Maza, A.; Parra, J. L., The Influence of Ionic Strength and Lipid Bilayer Charge on the Stability of Liposomes. *Journal of Colloid and Interface Science* 1994, *164* (1), 78-87.
98. Zhao, E.; Benson, G. C.; Lu, B. C. Y., Excess Enthalpies of Ternary Mixtures of Ethanol + Water + Sodium Chloride or Zinc Chloride at 298.15 K. *Journal of Chemical & Engineering Data* 1995, *40* (3), 665-668.
99. Zucker, D.; Marcus, D.; Barenholz, Y.; Goldblum, A., Liposome drugs' loading efficiency: A working model based on loading conditions and drug's physicochemical properties. *Journal of Controlled Release* 2009, *139* (1), 73-80.
100. Tremblay, C.; Barza, M.; Fiore, C.; Szoka, F., Efficacy of liposome-intercalated amphotericin B in the treatment of systemic candidiasis in mice. *Antimicrobial Agents and Chemotherapy* 1984, *26* (2), 170-173.
101. Mayhew, E.; Ito, M.; Lazo, R., Toxicity of non-drug-containing liposomes for cultured human cells. *Experimental Cell Research* 1987, *171* (1), 195-202.
102. Szoka, F. C.; Milholland, D.; Barza, M., Effect of lipid composition and liposome size on toxicity and in vitro fungicidal activity of liposome-intercalated amphotericin B. *Antimicrobial Agents and Chemotherapy* 1987, *31* (3), 421-429.
103. Velinova, M.; Read, N.; Kirby, C.; Gregoriadis, G., Morphological observations on the fate of liposomes in the regional lymph nodes after footpad injection into rats. *Biochimica et Biophysica Acta - Lipids and Lipid Metabolism* 1996, *1299* (2), 207-215.
104. Senior, J. H., Fate and behavior of liposomes in vivo: a review of controlling factors. *Crit Rev Ther Drug Carrier Syst* 1987, *3* (2), 123-193.

105. Parnham, M. J.; Wetzig, H., Toxicity screening of liposomes. *Chemistry and Physics of Lipids* 1993, *64* (1), 263-274.
106. Filion, M. C.; Phillips, N. C., Toxicity and immunomodulatory activity of liposomal vectors formulated with cationic lipids toward immune effector cells. *Biochimica et Biophysica Acta (BBA) - Biomembranes* 1997, *1329* (2), 345-356.
107. Chong, C. S.; Colbow, K., Light scattering and turbidity measurements on lipid vesicles. *Biochimica et Biophysica Acta (BBA) - Biomembranes* 1976, *436* (2), 260-282.
108. Yoshikawa, W.; Akutsu, H.; Kyogoku, Y., Light-scattering properties of osmotically active liposomes. *Biochimica et Biophysica Acta (BBA) - Biomembranes* 1983, *735* (3), 397-406.
109. Matsuzaki, K.; Murase, O.; Sugishita, K. i.; Yoneyama, S.; Akada, K. y.; Ueha, M.; Nakamura, A.; Kobayashi, S., Optical characterization of liposomes by right angle light scattering and turbidity measurement. *Biochimica et Biophysica Acta (BBA) - Biomembranes* 2000, *1467* (1), 219-226.
110. Pick, U., Liposomes with a large trapping capacity prepared by freezing and thawing of sonicated phospholipid mixtures. *Arch. Biochem. and Biophys.* 1981, *212* (1), 186-194.
111. Mayer, L. D.; Hope, M. J.; Cullis, P. R.; Janoff, A. S., Solute distributions and trapping efficiencies observed in freeze-thawed multilamellar vesicles. *Biochim. Biophys. Acta - Biomembranes* 1985, *817* (1), 193-196.
112. Castile, J. D.; Taylor, K. M. G., Factors affecting the size distribution of liposomes produced by freeze-thaw extrusion. *Int. J. Pharm.* 1999, *188* (1), 87-95.
113. Hwang, S. Y.; Kim, H. K.; Choo, J.; Seong, G. H.; Hien, T. B. D.; Lee, E. K., Effects of operating parameters on the efficiency of liposomal encapsulation of enzymes. *Colloids Surf., B* 2012, *94* (1), 296-303.
114. Colletier, J.-P.; Chaize, B.; Winterhalter, M.; Fournier, D., Protein encapsulation in liposomes: efficiency depends on interactions between protein and phospholipid bilayer. *BMC Biotechnology* 2002, *2* (1), 9.
115. Anzai, K.; Yoshida, M.; Kirino, Y., Change in intravesicular volume of liposomes by freeze-thaw treatment as studied by the ESR stopped-flow technique. *Biochim. Biophys. Acta - Biomembranes* 1990, *1021* (1), 21-26.
116. Tetko, I. V.; Gasteiger, J.; Todeschini, R.; Mauri, A.; Livingstone, D.; Ertl, P. P., V. A. ; Radchenko, E. V.; Zefirov, N. S.; Makarenko, A. S.; Tanchuk, V. Y.; Prokopenko, V. V., Virtual computational chemistry laboratory - design and description. *J. Comput. Aid. Mol. Des.* 2005, (19), 453-63.
117. Xu, X.; Khan, M. A.; Burgess, D. J., A quality by design (QbD) case study on liposomes containing hydrophilic API: I. Formulation, processing design and risk assessment. *Int. J. Pharm.* 2011, *419* (1-2), 52-59.
118. Talsma, H.; Van Steenbergen, M. J.; Crommelin, D. J. A., The cryopreservation of liposomes: 3. Almost complete retention of a water-soluble marker in small liposomes in a cryoprotectant containing dispersion after a freezing/thawing cycle. *Int. J. Pharm.* 1991, *77* (2-3), 119-126.
119. Siow, L. F.; Rades, T.; Lim, M. H., Characterizing the freezing behavior of liposomes as a tool to understand the cryopreservation procedures. *Cryobiology* 2007, *55* (3), 210-221.